



Handbook of LED and SSL Metrology

Günther Leschhorn

Richard Young

Günther Leschhorn, Richard Young

Handbook of LED and SSL Metrology

With contributions from

Richard Distl

Prof. Dr. Thomas Nägele

Dr. Thomas Attenberger

Dr. Đenan Konjhodžić

Dr. Matthias Höh

Published by

Instrument Systems GmbH

Munich, Germany

Library information of the Deutsche Nationalbibliothek

The Deutsche Nationalbibliothek listed this publication in the German National Bibliography.
The detailed bibliography data can be found at <http://dnb.d-nb.de>

Instrument Systems GmbH (editor)
Günther Leschhorn, Richard Young
Handbook of LED and SSL Metrology

Berlin: Pro BUSINESS 2017

ISBN 978-3-86460-917-6

1. Auflage 2017

© 2017 by Pro BUSINESS GmbH
Schwedenstraße 14, 13357 Berlin

All rights reserved. No part of this book may be reproduced or transmitted in any form or any means,
electronic or mechanical, including photocopying, recording, or any information storage and retrieval system,
without permission in writing from the copyright owner. Requests should be made through
Instrument Systems GmbH.

Produced and published by: Pro BUSINESS GmbH
Printed on ageing resistant paper
Printed in Germany
www.book-on-demand.de

Cover design, Layout: abc cross media GmbH, Munich
Cover image: ©tailex, fotolia.com

Also available:
Paperback: ISBN 978-3-86460-643-4
Hardcover: ISBN 978-3-86460-644-1

Preface

The first edition of the Handbook of LED Metrology was published in 1999 and maintained its popularity over 16 years. We received extremely positive feedback from customers and people interested in the field of LED measurement. The handbook was considered as a helpful introduction to basic terms and definitions and served as a good guideline to test setups and methodology for accurate measurements on LEDs. Although only about 40 pages long, it covered the basic principles of optical characterization of LEDs. The content of this first edition was sufficient at this early stage of the first wave of the Solid-State Lighting (SSL) revolution.

As time moved on, the SSL revolution continued and demanded a more comprehensive view on the subject of SSL and LED measurement. This led to the decision to intensively review and extend the existing manuscript. The outcome is the work at hand entitled Handbook of LED and SSL Metrology. The content is a summary of knowledge gained by Instrument Systems over the last 30 years. A lot of technical advances in the field of SSL measurements made it into scientific papers or were selected as contributions to proceedings of international conferences and symposia. As a matter of fact, numerous people assisted in preparing the scientific content of this handbook.

We want to take the advantage to acknowledge a number of people who contributed in a special way to the preparation of the manuscript and the technical content.

Thomas Nägele was one of the authors of the first edition and left us an excellent basis for this updated second edition.

As an application engineer, Đenan Konjhodžić contributed with measurements and evaluations to numerous chapters. We are very thankful for his contributions.

Thanks also to Matthias Höh who was deeply involved in the preparation of the manuscript for chapter 9 on LED measurements in the production line.

We are further thankful to Thomas Attenberger for technical editing of the entire manuscript. His experience in the field of LED and SSL measurements was greatly acknowledged.

Thanks to Christine Costa, Melanie Maier and Bei-Bei Chuang from the marketing team. They did a fantastic job in preparing the figures and coordinating the layout and print of this handbook.

Last but not least, we are sincerely grateful to Richard Distl. He was not only one of the authors of the first edition, but inspired and launched the preparation of this second edition during his time as president and CEO of Instrument Systems.

The authors

Contents

Preface	III
Contents	v
1 Introduction	1
2 Terms and Definitions in Photometry, Radiometry and Colorimetry	2
2.1 Photometric and Radiometric Quantities	2
2.1.1 Luminous Flux and Radiant Power	4
2.1.2 Luminous Intensity and Radiant Intensity	4
2.1.3 Illuminance and Irradiance	5
2.1.4 Luminance and Radiance	6
2.2 The Cosine Law	7
2.3 Colorimetry	9
2.3.1 Dominant Wavelength	10
2.3.2 Purity	10
2.3.3 Just Noticeable Differences and MacAdam Ellipses	11
2.3.4 Correlated Color Temperature	12
2.4 Color Rendering Index	13
2.5 Wavelength and Spectrum	15
2.5.1 Peak Wavelength λ_p	15
2.5.2 Spectral Bandwidth (FWHM)	16
2.5.3 Center Wavelength $\lambda_{0.5m}$	16
2.5.4 Centroid Wavelength λ_c	16
3 Standards and Recommendations Applying to LEDs and SSL Products	17
3.1 CIE 127-2007	17
3.2 IES LM-79-08	18
3.3 CIE S025 and EN 13032-4	18
3.4 IES LM-80-08 and TM-21-11	21
3.5 ANSI_NEMA C78.377-2008 and Energy Star®	22
3.6 IES TM-30-15	23
3.7 Zhaga Books	26
3.8 Laboratory Accreditation and Traceability.....	28
4 Basic Properties of LEDs	30
4.1 Package Design	30
4.2 Electrical Properties and Ambient Conditions	32

4.3	Thermal Properties of High Power LEDs	34
4.3.1	Thermal Modeling	34
4.3.2	Active Cooling	36
4.3.3	Testing Methods for HP LEDs	37
4.4	Characteristics of White LEDs	39
4.4.1	Phosphor-Converted White LEDs	39
4.4.2	3-Chip and 4-Chip White LEDs	40
4.4.3	Color Rendering and Efficacy of White LEDs	41
4.5	Basic Properties of OLEDs	42
5	Optical Measuring Instruments	44
5.1	Photometer Design	44
5.2	Comparison of Photometers and Spectroradiometers	47
5.3	Requirements for a Spectroradiometer	48
5.3.1	Scanning Spectroradiometer	49
5.3.2	Array Spectroradiometer	50
5.3.3	Selection Criteria	52
5.4	Stray Light Correction of Array Spectroradiometers	53
5.5	Calibration of Spectroradiometers	56
5.5.1	Wavelength Calibration	56
5.5.2	Spectral Calibration	57
5.5.3	Absolute Calibration and Verification	57
5.6	Imaging Photometers and Colorimeters	58
6	Basic Properties of Integrating Spheres and Goniometers ...	62
6.1	Integrating Spheres	62
6.1.1	Integrating Sphere Design	63
6.1.2	Integrating Sphere Theory	64
6.1.3	Coatings	65
6.1.4	Sphere Directional Response	67
6.2	Goniometers	68
6.2.1	Coordinate Systems	69
6.2.2	Goniometer Types	69
6.2.3	Burning Position Correction	72
7	Optical Characteristics of LEDs, Modules, SSL Lamps and Luminaires	76
7.1	Luminous Flux and Radiant Power	76
7.1.1	The Integrating Sphere Method	76
7.1.2	The Goniophotometer Method	80
7.2	Luminous Intensity and Radiant Intensity	82
7.3	The “Averaged LED Intensity” Concept	83
7.4	The “Partial LED Flux” Concept	84

7.5	Spatial Radiation Characteristics	85
7.6	Uniformity and Glare	90
8	Discussion of Sample Measurements with Error Analysis	92
8.1	Effects of the Dynamic Measuring Range.....	92
8.2	Influence of Stray Light on White LEDs	93
8.3	Influence of Bandpass	96
8.4	Performance Indices	97
8.5	External Influences	98
8.5.1	Accuracy and Stability of the Current Source	98
8.5.2	Quality of LED Test Sockets	99
8.5.3	Precision of Mechanical Setup	100
8.5.4	Temperature Stabilization Time	103
9	LED Measurements in the Production Line	105
9.1	Conditions and Requirements in Production Testing	105
9.2	Process Integration	106
9.3	Reproducibility and Accuracy	108
9.3.1	Correction Factors	108
9.3.2	Reproducibility.....	109
9.3.3	Accuracy	109
9.4	Field Installation of Measurement Equipment	111
9.4.1	Wafer Level Testing	111
9.4.2	Die Level Testing	114
9.4.3	Package Level Testing	115
9.4.4	Module Level Testing	116
9.4.5	OLED Testing	117
List of Figures	118	
List of Tables	126	
References	127	
About Instrument Systems	130	
The Authors	131	

1 Introduction

Rapid developments in LEDs over the past decade have created a major growth market with completely new applications. Full color displays for large areas only became possible with the introduction of high-intensity blue LEDs, while High Power white LEDs are now widely used in general lighting and the automotive industry. These applications have placed increasingly stringent demands on the optical characterization of LEDs, and Solid-State Lighting (SSL) lamps, modules and luminaires, which serves as the benchmark for product quality.

Specific expertise is needed in order to achieve precise and reproducible results. This handbook discusses the special characteristics of LEDs and emerging OLEDs. It provides an overview of state-of-the-art measurement equipment and gives recommendations for obtaining accurate measurement results. The main goal of this handbook is to give readers who are new to this subject an introduction into LED metrology. However, it also provides a useful reference work for more experienced readers.

As an introduction, basic terms and definitions used in photometry, radiometry and colorimetry are described. This develops into definitions of quantities and details such as the physical properties specific to LEDs and SSL products. Later sections describe the test setups and methodology required for accurate measurements. Possible sources of error arising from interactions between LEDs and measuring instruments are also discussed. The handbook concludes with a section devoted to the unique requirements of LED testing in a production environment.

Readers who are short of time can selectively read individual sections. However, it is recommended to read the entire handbook to obtain an in-depth understanding of this discipline.

2 Terms and Definitions in Photometry, Radiometry and Colorimetry

2.1 Photometric and Radiometric Quantities

This section provides a brief overview of important terms and definitions that are essential for an in-depth understanding and therefore correct use of measuring instruments. A distinction is drawn between radiometric quantities describing physical optical radiation properties, photometric quantities describing the perception of optical radiation by the human eye and colorimetry relating to the visual perception of color by human beings.

The relevant quantities reflect different conditions that are important to people in their everyday lives. For example, a distant traffic light will appear to get brighter as you approach it, until you see it as a circular disc rather than a point source. Then as you start to get closer it still seems to be getting bigger but not brighter. While the traffic light appears to be like a point source, luminous intensity is the relevant quantity, but at a shorter distance the luminance of the source is more appropriate. Other quantities of interest are illuminance (e.g. light falling onto the skin or illuminating an object) and total luminous flux (the entire light emitted in all directions).

Table 1:
Important radiometric
and photometric
quantities.

Radiometry	Symbol	Unit
Radiant power	Φ_e	W
Radiant intensity	I_e	W sr^{-1}
Irradiance	E_e	W m^{-2}
Radiance	L_e	$\text{W m}^{-2} \text{sr}^{-1}$
Photometry	Symbol	Unit
Luminous flux	Φ_v	lumen (lm)
Luminous intensity	I_v	$\text{lm sr}^{-1} = \text{candela (cd)}$
Illuminance	E_v	$\text{lm m}^{-2} = \text{lux (lx)}$
Luminance	L_v	cd m^{-2}

Table 1 shows similarities between the units of radiometric quantities and photopic quantities (see the “W” in radiometric quantities and “lm” in photometric quantities). Each photometric quantity has its corresponding radiometric quantity, where the suffix “e” in the symbols represents the radiometric quantity and “v” the photometric equivalent.

One watt of light at 555 nm corresponds to 683 lumens, fixing the relationship between the quantities radiant power and luminous flux. This factor varies with wavelength and the variation is defined by the Commission Internationale de l’Éclairage (CIE), also referred to by the translation

“International Commission on Illumination”, as the $V(\lambda)$ function (see Figure 1). The $V(\lambda)$ curve describes the spectral response function of the human eye in the wavelength range from 360 nm to 830 nm¹ normalized to 1. This curve is used to weight the radiometric quantity that is a function of wavelength λ in order to obtain its corresponding photometric quantity. If $Q_e(\lambda)$ is a spectral radiant quantity, the value of the corresponding photometric quantity Q_v is derived by integration of $Q_e(\lambda)$ as follows:

$$Q_v = K_m \int_{360nm}^{830nm} Q_e(\lambda) \cdot V(\lambda) \cdot d\lambda$$

The constant $K_m = 683 \text{ lm W}^{-1}$ refers to the (physical) radiometric unit of the watt and the (physiological) photometric unit of the lumen.

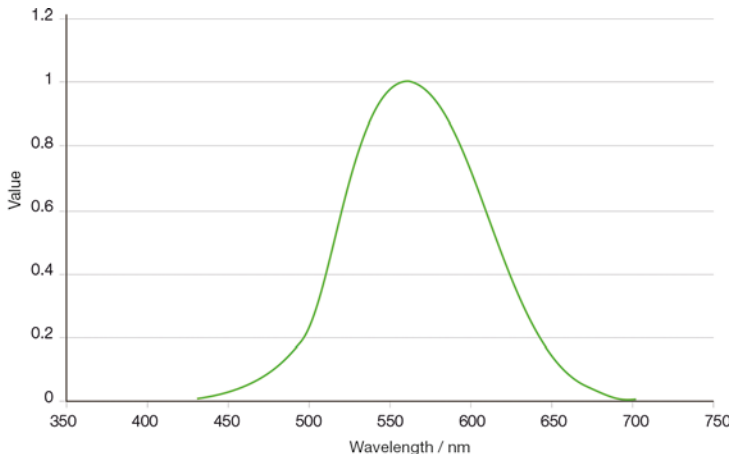


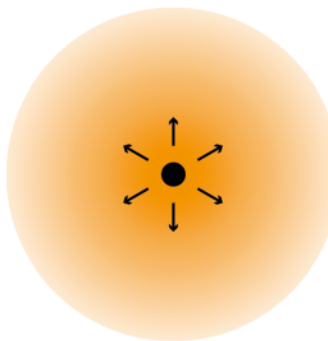
Figure 1:
Diagram showing the $V(\lambda)$ curve (human eye response function).

There are four basic radiometric and photometric quantities which are described in the following sub-chapters.

¹ The full range is 360 nm to 830 nm but values are very small at the extremes and it is often limited for practical purposes to the useful range of 380 nm to 780 nm.

2.1.1 Luminous Flux and Radiant Power

Figure 2:
Luminous flux and
radiant power geometry.
Light from the source
spreads in all directions.
The flux is the amount
of optical radiation (or
visible light) emitted by
the source.



Light is electromagnetic radiation and thus a kind of energy. Radiant power Φ_e is defined as the energy dQ_e of optical radiation emitted by a source per unit time dt . The unit of radiant power is the watt [W].

$$\Phi_e = \frac{dQ_e}{dt}$$

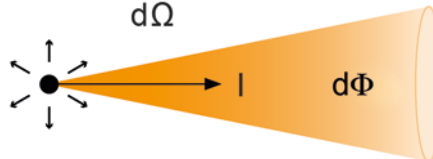
As radiant power relates to light emitted in all directions, it is sometimes called total radiant flux or is even referred to simply as radiant flux (see Figure 2).

The corresponding photometric value is called luminous flux and is obtained by integrating spectral radiant power $\Phi_e(\lambda)$ as follows:

$$\Phi_v = K_m \int_{360nm}^{830nm} \Phi_e(\lambda) \cdot V(\lambda) \cdot d\lambda$$

2.1.2 Luminous Intensity and Radiant Intensity

Figure 3:
Luminous intensity and
radiant intensity
geometry. Radiation from
a point source emitted
per unit solid angle in a
given direction.



Radiant intensity I_e is defined as radiant power $d\Phi_e$ emitted per unit solid angle $d\Omega$ in a given direction (refer to Figure 3). It is expressed in watts per steradian [W sr⁻¹].

$$I_e = \frac{d\Phi_e}{d\Omega}$$

A detector with an active area dA positioned at distance r from a light source measures radiant flux $d\Phi_e$. This configuration assumes a point source and therefore that the inverse square law holds true. In this geometry, the distance r and the detector area dA define the solid angle $d\Omega$ (see also Figure 4).

$$d\Omega = \frac{dA}{r^2} \quad \text{where } dA \ll r^2$$

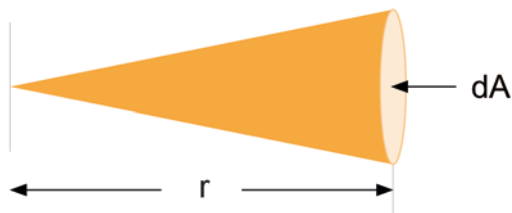


Figure 4:
The solid angle $d\Omega$ of a cone is defined as the ratio of the area dA cut out on a spherical surface to the square of the radius r of the sphere.

Luminous intensity I_v is obtained from spectral radiant intensity I_e using the equation:

$$I_v = K_m \int_{360nm}^{830nm} I_e(\lambda) \cdot V(\lambda) \cdot d\lambda$$

2.1.3 Illuminance and Irradiance

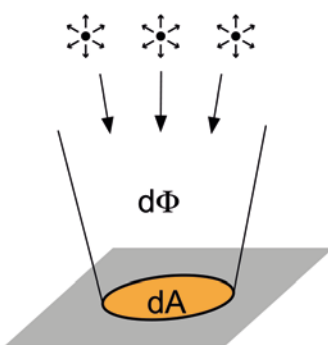


Figure 5:
Illuminance and irradiance geometry. A surface of area dA is illuminated by a light source or ambient light.

Irradiance E_e is obtained from the ratio of the radiant power $d\Phi_e$ falling onto a surface element dA . This quantity is expressed in watts per square meter [W m^{-2}]:

$$E_e = \frac{d\Phi_e}{dA}$$

The following relationship between radiant intensity I_e and irradiance E_e for a point light source is derived from the above formula for irradiance E_e :

$$E_e = \frac{d\Phi_e}{dA} = \frac{I_e \cdot d\Omega}{dA} = \frac{I_e}{r^2}$$

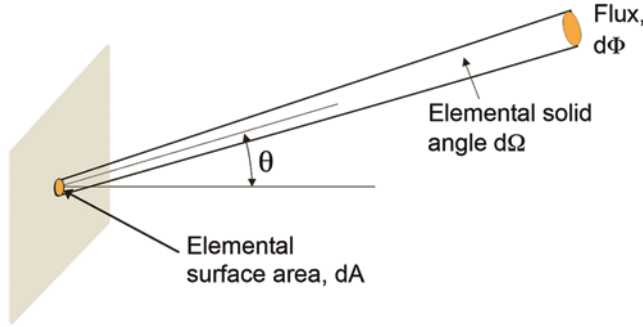
Irradiance can come from any direction, any (even multiple) sources and from any distance (see Figure 5). Although irradiance is often referred to in relation to a lamp, irradiance is not actually a property of a source but is instead a property of the light at a given surface. When referring to the irradiance of a lamp we are implying the following conditions: the irradiance obtained at a surface when the lamp is the only light source and is arranged at a given distance and orientation relative to the surface and the optical axis.

Illuminance E_v can be calculated from spectral irradiance E_e using the following formula:

$$E_v = K_m \int_{360nm}^{830nm} E_e(\lambda) \cdot V(\lambda) \cdot d\lambda$$

2.1.4 Luminance and Radiance

Figure 6:
Luminance and radiance geometry. Light is emitted from a surface of area dA in a solid angle $d\Omega$ and a given direction.



Radiance L_e is measured for extended light sources (i.e. not a point source) and is defined by the equation:

$$L_e = \frac{d\Phi_e}{\cos \theta \cdot dA \cdot d\Omega}$$

where

$d\Phi_e$ represents the radiant flux transmitted by an elementary beam passing through a given point and propagating in the solid angle $d\Omega$, containing a given direction;

- dA is the area of the section of the beam containing the given point;
- θ is the angle between the normal to that section and the direction of the beam.

Radiance is expressed in watts per steradian per square meter [W sr⁻¹ m⁻²]. Note, that the equation for radiance and luminance does not represent a derivative (i.e. a rate of change of flux with solid angle or area) but rather the quotient of an element of flux by an element of solid angle and an element of area (see Figure 6). In strict mathematical terms the definition could be written as follows:

$$L_e = \lim_{A, \Omega \rightarrow 0} \frac{\Phi_e}{\cos \theta \cdot A \cdot \Omega}$$

In practical measurements, A and Ω should be small enough for directional variations in Φ_e not to affect the result. Otherwise, the ratio $\Phi_e / (\cos \theta \cdot A \cdot \Omega)$ gives the average radiance and the exact measurement conditions must be specified. Luminance L_v can be calculated from spectral radiance L_e using the following formula:

$$L_v = K_m \int_{360nm}^{830nm} L_e(\lambda) \cdot V(\lambda) \cdot d\lambda$$

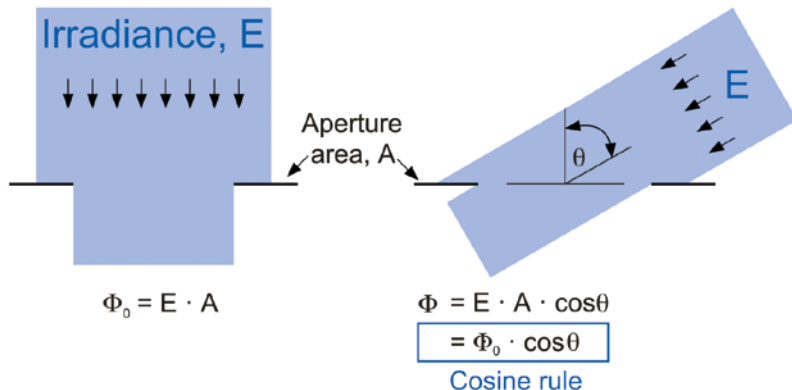
2.2 The Cosine Law

Certain quantities, such as radiance and luminance described above, include a cosine relationship with respect to the viewing angle of the observer or detector. Moreover, certain descriptions inherently imply this cosine relationship; for instance “cosine collector” or “Lambertian emission”.

The cosine relationship originates directly from the fact that these quantities include a plane in their definition. We can define an area within the plane, but when we “view” the area from an angle the apparent size changes. Obviously, when viewed from normal to the plane ($\theta = 0^\circ$) the apparent area is largest, and when viewed from within the plane ($\theta = 90^\circ$) the apparent area is zero (you can try looking at a sheet of paper face-on and edge-on for a visual demonstration). At these, and all other angles, the apparent area is the actual area multiplied by the cosine of the angle (see Figure 7).

Figure 7:

Drawing to illustrate the cosine law. The apparent area becomes smaller as the angle increases with respect to normal.

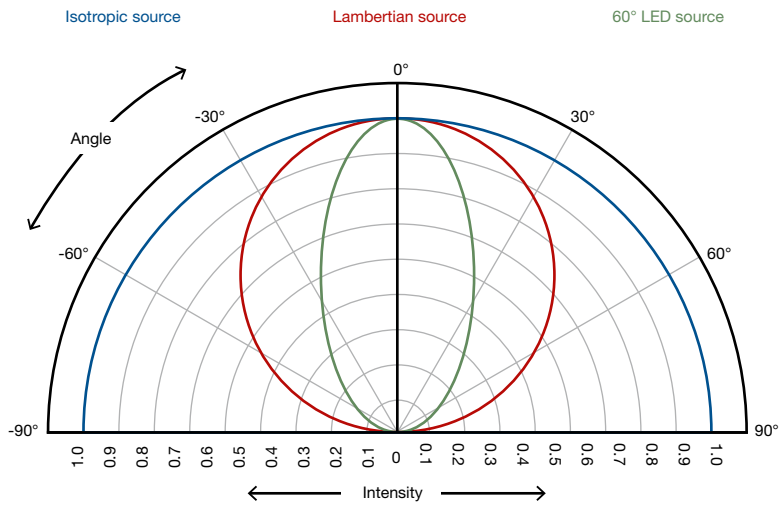


In order to correctly measure the irradiance at a plane, the detector must feature this cosine response so that light from all angles is weighted correctly. A source of radiance that includes a good cosine distribution is called a Lambertian source. A perfect diffuse reflector will scatter light so that the reflection is Lambertian (a cosine distribution) irrespective of the direction of illumination used.

The response of detectors and the angular distribution of source emission are often shown on a radial plot. This shows angles around a circle or semi-circle and intensity or response as the distance from the center, as illustrated in Figure 8.

Figure 8:

A radial plot showing examples of sources: Isotropic (same intensity in all directions), Lambertian (the value changes with the cosine of the angle) and an LED with 60° view angle.



The cosine law therefore represents an ideal behavior, and the quality of sources, detectors and diffuse reflectors are usually measured by the degree of deviation from this ideal [1].

2.3 Colorimetry

Colorimetry relates to the visual perception of color by the human eye and provides a quantitative and qualitative description of color. In 1931 the CIE established the X , Y , Z tristimulus system which is based on the assumption that every color is a combination of the three primary colors red, green and blue [2]. The X , Y , Z tristimulus values are obtained by integrating the product of the spectral power distribution of radiation $S(\lambda)$ and the three color matching functions $\bar{x}(\lambda)$, $\bar{y}(\lambda)$ and $\bar{z}(\lambda)$ (see Figure 9, left) over the 360 nm to 830 nm wavelength range.

$$X = K_m \int_{360\text{nm}}^{830\text{nm}} S(\lambda) \cdot \bar{x}(\lambda) \cdot d\lambda$$

$$Y = K_m \int_{360\text{nm}}^{830\text{nm}} S(\lambda) \cdot \bar{y}(\lambda) \cdot d\lambda$$

$$Z = K_m \int_{360\text{nm}}^{830\text{nm}} S(\lambda) \cdot \bar{z}(\lambda) \cdot d\lambda$$

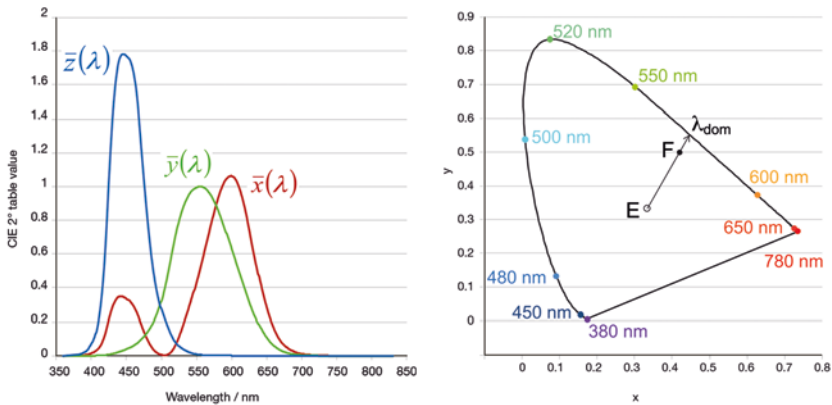
Since the eye response curves depend on the field of view, two sets of color matching functions have been defined by the CIE. The 2° observer is commonly used for light sources whereas the 10° observer is more suitable for color evaluation of objects with a large surface area.

The well-known CIE chromaticity coordinates x , y and z are then derived from the tristimulus values (X , Y and Z) by normalizing to the sum $X+Y+Z$. As $z = 1-(x+y)$, chromaticity is uniquely represented by just x and y coordinates. Plotting values of y and x gives the distinctive shoe shape for monochromatic wavelengths (the monochromatic locus). All real sources must be combinations of one or more monochromatic components, so all must lie within the area bounded by the monochromatic locus.

$$x = \frac{X}{X+Y+Z} \quad y = \frac{Y}{X+Y+Z} \quad z = \frac{Z}{X+Y+Z} = 1 - (x+y)$$

The right side of Figure 9 shows this chromaticity space according to CIE 1931 for the 2° observer. There are other chromaticity spaces, e.g. more uniform chromaticity scales (CIE 1960 u v and CIE 1976 u' v') or $L^*a^*b^*$ that can be calculated by transformation of the x , y and z values. The CIE 1960 u v chromaticity space is for example used to calculate correlated color temperature (see also Section 2.3.4 on page 12).

Figure 9:
The CIE 2° observer color matching functions (left). 1931 CIE chromaticity diagram for 2° observer (right).



2.3.1 Dominant Wavelength

The dominant wavelength λ_{dom} is determined from the chromaticity coordinates of the measured spectrum. A straight line is taken through the color coordinates of a reference illuminant and the measured chromaticity coordinates F in the chromaticity diagram (see Figure 9 right side). The equal energy point E with chromaticity coordinates $x = 0.333$ and $y = 0.333$ is generally taken as the reference illuminant. The intersection between the straight line and the boundary of the color diagram (i.e. the monochromatic locus) gives the dominant wavelength. It is a measure of the color sensation (hue) produced in the human eye by the light source.

The straight line connecting the end points of the monochromatic locus is called the purple line. Points on the purple line do not correspond to specific wavelengths of monochromatic light. Hence, a dominant wavelength is not defined. Instead of a dominant wavelength, a complementary wavelength can be assigned. Subtraction of the complementary wavelength from white light yields the color on the purple line.

2.3.2 Purity

Purity, P_e , is defined from CIE 1931 x y chromaticity coordinates² as:

$$P_e = \frac{y_F - y_0}{y_d - y_0} = \frac{x_F - x_0}{x_d - x_0}$$

where the suffix 0 indicates the white reference point (usually the equal energy point E), F is the test source, d is the dominant wavelength intersection.

² other color spaces may yield slightly different values

Most single color LEDs are narrow wavelength band radiators with a purity of between 90 % and 100 %, i.e. their color cannot be distinguished from a monochromatic beam.

Purity is a measure of colorfulness, known as chroma. Colors close to the white point are desaturated and those close to the monochromatic locus are saturated.

2.3.3 Just Noticeable Differences and MacAdam Ellipses

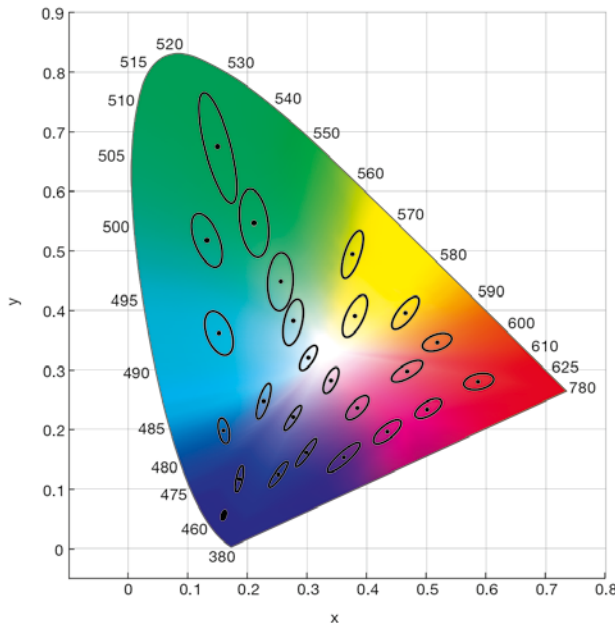


Figure 10:
MacAdam ellipses
shown at 10x actual size.

The CIE 1931 x y diagram shows color, but it is apparent from the work of MacAdam [3] that this color space is not uniform. If, for example, a stimulus of a certain chromaticity has monochromatic light at some wavelength added to it, how much does the chromaticity need to change before humans can see it as a different color? This is the essence of a just noticeable difference (JND) test. MacAdam found that the shape of a JND around the test chromaticity formed an ellipse. Figure 10 shows that the size, shape and orientation of the ellipse changed with color. Uniform color spaces (u v and u' v') were later introduced in order to make these ellipses more circular.

Results from MacAdam were used for specific examples. For general “MacAdam ellipses” at other chromaticities these are taken as $\Delta E = 1$ in $L^*a^*b^*$ space [4] and transformed to other spaces.

2.3.4 Correlated Color Temperature

An important property for white light sources is the correlated color temperature (CCT) expressed in Kelvin. Table 2 shows general classifications of CCT and provides typical examples.

Table 2:
General classification
of correlated color
temperature and
examples.

Description	CCT	Example
Warm white	approx. 2700 K	Incandescent lamp
Neutral white	3000 to 3500 K	Halogen lamp
Cool white	4100 to 5000 K	Compact fluorescent lamp

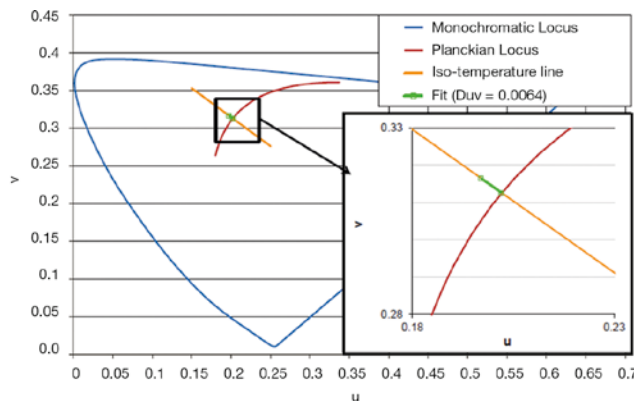
As a blackbody³ heats up it goes through red, orange, yellow, warm white and cool white. At each temperature the blackbody has specific chromaticity coordinates and the line formed by these coordinates is called the Planckian locus. Conversely, if the chromaticity of a blackbody is known the temperature can be determined – this is the color temperature.

Most sources are not blackbodies and hence may not lie on the Planckian locus. The correlated color temperature relates to the blackbody nearest to the chromaticity of the source when expressed in CIE 1960 u v space. This is the only CIE space where the iso-CCT lines (lines of equal correlated color temperature) are perpendicular to the Planckian locus.

$$u = \frac{4x}{12y - 2x + 3} \quad v = \frac{6y}{12y - 2x + 3}$$

The correlated color temperature of a source can therefore be calculated from the u v chromaticity coordinates by finding the temperature of the blackbody closest to it, as illustrated in Figure 11. As all blackbodies lie on the Planckian locus, all sources with the same CCT lie on a line at a right angle to the locus.

Figure 11:
CIE 1960 u v diagram,
showing a test source
chromaticity and
the corresponding
chromaticity on the
Planckian locus joined
by the iso-temperature
line (Fit). The temperature
of the blackbody on
the Planckian locus is
the correlated color
temperature. Duv is the
distance between the
chromaticities.



³ A blackbody is an ideal radiator, also called Planckian radiator, i.e. the emission is described by the Planck Law of radiation. Glowing metal like a filament can be described as a blackbody source to a certain extent.

Although an iso-temperature line may extend to greens and purples, a green or purple blackbody does not exist. Care must be exercised when interpreting CCT values that lie far from the Planckian locus to ensure conclusions are valid. It is not uncommon to use the value of Duv , the distance from the Planckian locus, in order to ensure that valid CCT values are obtained.

In addition, the Planckian locus ends in the middle of the CIE u v diagram, corresponding to the chromaticity of a blackbody at infinite temperature. The iso-temperature line from this point represents a limit of CCT and this excludes much of the blue region of the diagram. It is possible for LEDs and other sources to have chromaticities in this region so they would not have an equivalent CCT. Example spectra for typical sources with their respective CCT are shown in Figure 12.

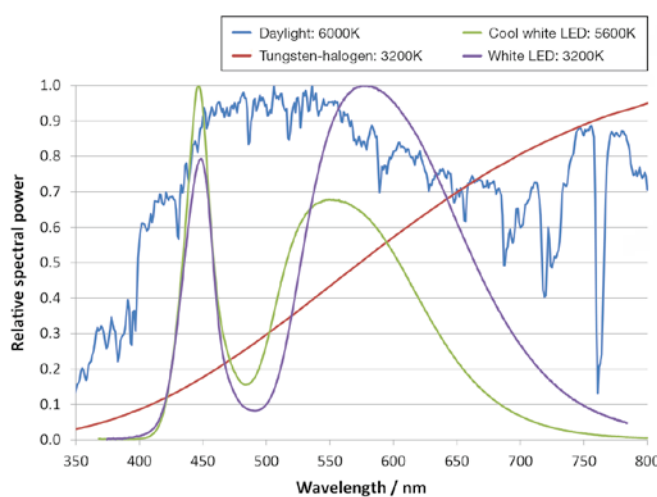


Figure 12:
Examples of source spectra with their respective CCT.

2.4 Color Rendering Index

When a light source is used to illuminate objects, the colors of the objects depend on the spectral distribution of the source. Two sources with the same chromaticity but different spectral distributions will not render objects in the same way. Color rendering index (CRI) provides a value for how well or badly a test source would render colors compared to a reference source.

Figure 13:
Representation of the rendering of the 14 tiles used in color rendering index calculations under test and reference sources. A white tile is included for reference.

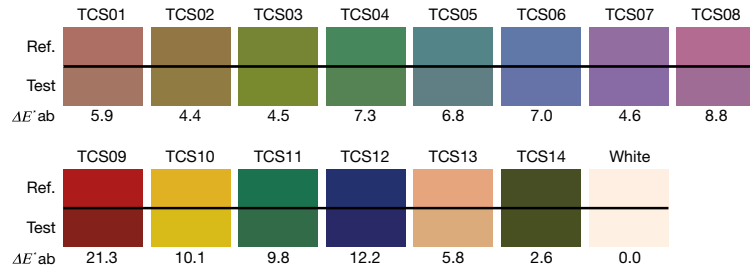


Figure 13 shows an example for rendering of Test Color Samples (TCS) by two sources. CIE Publication 13.3 [5] describes the recommended calculation of the CRI. Details of the calculation will be omitted here but essentially the method follows these steps:

- The CCT is calculated. This means that if there is no valid CCT the CRI is also not valid. The recommendation is for D_{uv} to be less than 0.0054 for valid results.
- The reference illuminant is then selected to be the same CCT as the test lamp. For a CCT of less than 5000 K the reference is a blackbody and for greater temperatures it is a calculated spectral distribution representing different phases of daylight.
- Human vision adapts to various illumination conditions by shifting colors, so the next stage is to apply chromatic adaptation corrections.
- After this the colors are represented on a uniform color space known as $W^*U^*V^*$ and the color differences between the test source and reference illuminant are then calculated. These differences are scaled so that a value of 100 represents a perfect match to the reference and the value decreases as the color rendering deteriorates.
- The first 8 tiles are desaturated colors, whereas tiles 9 to 12 are more saturated. To some extent, tile 13 simulates Caucasian skin tones and tile 14 is a strong green. Each of the 14 colored tiles⁴ has a special color rendering index, R_1 to R_{14} . The average of the first 8 tiles is called the general color rendering index, R_a , and it is this single value that is most used. Since its publication in 1995, the color rendering index has become synonymous with the general color rendering index, R_a , unless specified otherwise.

⁴ Some non-CIE color samples exist, but are rarely used. Tile 15, for example, simulates Asian skin tones.

For normal lighting a CRI of at least 80 is generally acceptable, but high quality applications require a CRI of 90 or more. Special lighting applications may need values close to 100 for critical rendering purposes. The CRI, however, is irrelevant for single color LEDs (e.g. wall washers for buildings).

2.5 Wavelength and Spectrum

The spectral power distribution of the optical radiation emitted by single color LEDs differs in many ways from other radiation sources. It is neither monochromatic like a laser nor broadband like a tungsten lamp, but rather lies somewhere between these two extremes. The spectrum of such LEDs has a specific peak wavelength λ_p depending on the manufacturing process, where the spectral bandwidth (FWHM) is typically a few tens of nanometers (see Figure 14). The spectral parameters of LEDs are described in the following sub-chapters.

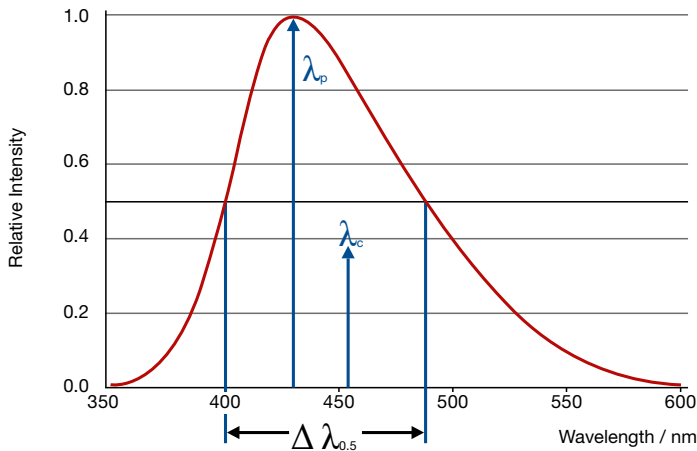


Figure 14:
The spectral power distribution of a blue LED and relevant spectral parameters.

2.5.1 Peak Wavelength λ_p

The peak wavelength is at the maximum intensity of the spectrum. It is easy to define and is therefore generally given in LED datasheets. However, the peak wavelength has little significance for practical purposes, since two LEDs may well have the same peak wavelength but different color perception.

Modern thinking and emerging recommendations do not advise use of the peak wavelength except for information purposes. Centroid wavelength is the quantity of choice when specifying the characteristics of a monochromatic source.

2.5.2 Spectral Bandwidth (FWHM)

The spectral bandwidth at half intensity $\Delta\lambda_{0.5}$ is calculated from the two wavelengths $\lambda'_{0.5}$ and $\lambda''_{0.5}$ on either side of λ_p : $\Delta\lambda_{0.5} = \lambda'_{0.5} - \lambda''_{0.5}$, where the intensity falls to half of its maximum.

2.5.3 Center Wavelength $\lambda_{0.5m}$

The center wavelength corresponds to the wavelength halfway between the half-wavelengths $\lambda'_{0.5}$ and $\lambda''_{0.5}$.

2.5.4 Centroid Wavelength λ_c

The centroid wavelength λ_c corresponds to the “center of gravity” of the plot in Figure 14. Hence it is the wavelength that divides the area below the spectrum graph into two equal parts according to the following formula:

$$\lambda_c = \frac{\int_{\lambda_1}^{\lambda_2} \lambda \cdot S(\lambda) \cdot d\lambda}{\int_{\lambda_1}^{\lambda_2} S(\lambda) \cdot d\lambda}$$

The centroid wavelength is ideal for characterizing the radiometric properties of LEDs (e.g. ultraviolet and infrared LEDs).

3 Standards and Recommendations

Applying to LEDs and SSL Products

The CIE is the main organization providing document standards for general optical measurement of LEDs. Standards published by CIE are sometimes mirrored by other organizations such as ISO (International Organization for Standardization), DIN (Deutsches Institut für Normung e.V.), IEC (International Electrotechnical Commission), JSA (Japanese Standards Association), ANSI (American National Standards Institute), etc. The same effective standard (often with minor changes, language or convention translations) may appear by another designation and number when published by these other organizations.

Some organizations produce standards or recommendations that relate to LED testing in or for specific applications. These include: IES (Illumination Engineering Society) and IESNA (Illumination Engineering Society of North America), ASTM (American Society for Testing and Materials), NEMA (National Electrical Manufacturers Association), SAE (Society of Automotive Engineers), SID (Society for Information Display), VESA (Video Electronics Standards Association), FAA (Federal Aviation Administration), etc.

The following sections give an overview of the most important standards and recommendations for measurement of LEDs and SSL products.

3.1 CIE 127-2007

CIE 127-2007 [6] deals with single packaged LEDs up to 10 mm in diameter. Larger LEDs, OLEDs and units containing multiple LEDs should be measured according to other recommendations, and many of these are currently under discussion but as yet unpublished. In particular, Solid-State Lighting (SSL) applications have received much recent attention with the publication of IES LM-79-08, EN 13032-4 and CIE S025.

The CIE publication 127-2007 is probably the best known and most widely adopted document for LED testing. Although technically a recommendation, it is recognized as a de facto standard by the industry⁵. The publication includes optical measurements that are based on fixed geometries and require specific equipment:

- Averaged LED intensity
- Partial LED flux
- Total flux

⁵ CIE Technical Committee 2-46 "CIE/ISO Standards on LED Intensity Measurements", which was set up to establish a standard based on CIE Publication 127:2007, was discontinued in 2010 due to the fact that the CIE Publication was already considered a de facto standard.

The first two measurement types include “LED” to emphasize that they are special definitions applying to LEDs only. Total flux is defined in the same way as for any other source, but with recommendations on the design and size of integrating spheres that should be used. These measurement methods are described in detail in Chapter 7.

3.2 IES LM-79-08

LM-79-08 [7] is an approved North American method developed by IES. It is not an internationally accepted standard. Nevertheless, LM-79-08 was widely used worldwide and much content was adopted by the first internationally agreed measurement standard for SSL sources CIE S025 (see Section 3.3). The method describes procedures and precautions to perform reproducible measurements on Solid-State Lighting products. These sources are tested for total flux and, if required, spatial distribution. Sources should be measured at $25 \pm 1^\circ\text{C}$ ambient in still air such that any mounting fixtures do not add extra heat sinking. Self-absorption correction is required and the integrating sphere used for measurement of luminous flux must be large compared to the source. If spatial distribution is required, a type C goniometer must be used. IES LM-79-08 shows differences to the more general IES LM-78-07 [8] which deals with general lighting total luminous flux measurements in an integrating sphere. A major difference is the inclusion of 2π measurement geometry for applicable SSL sources.

3.3 CIE S025 and EN 13032-4

As a purely North American standard, LM-79 lacked the coverage of worldwide accreditation. A number of national documents, such as the draft standard DIN 5032-9 in Germany, the CQC and GB Standards in China or the JIS Test Methods in Japan, existed in parallel to the North American standard. Over a period of many years, standardization committees have been working to close this gap by creating an international standard. 2013 therefore saw publication of the European standard prEN 13032-4:2013 which had been developed by the Working Group WG7 “Photometry” of the Technical Committee CEN/TC 169 “Light and Illumination”. The secretariat of this committee is managed by the DIN German Standards Organization. The “Photometry” Working Committee of the Light Metrology Standards Committee (FNL) within the DIN German Standards Organization was responsible for drawing up the German national version. Simultaneously and in close cooperation with the WG7 Working Group, the TC2-71 Technical Committee of the CIE was working on a reference standard with the same content.

In 2015, the standard CIE S025:2015 [9] was published. This represents a milestone in the development of an international standard for the analysis and presentation of photometric data from lamps, luminaires and modules based on LEDs. In contrast to LM-79, which does not include LED modules, the standard encompasses LED modules, LED lamps, LED light engines and LED luminaires. The only devices not included in this standard are LED packages and products based on OLEDs. Adoption of CIE S025 as an ISO/CIE/IEC “Triple Logo” Standard is anticipated.

The measured quantities covered by the standard include measurement of luminous flux (including partial luminous flux and derived parameters, such as luminous efficacy), luminous intensity distributions, luminance and colorimetric quantities, such as chromaticity coordinates, correlated color temperature (CCT), distance from the Planckian locus (D_{uv}), color rendering indices and angular color uniformity. Appropriate test setups recommended for all measured quantities are defined. In the case of luminous flux, for example, integrating sphere photometers and integrating sphere spectroradiometers are recommended for modules, lamps, and small luminaires.

	Standard test condition	Tolerance interval	Applicable for
Ambient temperature	25.0 °C	±1.2 °C	LED lamps/luminaires, light engines
Surface temperature	Nominal operating temperature t_p	±2.5 °C	LED modules
Air movement	Stationary air	0 m/s to 0.25 m/s	
Test voltage/ Test current	Nominal voltage, nominal current	±0.4 % for root mean square value (RMS) AC voltage; ±0.2 % for DC voltage and current	

Table 3:
The standard test conditions and tolerance intervals of CIE S025.

CIE S025 defines uniform standard test conditions (see Table 3), as well as special requirements and instrumentation (see Table 4). These conditions are specified for the laboratory, the environment, and the test instruments. Each standard test condition is subject to a set value and a tolerance condition which is specified by a tolerance interval (see Figure 15). Since the definition of the tolerance interval does not take account of measurement uncertainty, different accuracy characteristics can be accepted for the measuring device. The range yielded by deduction of the extended calibration uncertainty (twofold standard deviation) of the instrument being used is known as the acceptance interval.

Table 4:
Summary of special requirements defined by the CIE S025 standard for measuring instruments.

	Requirement
Calibration uncertainty for voltmeters and ammeters	AC: $\leq 0.2\%$ DC: $\leq 0.1\%$
Calibration uncertainty and bandwidth of AC power meters	$\leq 0.5\%$ bandwidth $\geq 100\text{ kHz}^1$
Internal impedance voltmeter	$\geq 1\text{ M}\Omega^2$
Drift and fluctuation of the voltage supply	Within the acceptance interval for test voltage and test current
Harmonic content and frequency uncertainty of operating voltage	$\leq 1.5\%^3$ $\pm 0.2\%$ of the required frequency
AC component for direct-current supply	$\leq 0.5\%$ (rms)
Electric and photometric stabilization for the device under test	LED lamps and luminaires: $\geq 30\text{ min}$ and relative difference of maximum and minimum measured values of the previous 15 minutes $<0.5\%$ LED modules: Operating temperature t_p achieved and retained for 15 min in an interval of $\pm 1^\circ\text{C}$
Spectral sensitivity photometer	$V(\lambda)$ mismatch index $f_1' \leq 3\%$
Surface of device under test for measurements with integrating sphere	$4\pi: \leq 2\%$ of the inside surface of the sphere $2\pi: \text{diameter of the sphere port} \leq 1/3 \text{ of the sphere diameter}$
Cosine correction of the detector for measurements with integrating sphere	Cosine correction index $f_2 \leq 15\%$
Repeatability for sphere opening/closing	$\pm 0.5\%$
Stability of the spectral sensitivity of a sphere between recalibrations	$<0.5\%$
Wavelength range and wavelength uncertainty for the spectroradiometer	380 – 780 nm $\leq 0.5\text{ nm (k = 2)}$
Bandwidth and scanning interval spectroradiometer	$\leq 5\text{ nm}$
Angular alignment and resolution angular display goniometer	$\pm 0.5^\circ$ $\leq 0.1^\circ$
Photometric (test) distance for samples with a maximal luminous dimension D	Beam angle $\geq 90^\circ: \geq 5xD$ Beam angle $\geq 60^\circ: \geq 10xD$ Narrow angular distribution / steep gradients: $\geq 15xD$ Large non-luminous areas with maximum distance S: $\geq 15x(D+S)$
Burning position	Measurement in specific burning position or correction to behaviour of the device under test in the specified burning position (e.g. with the auxiliary photometer method) ⁴

¹ 5 kHz or 30 kHz are authorized without high-frequency components

² An even higher internal impedance of the measuring instrument is necessary for devices under test with high impedance

³ $\leq 3\%$ for power factors >0.9

⁴ Not necessary for LED modules with temperature regulation

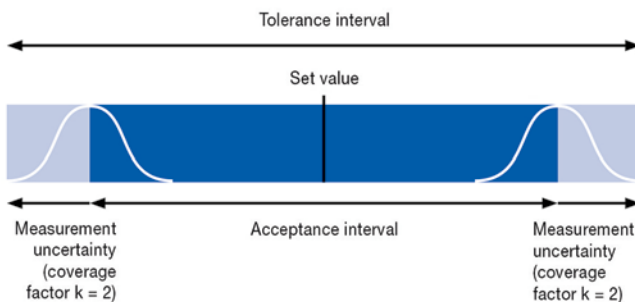


Figure 15:
Relationship between set value, expanded measurement uncertainty, tolerance and acceptance interval. The definition of the tolerance interval does not take account of measurement uncertainty.

The measured parameter must be within the acceptance interval for a standard-compliant measurement. The measuring results can be corrected to the set value of the tolerance interval in order to reduce the measurement uncertainty. The special requirements for the test setup may also be corrected in some cases.

Concerning goniophotometry, a measurement of the source in the burning position specified by the manufacturer is not mandatory. If the device under test is not measured in its designed burning position, a correction (e.g. with the so called auxiliary photometer method) can be applied. This method is covered in more detail in Section 6.2.3.

3.4 IES LM-80-08 and TM-21-11

LED sources may fail, but as there is no filament, the failure mode is somewhat different from incandescent sources. They will normally just continue to emit a lower level of light throughout their life. Catastrophic failures are rare and attributable to mechanical causes, e.g. stress due to the differential expansion rates of dies and encapsulant. It is therefore difficult to define the lifetime of LEDs by failure rate. IES LM-80-08 [10] deals with lumen depreciation of LEDs and modules. It recommends measuring the lumen output and chromaticity over a long period of operation. A spectroradiometer is the recommended equipment for making such measurements. The LEDs or modules are driven according to the manufacturer's instructions at three different case temperatures (55 °C, 85 °C and a manufacturer-selected temperature). Luminous flux and chromaticity measurements are made at intervals of less than 1,000 hours and for a total duration of at least 6,000 hours, though more frequent and longer measurements of up to 10,000 hours are preferred. Results are reported but LM-80-08 provides no recommendation for estimations of expected lifetime or lumen output beyond the test period.

IES TM-21-11 [11] provides a measure of usable lifetime for LEDs and modules. The testing procedure is similar as for LM-80-08 and an average of at least 20 samples at each temperature is used. An exponential decay of

the form $\Phi(t) = B \exp(-\alpha t)$, where α is the time constant and B is a scaling constant, is fitted to the last 5,000 hours data (of 6,000 or 10,000 hour tests) using a least squares method. The projected “life” over which the lumens are maintained above the level p [%] is then

$$L_p = \frac{\ln(B/p)}{\alpha}$$

The lumen maintenance “life” is then expressed as, e.g. $L_{70}(6k) = 30,000$ hours. $L_{70}(6k)$ is the estimated time up to which the source will emit more than 70 % of its initial luminous flux on a 6,000 hours testing base.

Calculated lifetimes in excess of 6 times test duration should be expressed as, e.g. $L_{70}(6k) > 36,000$ hours.

3.5 ANSI_NEMA C78.377-2008 and Energy Star®

Energy Star®, a US-government backed program to lower energy consumption by lamps, provides a set of specifications for lighting components so that performance and energy saving are simultaneously achieved. Although this is not in itself a standard, it provides important criteria by which LEDs can be used in applications ranging from exit signs to general lighting.

Packaging of lamps according to Energy Star® [12] recommendations should include an educational tool to indicate the CCT.

Figure 16:
CIE x y chromaticity diagram showing the 8 Energy Star® nominal quadrangles defining color binning. The red line is the Planckian locus. 7-step MacAdam ellipses are shown as a reference.
Source: ANSI_NEMA_ANSLG C78.377-2008

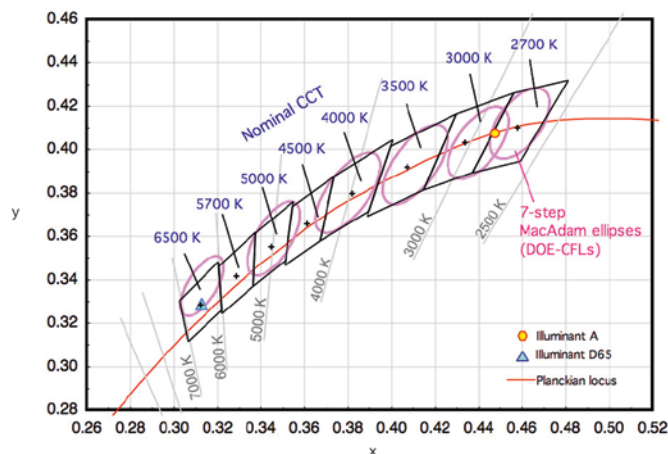


Figure 16 shows the Energy Star® binning limits for integral LED lamps. This principle of color binning is adopted from the American National Standard ANSI_NEMA C78.377 “Specifications for the Chromaticity of Solid-State

Lighting Products” [13]. The iso-temperature lines (lines where the color of the source is closest to the blackbody temperature at the intersection with the Planckian locus) are shown for comparison. As discussed in Section 2.3.4, correlated color temperature is defined by the intersection with the Planckian locus of an iso-temperature line that includes the source chromaticity. This process is only valid close to the Planckian locus. The combination of CCT limits and acceptable distance from the locus leads to a quadrangle shaped definition of color binning. ANSI C78.377 defines 8 nominal⁶ CCT categories that are used to specify and communicate white light chromaticity information (see Table 5). The specified quadrangles are shown in Figure 16 together with 7-step MacAdam ellipses as a reference.

Nominal CCT [K]	Target CCT and tolerance [K]	Target D_{uv} and tolerance
2700	2725 ± 145	0.000 ± 0.006
3000	3045 ± 175	0.000 ± 0.006
3500	3465 ± 245	0.000 ± 0.006
4000	3985 ± 275	0.001 ± 0.006
4500	4503 ± 243	0.001 ± 0.006
5000	5028 ± 283	0.002 ± 0.006
5700	5665 ± 355	0.002 ± 0.006
6500	6530 ± 510	0.003 ± 0.006

Table 5:
Nominal CCT categories according to ANSI_NEMA C78.377-2008.

Where white LEDs are used in general lighting they should ideally be the desired class or bin of white with good color rendering properties. As well as the CCT, color rendering depends on the spectral distribution of light. The quality of color rendering required by the user is normally task-based but Energy Star® [14] states that $R_a \geq 80$ is generally required. A perfect score is 100 and the closer to this one gets the better the color rendering properties of the lamp. For applications involving critical color discrimination it is not unusual to require a R_a value in excess of 90 or even 95. CRI is considered for a revision [15] by the CIE. A brief introduction of the calculation procedure is given in Section 2.4.

3.6 IES TM-30-15

CRI has been the industry reference for decades when it comes to measuring the color quality of light and has a charming simplicity that makes it easy for the end user to understand and work with. Nevertheless, CRI is a pure fidelity (magnitude of difference to original image) metric, based on a very limited set of color samples and therefore has some substantial drawbacks. The most severe methodological issues are the small sample set, the choice

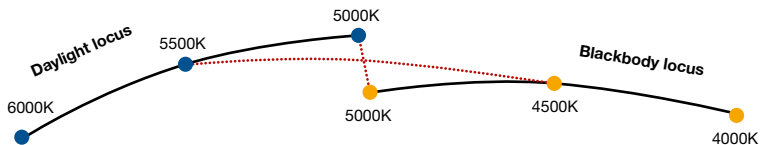
⁶ Nominal CCT is a CCT value at 100 K steps that is closest to the target CCT of the product (value that the product is designed to produce).

of the reference source and the inherent averaging over the test colors which leads to a loss of information and induces ambiguity. Moreover, CRI does not convey exact color appearance e.g. saturated colors and red in particular are not rendered accurately.

Over time, numerous indices have been proposed as a successor for CRI. The most important are the Color Quality Scale (CQS), Gamut Area Index (GAI) and Television Lighting Consistency Index (TLCI). Although some manufacturers of SSL products use and publish these indices, they have not accomplished international agreement as a successor for CRI up to now.

In 2015, the Illuminating Engineering Society published IES TM-30-15 [16] as a method for evaluating the color rendition of light sources. Although it is not finally clear that CIE will follow the IES proposal and make this method an internationally agreed color metric standard, the chances for a revised version are quite high. TM-30 is a more accurate fidelity and also a gamut metric with additional information and graphical representations. It uses a modern and uniform color space⁷ and is built on a set of 99 Color Evaluation Samples (CES) with spectral properties of real, everyday objects (e.g. paints, textiles, inks). Like CRI, TM-30 uses a combination of daylight and blackbody locus as reference source. The main difference to CRI is that TM-30 avoids the discontinuous step at 5000 K and realizes a smoother transition by blending reference sources in the range of 4500 K to 5500 K (see Figure 17).

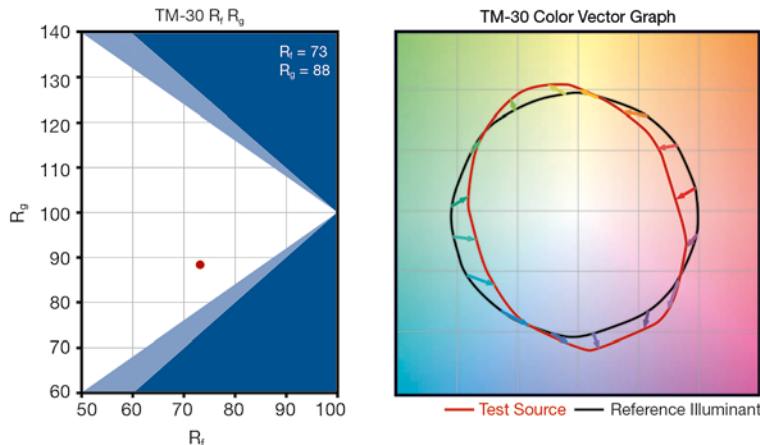
Figure 17:
Smooth transition of
daylight and blackbody
locus as reference
source for TM-30-15.



The main result of a TM-30 calculation is the Fidelity Index R_f and the Gamut Index R_g . R_f scores from 0 to 100 and can be interpreted as a more accurate version of CRI⁸. The value set of the Gamut Index depends on the achieved Fidelity Index. It scores from 60 to 140 when $R_f > 60$. $R_g < 100$ means decreasing overall saturation and $R_g > 100$ means increasing overall saturation.

⁷ Three dimensional CIE CAM02-UCS

⁸ R_f tends to produce values a little lower than CRI in direct comparison.



The score of a typical white light source (red dot) in Figure 18 left, indicates an overall desaturation of $R_g = 88$ with a Fidelity Index of $R_f = 73$.

One of the basic concepts of TM-30 is the sub-division of the color space into 16 so-called hue bins in a radial pattern. For each hue bin, an R_f value can be calculated (see Figure 19), and chroma and hue shifts can be illustrated graphically by a Color Vector Graph (see Figure 18 right side). The resulting vectors for each hue bin can be easily interpreted when compared to the reference. The whole graph is scaled in a way that the reference has a circular shape (black circle in Figure 18 right). Tangential vectors to the reference circle indicate pure hue shifts. Vectors pointing inside or outside the reference circle indicate decreased or increased saturation for the specific color, respectively. A perfect match for the source under investigation would be to exactly hit the reference circle. For the given example in Figure 18, the simple interpretation would be: The source tends to decrease saturation for green and red colors, while it tends to have a pure hue shift for turquoise and orange colors.

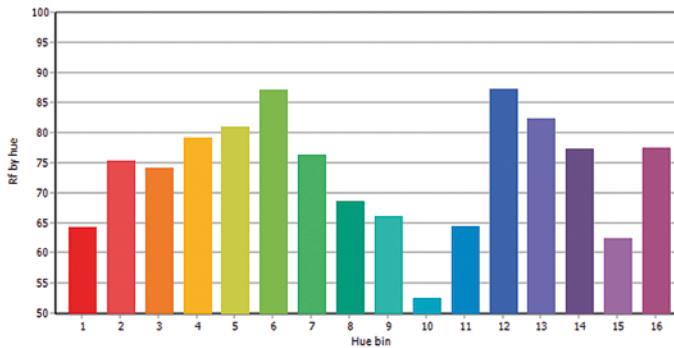


Figure 18:
Gamut Index versus Fidelity Index with approximate limits for the combination of the two measures (left). The shaded areas are not achievable for practicable white light sources and for sources on the Planckian locus. Color Vector Graphic for a typical white light source (right). Tangential vectors to the reference circle indicate hue shifts. Vectors pointing inside/outside the reference circle indicate decreased/increased saturation for the specific color.

Figure 19:
Fidelity Index R_f by hue bin.

3.7 Zhaga Books

Zhaga is an international consortium of the lighting industry, which develops specifications that enable the interchangeability of LED-based light sources made by different manufacturers. Zhaga's members include hundreds of companies from throughout the global lighting industry. The cooperation is governed by a consortium agreement that defines rules regarding confidentiality, intellectual property and decision making. Zhaga's ultimate goal is to bring consensus and simplification in applications for general lighting by establishing clearly defined interface specifications.

The Zhaga specifications, so called "Books", which are still in development, describe the interface between LED luminaire and LED light engine (LLE). An overview of Book 1 to Book 18 gives Table 6 and some examples of socketable, circular LED modules according to Book 5 are shown in Figure 20.

Table 6:
Overview of the Book 1
to Book 18 published or
in development by the
Zhaga Consortium.

Book number	Description	Current status
Book 1	Overview and common information relating to the other Books	Approved
Book 2	Socketable drum-shaped LLE with integrated electronic control gear (ECG), maximum 70 mm diameter, mainly used in downlight applications	Approved
Book 3	Circular LED modules with 50 mm diameter and separate ECG, mainly used in spot lighting	Approved
Book 4	Rectangular LED modules with separate ECG, for high-intensity outdoor and industrial applications	Approved
Book 5	Socketable, circular LED module with 70 mm diameter separate ECG	Approved
Book 6	Compact, socketable, circular LLE with integrated ECG	Approved
Book 7	Rectangular LED modules with separate ECG, for indoor lighting applications	Approved
Book 8	Socketable drum-shaped LLE with integrated ECG, maximum 95 mm diameter, for downlight applications	Approved
Book 9	Ring-shaped LED modules with a 12 mm or 25 mm light-emitting surface (LES) with separate ECG	Approved
Book 10	Circular LED modules with 75 mm diameter and separate ECG, mainly used in spot lighting	Approved
Book 11	Circular LED modules with 35 mm diameter and separate ECG, mainly used in spot lighting	In development
Book 12	Rectangular and square LED chip-on-board modules with a circular LES with separate ECG	Approved
Book 13	LED drivers	Approved
Book 14	Socketable linear LLEs with integrated driver	In development
Book 15	Modules to fit with lens arrays	In development
Book 16	Planar circular LLEs with integrated driver	In development
Book 17	Spotlight LLEs with integrated driver	In development
Book 18	Connectivity socket	In development



Figure 20:
Example of socketable, circular LED modules designed according to Zhaga Book 5.
Source: GE Lighting Infusion LED module product family

Each book defines at least the following set of interfaces between the LED light engine and LED luminaire: mechanical, photometric, electrical, thermal, and control interface.

For characterizing the photometric interface, different measurements have to be performed which include a goniophotometric analysis and a two dimensional imaging analysis of luminance for some books. In general, the measurement of luminous flux, luminous intensity distribution, correlated color temperature and color rendering index is required. The values of CCT and CRI are communicated using a three-digit code according to IEC/TR 62732:2012 [17]. A goniophotometric measurement is required to ensure that the luminous intensity distribution is as close as possible to a Lambertian intensity distribution. For that purpose thresholds of partial luminous flux in 4 so-called CIE flux zones have to be maintained (see Table 7).

		Relative Partial Luminous Flux		
CIE flux zone	y-angle (all C-planes)	Lambertian light source (reference)	Min. value of spot light LLE	Max. value of spot light LLE
FC1	0° - 41.4°	43 %	39 %	56 %
FC2 – FC1	41.4° - 60°	32 %	31 %	37 %
FC3 – FC2	60° - 75.5°	18 %	11 %	22 %
FC4 – FC3	75.5° - 90°	7 %	0 %	7 %

Table 7:
Relative partial luminous flux tolerances from Zhaga Book 3. Ideal values of a Lambertian light source are given for reference.

For the evaluation of luminance properties, a circular light-emitting surface is for example divided into five segments as shown in Figure 21. With the measurement of the average luminance of the five segments, parameters such as luminance rotational symmetry, luminance center balance and luminance uniformity can be calculated. For these parameters, Zhaga states limits and criteria that may vary from Book to Book.

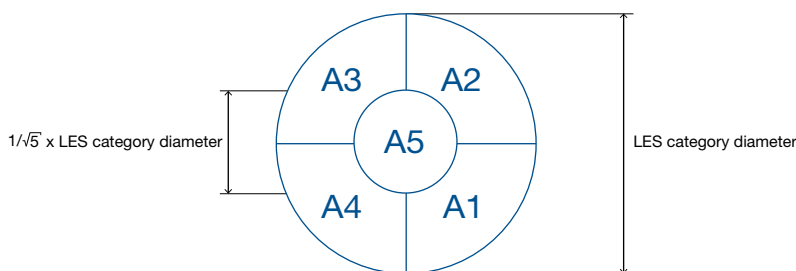


Figure 21:
Luminance property evaluation areas according to Zhaga Book 3.

3.8 Laboratory Accreditation and Traceability

Standards apply not only to LEDs, modules, lamps and luminaires; they can also apply to the laboratories measuring them. Probably the most basic and best known of common standards is the ISO 9000 series [18] for quality management systems. This is a general quality management standard that applies to all industries, not just laboratories, and does not directly address the correctness of measurements or appropriateness of methods.

ANSI/NCSL Z540 is an old but continuing American standard [19] that deals specifically with laboratories calibrating measurement and test equipment. For most laboratories making optical measurements of LEDs, ISO/IEC 17025 [20] is the current international standard to be met⁹. The ISO/IEC 17025 standard not only ensures a rigorous quality management system, but also addresses the competence of laboratories to make specific measurements or calibrations.

Accreditation to a particular standard guarantees that the laboratory conforms to the standard in every respect. Accreditation differs from certification in that it involves a third party, the accrediting body, attesting to technical competence within a laboratory in addition to its adherence and operation under a documented quality system. The accrediting body is itself regulated by the International Laboratory Accreditation Cooperation (ILAC) so that adherence is equivalent worldwide.

A laboratory that is accredited to ISO/IEC 17025 must therefore not only have the correct quality management systems in place to ensure competence in the calibration or measurement quantity, it must also continue to demonstrate this competence to the accrediting body in an ongoing series of in-depth audits. These are essential to provide demonstrative proof of competence by the laboratory, as well as international confidence in the measurement and calibration procedures and results.

Traceability is defined as “A property of a measurement result whereby the result can be related to a reference through a documented unbroken chain of calibrations, each contributing to the measurement uncertainty”.

In most laboratories, the calibration of instruments or sources requires physical artefacts (lamps, detectors, resistors, meters, etc.) and these in turn must be calibrated. Their calibration must be traceable to a National Metrology Institute (NMI)¹⁰ reference by an unbroken chain of calibrations complete with uncertainties for each measurement stage. A lack of documentation or uncertainty budget for any part of the chain means the chain is broken and the artifact is no longer traceable.

⁹ That standard was also duplicated to national standards like DIN EN 17025.

¹⁰ Examples of NMIs can be found in many countries and include NIST (National Institute of Standards and Technology, USA), NPL (National Physical Laboratory, UK), PTB (Physikalisch-Technische Bundesanstalt, Germany), NMIJ (National Metrology Institute of Japan, Japan), KRISS (Korea Institute of Standards and Science, South Korea), NIM (National Institute of Metrology, China), etc.

When making a measurement or calibration, the laboratory should use the unbroken traceability chain of all calibrated artifacts to derive the traceability and uncertainty of their result value.

Traceability is an essential part of calibration and measurements to ensure correct results. The longer the traceability chain, i.e. the more measurements and stages between an artefact used in calibration or measurement and the original calibration by the NMI, the greater the uncertainty in the result. It is important therefore to keep the traceability chain as short as possible.

4 Basic Properties of LEDs

This section describes the basic physical properties of LEDs. Some of these properties have a significant influence on optical measurements.

4.1 Package Design

Radiation from LEDs is generated by a semiconductor chip that has been mounted in a package or sometimes directly on a circuit board. The chip itself will most often have almost Lambertian emission properties (modified by internal reflections and refractions so it is never perfectly Lambertian). Lenses, mirrors, diffusers and phosphors can be built into the package to achieve specific spectral and spatial radiation characteristics. LEDs can now be obtained in a wide range of designs and types each with its own spatial radiation characteristics (see for example Figure 22). In the following, the most important LED package types are explained.

Dual/Direct In-line Package (DIP) LEDs

Direct In-line Packages (DIP) are inserted into a pre-drilled printed circuit board (PCB). This process is known as “through-hole” mounting. The legs are then soldered onto the opposite side of the PCB. DIP modules are typically used for outdoor applications. Having separate encapsulated diodes, heat dispersion and weather resistance are better compared to, for example, SMD modules.

Surface Mount Device (SMD) LEDs

In contrast to through-hole technology, SMD LEDs can be mounted directly onto a PCB. This technology is very popular because it is a cost-effective and versatile solution that makes for compact and light-weight designs. SMD LEDs can have a wide viewing angle, due to the fact that it does not have the DIP LED's epoxy enclosure that focuses the beam¹¹. A great variety of this type of LED is on the market, including one-chip LEDs and multi-chip LEDs. SMD LEDs are most often used in the low- or mid-power regime and are the perfect choice, for example, for LED strips.

¹¹ Variants of SMD LEDs feature a focussing lens to address applications where a small emission angle is necessary.



Figure 22:
Illustration of different package designs for LEDs. From left to right: Traditional Dual In-line Package (DIP), Surface Mount Device (SMD) LED, Chip on Board (COB) LED module.

Chip On Board (COB) LED modules

Similar to SMD, COB LED modules have multiple diodes on the same chip. SMD requires a circuit for every diode on the chip. COB devices have only 1 circuit and 2 contacts for the entire chip, regardless of the number of diodes. This single circuit design leads to simplicity and improved lumen-per-watt ratios in comparison to other LED packaging technologies. COB technology is very efficient and powerful for single-color applications like spot and floodlights. Moreover, it is very popular with flash applications in smartphones or cameras, because this technology produces a large amount of lumens while consuming little energy.

High Power (HP) LEDs

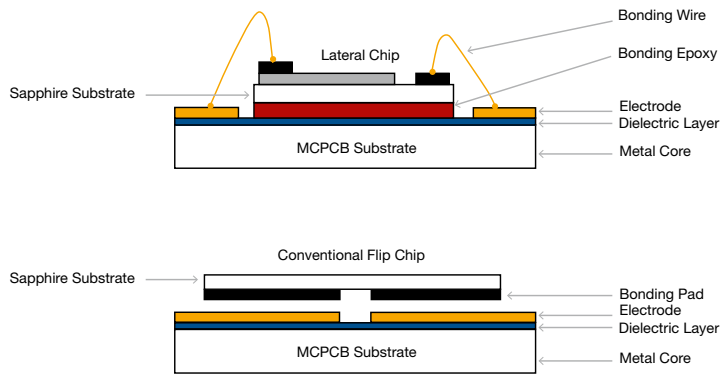
The definition of a HP LED is that it requires a heat sink or other means of thermal management for normal operation. As HP LEDs are designed to be heat sunk during their normal operation, a LED packaging to establish an efficient heat conduction path from the LED's active area (the pn-junction) towards the ambient is required. HP LED packages are provided with an exposed cooling surface (often referred to as case). Most of the heat generated at the junction leaves the package through this surface. Very often, HP LED packages use a SMD or COB technique. To achieve proper thermal conditions for testing HP LEDs, their exposed cooling surface should be attached to a temperature controlled thermal platform.

Flip-Chip Technology and Chip Scale Package (CSP)

Shrinking the size of a LED package is a trend in LED technology. In Flip-Chip LEDs the diode is mounted upside down, compared to traditional LEDs. Flip-Chip LEDs have no bonding wire to the electrodes of the dielectric layer, as do conventional lateral chips (see Figure 23). This provides for higher reliability and shortens the production process because a whole production step is omitted. It also significantly reduces thermal resistance, resulting in higher heat dissipation rates. In addition, there is no shadowing of light, due to the absence of a lead frame.

Chip Scale Packages are equal or slightly larger than a die. With this, higher packaging density is achieved, due to the reduced footprint.

Figure 23:
Comparison of a conventional lateral chip design with bonding wires and Flip-Chip Technology.



4.2 Electrical Properties and Ambient Conditions

Light is emitted from LEDs when a forward voltage causes electrons to combine with holes. The efficiency of this process, and hence the intensity emitted, is temperature-dependent.

LEDs are normally operated at a constant current¹². The emitted light is a function of the forward current I_F , and the forward voltage V_F . Experiments show that the voltage is not instantly stable after applying the forward current. V_F stabilizes as the temperature T_j of the diode junction reaches equilibrium. The temperature increases due to the electrical power consumed by the LED chip and then stabilizes at some junction temperature value $T_j > T_{\text{Ambient}}$ after a period of time when the heat generated is balanced by the heat lost. Unlike incandescent lamps, heat loss by radiation is not significant. Heat is lost by conduction through electrical or thermal connections, usually to a heat sink or active thermal cooling system. Because the forward voltage at a fixed current depends on the junction temperature, the emitted light is not stable until a constant forward voltage is attained.

Figure 24 shows the stabilization over time of a white LED. Luminous intensity and forward voltage are obtained when a current begins to flow through the LED, lasting until a constant forward voltage and luminous intensity value is achieved.

¹² AC LEDs which can operate directly from an AC power supply or AC mains is an interesting field of investigation. The concept provides several advantages as power is transmitted and used much more efficiently, and AC/DC conversion electronics are rendered obsolete.

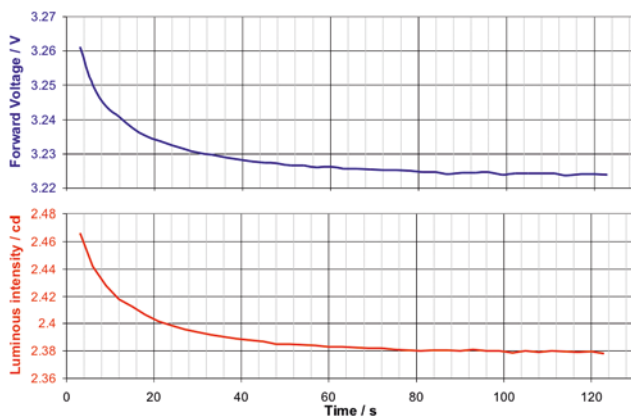


Figure 24:
Stabilization period of a white LED. Time [s] is entered on the x-axis and luminous intensity [cd] and corresponding forward voltage [V] on the y-axes.

The stabilization procedure can last several seconds or up to a minute. When thermal equilibrium has been reached in the chip, the value T_j results from a balance of input power and heat exchange with the ambient surroundings. The heat sinks used with High Power LEDs often have considerable thermal mass and larger size, so they may take much longer to reach equilibrium.

Since the heat from the junction must be somehow dissipated into the ambient air, changing the ambient temperature affects the junction temperature and hence the emitted light¹³. A typical temperature coefficient for the forward voltage with a constant current is approximately -1.5 to -5 mV/K [21], depending on the LED type (GaN, AlGaN etc.) and color. At a given current, therefore, the measured forward voltage is lower at higher temperatures.

If the LED junction temperature rises, the entire spectral power distribution is shifted in the direction of the longer wavelengths¹⁴. The shift in peak wavelength is typically about 0.1 to 0.3 nm/K. This effect has only a negligible influence on the photometric values of green, yellow or amber LEDs because their peak wavelength is at the flatter portions of the $V(\lambda)$ curve. However, the peak wavelength for red and blue LEDs are on the much steeper slopes of the $V(\lambda)$ curve, and this can lead to significant changes in the photometric values. In case of a phosphor-converted white LED, a shift in peak wavelength of the blue pump LED leads to a change in excitation of the phosphor. This results in a considerable change in color coordinates and CCT of the white LED. Therefore, current and temperature stabilization is important for attaining constant spectral properties.

If the forward current is not constant, i.e. modulated, the temperature may fluctuate. The average radiant power then no longer corresponds to the radiant power under constant current conditions. Similar problems apply to pulsed

¹³ An exception to this is when active cooling is used to maintain the heat sink temperature even when the ambient temperature changes.

¹⁴ Except for blue LEDs.

LEDs, where a high current is switched on and off periodically. Differences in the value for luminous intensity may arise between multiplex operation and constant-current operation despite comparable power consumption.

4.3 Thermal Properties of High Power LEDs

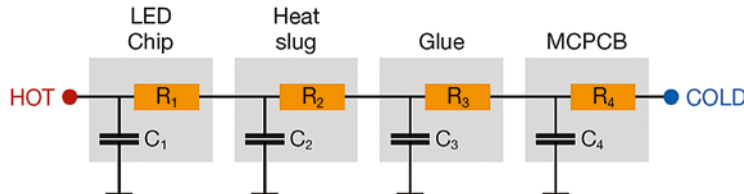
High Power LEDs require a thermal management. There are complex thermal processes inside the LED and at the connection to the ambient atmosphere that need to be modelled. In many cases, active thermoelectric cooling is required to perform accurate testing of HP LEDs. The following sub-chapters address the basic ideas behind these concepts.

4.3.1 Thermal Modeling

Thermally, the LED can be thought of as several parts that are joined: the chip generates heat as well as light, and that heat must flow through the chip material before it can reach the heat slug. The heat then flows via a thermal interface material (e.g. thermal grease, epoxy, solder etc.) to the Metal Core PCB. Heat flow continues on through further layers of thermal interface material and heat sinks until it reaches the atmosphere or active temperature control layer.

Each of these stages has two main thermal properties – thermal resistance (that slows down the heat flow) expressed in K/W and thermal capacitance (that absorbs heat energy) expressed in J/K.

Figure 25:
Thermal model of a simple LED package.
“Hot” is the p-n junction of the LED and “cold” is the thermal connection to the outside world.



Under steady-state conditions the thermal capacitance is not significant and only the thermal resistances need to be considered. Figure 25 looks like an electrical series circuit diagram and like the electrical quantity the total thermal resistance is the sum of all the individual thermal resistances, i.e.

$$R_{\text{package}} = R_1 + R_2 + R_3 + R_4$$

With this, the temperature difference from the junction to the cold contact can be calculated if the input power is known. This is a simple model often advocated by LED manufacturers advising on practical thermal design and is a useful first approximation. In practice, thermal resistance may not be a constant and can depend on power to the chip [22] just as electrical resistance can vary with the current passing through.

When operating a LED immediately after switch-on or in pulsed mode, it is not in an equilibrium condition. How the temperature changes with time and its relationship to measurement timing is important if optical measurements in the non-equilibrium condition are to be correlated with equilibrium measurements. In this non-equilibrium condition the dynamic thermal impedance of the device is important, and this includes the thermal capacitance of each stage as shown in Figure 25.

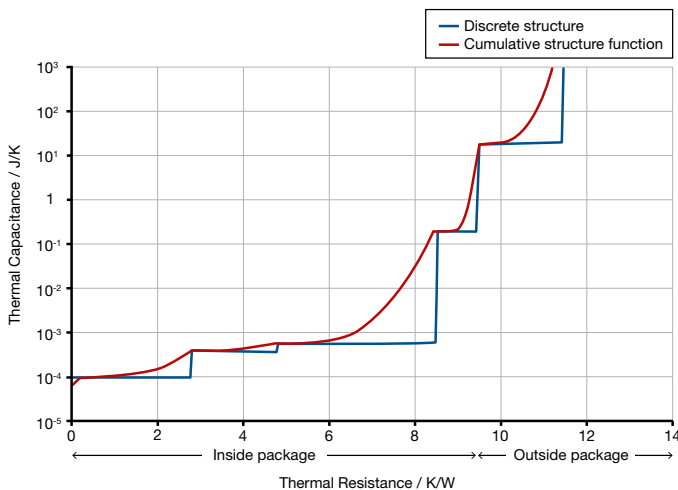
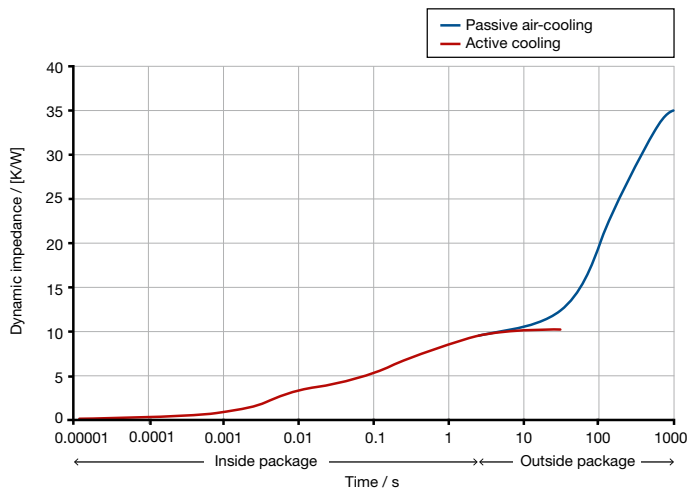


Figure 26:
Simulated cumulative structure function (thermal capacitance versus thermal resistance) and the discrete structure for the package in Figure 25.

Figure 26 shows an example of the cumulative structure function (thermal capacitance vs thermal resistance) that can result from such a package structure. This can be readily calculated from the inherent material properties and dimensions within the structure. The dynamic impedance shown in Figure 27 graphically illustrates that the LED chip will see different thermal resistance to the outside world, depending on time. This can be calculated using computer models [23] or measured using transient analysis [24]. At short times the heat flows within the package and all external heat sinks are irrelevant. It should be noted however that some periods of relative stability are seen and measurements during these periods are more reproducible. At longer times the heat now flows to external components. Those external components that absorb this heat most readily, such as active cooling systems, will stabilize quickest and with least added thermal resistance. As shown in Figure 27, an active cooling system (red line) stabilizes in around 10 seconds in this example,

whereas the convection cooled system is still not stable in 1,000 seconds. Moreover, the actively cooled system will stabilize the LED junction at a temperature 25 K lower than the convection-cooled system in this example.

Figure 27:
Simulated dynamic impedance for the package in Figure 25. The red curve describes an active cooling and the blue curve a passive air-cooling system. Outside the package, the active cooled system stabilizes much faster.

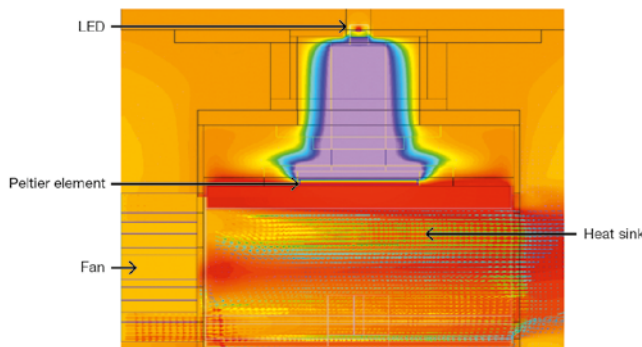


4.3.2 Active Cooling

Active cooling can employ water cooling or Peltier (thermoelectric) cooling elements. Peltier cooling is easier and more widely used. Without large volumes of water to heat and cool, it is also quicker to come to equilibrium at a desired temperature.

As current flows through a Peltier element, one side gets hot while the other becomes cold. The temperature difference depends on the current supplied. The cold side is connected to the LED and the hot side to a heat sink and fan to dissipate heat to the air (see also the thermal map in Figure 28). By controlling the current to the Peltier element, the temperature of the cold side can be regulated to maintain a desired temperature.

Figure 28:
Thermal map of a High Power LED connected to an active cooling system.



The temperature difference across the Peltier elements depends on the current supplied and the heat load (watts) it is required to dissipate. As the heat load increases the temperature difference decreases so the current must be increased to compensate. It is important to not exceed the maximum heat load of the Peltier cooler if temperatures are to be tuned over the full temperature range, but higher loads can be tolerated if lower temperatures are not required.

The temperatures of the LED junction may be controlled by using the forward voltage of the LED to adjust the current to the Peltier element. A constant forward voltage is the best indicator of constant temperature. Not all LEDs and modules have the forward voltage available, and for these the best control is to regulate the temperature of the LED or module thermal contact. Unlike the forward voltage, the latter method provides actual temperatures in addition to regulation, which may be an advantage in comparing devices.

Unlike convection or forced cooling using a simple heat sink, active cooling can be used at any desired temperature, even those below ambient. In such a case, care must be taken to handle condensation or even the build-up of ice, which has a negative effect on the electrical connections and hence the measurement results.

4.3.3 Testing Methods for HP LEDs

High Power LEDs present unique problems concerning measurement and test methods. The results of bare component tests can no longer be directly equated with final application tests, as the latter must include heat sinking whereas the former may not. To avoid overheating, component tests are usually performed with short current pulses (typical of production environments) or with heat sinks that simulate the anticipated final thermal environment. Alternatively, a test can be done at any temperature (i.e. with any heat sink) and the results corrected to the anticipated application temperature if the temperature coefficient is known.

When several High Power LEDs are used together, for instance in a module or luminaire, the forward voltage may no longer be available (unless wired in a simple series circuit). In the case of a module, most manufacturers specify a thermal test point at which the temperature can be measured. For luminaires, it is usual to measure the air temperature close to the luminaire, as these normally include all thermal dissipation mechanisms to ambient. Some sources, e.g. recessed down-lights, may also require special fixtures to simulate final installation environments.

Different approaches to testing HP LEDs are currently under discussion¹⁵. There are two alternative methods of testing in equilibrium conditions at known temperature. A suitable laboratory setup consisting of a test adapter with a thermoelectric cooler (TEC) attached to a medium sized integrating sphere can be seen in Figure 29.

Figure 29:
Laboratory test setup for High Power LEDs. A TEC test adapter providing active temperature control is mounted at the side port of a medium sized integrating sphere.



One method for tests in a laboratory setup is to stabilize the LED in the off state at the required temperature and then apply the drive current while monitoring the forward voltage. Fast data recording allows accurate extrapolation of data to obtain the forward voltage at time = 0. The LED is then operated at the drive current and while the temperature is controlled to achieve the same forward voltage, ensuring the desired temperature is again obtained, but this time under equilibrium conditions. Optical measurements are then made.

A second method in a laboratory setup is to stabilize the LED in the off state at the required temperature and then apply a small current, small enough that heating is not significant, and measure the forward voltage. Subsequently, during testing at a higher current, the current is reduced for a very short time to this small current in order that the forward voltage can again be read. The LED temperature is regulated to maintain this small current forward voltage at the desired temperature.

Methods for testing in production environments where equilibrium conditions cannot be obtained are different to the two methods discussed above. Current is applied in a very short pulse or series of pulses, and all measurements (optical and electrical) are made during this time. The characteristics of the device are determined separately, so that the pulse test data can be correlated to standard conditions, e.g. those specified in CIE 127:2007.

¹⁵ CIE Technical Committees: CIE TC2-63 "Optical Measurement of High Power LEDs" and CIE TC2-64 "High speed testing methods for LEDs".

In many practical uses of HP LEDs the thermal contact temperature (T_c) is regulated, because it is accessible more easily than the LED junction temperature (T_j). Compensation to T_j – if required – is achieved using the manufacturer's values for thermal resistance of the device under test.

4.4 Characteristics of White LEDs

Many designs are in common use in the construction of white LEDs. These differ in their spectra and properties.

4.4.1 Phosphor-Converted White LEDs

Phosphors absorb light of short wavelength and emit light of longer wavelengths. Most commonly the phosphor has a broad emission spectrum with a yellow color. When placed over a blue LED some of the blue light is converted to yellow by the phosphor (phosphorescence) and the resulting spectrum is perceived as white by the human eye (see Figure 30). The wavelength of the blue peak, the type and thickness of phosphor are all variables that can lead to different chromaticities. The phosphor is often applied directly to the LED chip by various coating techniques. Some manufacturers are embedding the phosphor in a sheet material, such as ceramics or silicone, which is then attached to the chip to allow for an easier handling and even a spectral matching of the individual phosphor plate and the blue chips. In the increasingly popular remote phosphor designs, the phosphor is applied to a separate substrate and illuminated from some distance by one or several blue chips.

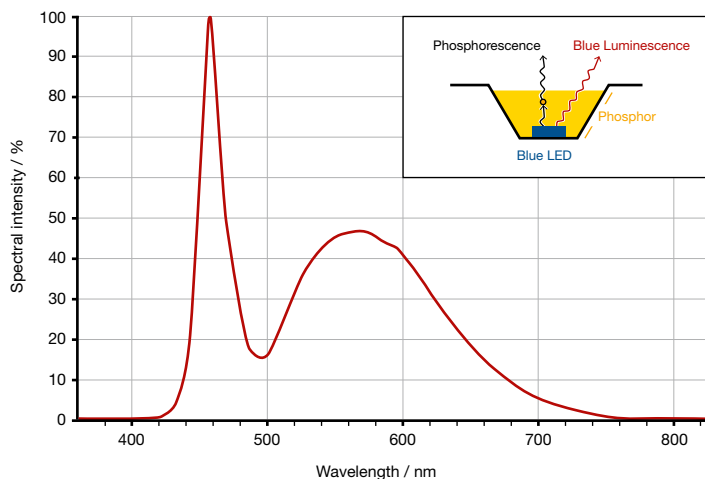


Figure 30:
Spectrum of a typical phosphor-converted white LED. The blue luminescence peak at 460 nm and the broad phosphorescence peak from approximately 500 to 650 nm are clearly visible. The resulting spectrum is perceived as white by the human eye.

Because the blue LED light must pass through the phosphor, which may not be of even thickness or cover the entire chip, color variations with angle are common in this design. In particular, at some angles the color may be very blue rather than the desired white color.

The shorter wavelength photons absorbed have more energy than the longer wavelength photons emitted. This is seen from the formula $E = hc/\lambda$ where h is Planck's constant, c is the speed of light, λ is the wavelength and E is the energy per photon.

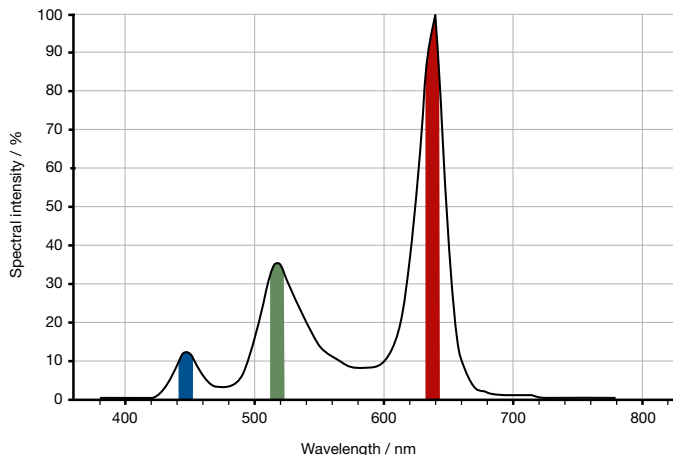
The energy difference between the absorbed and emitted photons is converted to heat leading to an inherently lower efficiency of phosphor conversion white LEDs compared to the blue chips.

4.4.2 3-Chip and 4-Chip White LEDs

Red, green and blue LEDs when mixed in the right proportions will create a white perception. The exact details of the spectral distributions and their mixing vary from design to design (see for example Figure 31). Some LEDs even include altering the mix so the color and rendering of the LED can be tuned for specific applications.

For critical color rendering applications some LEDs use 4 chips: blue, green, yellow and red to produce the desired white.

Figure 31:
Example of a 3 chip RGB LED spectrum.



As the chips are physically separated, any imaging optics will tend to direct the light of each chip at a different angle. This means that in applications such as displays the colors can vary markedly with the observation angle. For general lighting applications, care is usually taken to combine the light from each chip using non-imaging optics to prevent uneven illumination and color separation.

4.4.3 Color Rendering and Efficacy of White LEDs

The main driving force for Solid-State Lighting lies in the potential of huge energy savings on the national or global scale. Thus, when considering spectra of light sources for general illumination it is important to consider luminous efficacy (lumens per watt). The term luminous efficacy is normally used for the conversion from the input electrical power (watts) to the output luminous flux (lumens). The luminous efficacy of a source comprises two factors: the conversion efficiency from electrical power to optical power (called radiant efficiency or external quantum efficiency) and the conversion factor from optical power (watts) to luminous flux (lumens). The latter is called luminous efficacy of radiation (LER). Since LER and color rendering are determined solely by the spectrum of the source, white LED spectra should be optimized for both of these aspects.

The difficulty is that color rendering and LER are generally in a trade-off. Based on the CRI, color rendering is best achieved by broadband spectra distributed evenly throughout the visible region, while luminous efficacy is highest with monochromatic radiation at 555 nm. This trade-off is evident in many existing lamps. By studying the CRI, some people are led to believe that white LED spectra should mimic the spectrum of the sun or a blackbody. While such spectra would give high CRI values, they would suffer significantly from low LER. The challenge in creating LEDs for use as illumination sources is to provide the highest possible energy efficiency while achieving best color rendering possible.

In considering radiant efficiency, blue and UV LEDs are normally efficient but then lose efficiency owing to the phosphor conversion process. Red single color LEDs are also efficient but green and yellow LEDs are much less so.

In considering CRI, the broadband emission of the phosphor generally helps to increase values, whereas the single color LED components of a 3- or 4-chip LED can render some of the tiles well, while rendering others poorly. In fact, the single colors often drive some of the tiles towards saturation; a phenomenon that is often esthetically pleasing but penalized by CRI (which only looks at the color change, irrespective of whether the change is perceived as "good" or "bad").

By changing the formulation of LED/phosphor or multi-chip LED, a large number of possible spectra and efficacies are possible. Broadening the spectrum to enhance color rendering can also be achieved by developing multi-phosphor LEDs or using hybrid technologies (e.g. add an additional red LED to a phosphor converted white LED). These approaches get more and more popular in modern LED development.

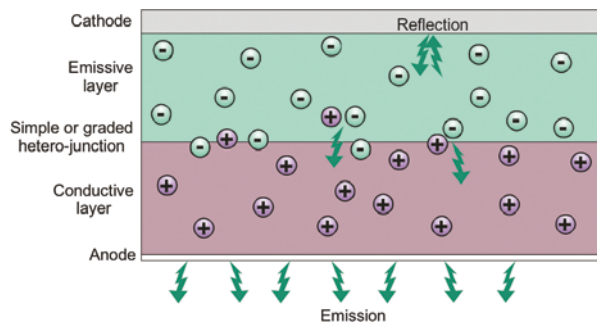
Simulations [25] indicate a LER of around 400 lm/W is possible with a CRI of 80. Low CCT sources will generally have lower LER however, since lower temperature blackbodies (the reference) have more red and the $V(\lambda)$ function

is low in red. Adding more red to the LED source therefore improves the CRI but lowers the LER.

4.5 Basic Properties of OLEDs

Organic Light Emitting Diodes (OLEDs) show much potential in SSL applications. Luminance tends to be low but the devices are large. In applications where large diffuse illumination is desired, these devices are inherently suited as they require no other optics to distribute the light.

Figure 32:
Basic structure of an OLED. Graded hetero-junction devices are gaining in popularity owing to their inherently higher efficiency.



Several types of organic layers can be included in a single OLED device, allowing a range of emission colors. This often means white or near-white sources can be made without the need for further combinations or conversions. Figure 32 shows the basic structure of an OLED with emissive and conductive layer separated by simple or graded hetero-junction¹⁶. In contrast to the generally quasi-monochromatic emission of inorganic LEDs, the spectra of OLEDs are generally broadband although they may show structure. Figure 33 shows example spectra of different sources used in general lighting.

The layered structure of the OLED can give rise to interference effects that change the spectral characteristics with angle, but most modern devices feature a diffuser exit layer to reduce this effect. As the area of the device can be very large, it is also common to employ a metallic busbar to increase conductivity to the junction by reducing the length of less conductive paths.

¹⁶ A graded hetero-junction alters the composition of hole and electron transport materials by a dopant emitter. This technique increases the quantum efficiency of OLEDs significantly compared to simple hetero-junction devices.

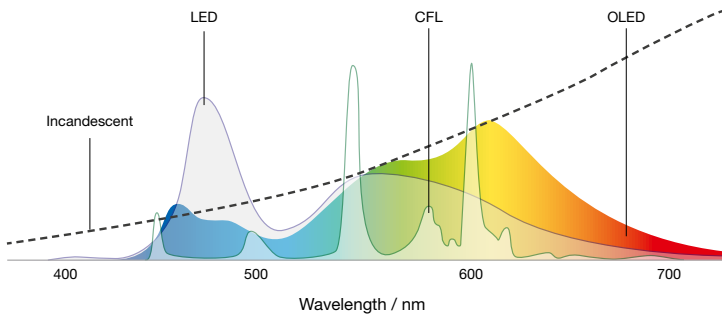


Figure 33:
Spectra of different sources used in general lighting. The OLED spectrum is generally broadband, showing some structure due to several types of organic layers.

The emitted luminous flux is roughly proportional to the forward current. The diode characteristics will determine how this then changes with forward voltage or power. This contrasts with the inorganic LED, where flux is often non-linear with current. The difference may lie with the lower self-heating temperature changes as the current is spread over a much larger area.

As the emitted flux is much more sensitive to forward voltage than to current, testing should employ current regulated supplies and be operated at the manufacturer's rated current.

Even though self-heating is low, OLEDs are still sensitive to the ambient temperature; changing both flux and chromaticity. The direction of chromaticity changes with increasing temperature varies with the materials used. Low self-heating does not imply insignificance, and an orientation dependence of the flux is often observed as a panel "stabilizes" in different orientations. Also luminance, chromaticity and temperature variations are seen across the panel that can change with panel orientation.

OLED panels can take a long time to fully stabilize after switch-on, depending on their size and construction. However, most are stable to within 0.5 % of their final value after 10 minutes of operation. Any changes to the OLED orientation must be accompanied by a new stabilization period because luminous flux and luminance uniformity changes following a new orientation are slow.

5 Optical Measuring Instruments

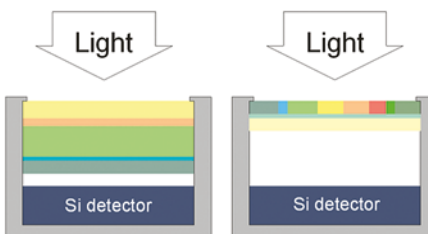
This section describes the most important properties and concepts of optical measuring instruments relevant to the precise measurement of optical LED parameters. There are two measuring procedures for determining the photometric and colorimetric values of light radiation. One is the integration method based on a photometer or imaging colorimeter. The quality of a measurement with this technique depends on the spectral matching of physical filters to the response of the human eye. The other one is the spectral resolution method based on a spectroradiometer. The spectral power distribution is used together with the definition of human perception ($V(\lambda)$) curve and color matching functions) to calculate photometric and colorimetric values.

5.1 Photometer Design

One of the functionally simplest devices to measure light is a photometer. This is a detector, usually a silicon photodiode, with a filter designed such that the combined system response mimics the perception of the human eye. Such detectors are used to measure luminance (e.g. the emission from a computer monitor or TV), illuminance (e.g. the light illuminating a sheet of paper), luminous intensity (e.g. light seen from small or distant light sources) or luminous flux (the total light emitted by a source).

Several types of photometers exist (see figure 34) and their quality depends, among other things, on how well they match the human eye response.

Figure 34:
A simple photometer with a filter stack (left) and with a mosaic filter (right). Practical mosaic detectors may include some stack elements as well as mosaic elements.



The filter stack (also called full filtering) method allows the light to pass through each layer over the full lateral extension of the photometer. A good filter stack will have up to 5 or more individual filter components. Since the light must pass through each layer in turn, the overall transmittance of the stack is the product of each of the individual layers' transmittance. This co-dependence means this type of filter requires very careful attention to detail, but when done properly can yield extremely good and stable devices.

The mosaic filter (also called partial filtering) places filter components side-by-side and hence only part of the light passes through each filter. The transmittance through the filter is additive, depending only on the area and transmittance of each “element”. This allows the properties to be manipulated more easily and hence it can produce very accurate spectral matches. However, the transmittance of the device depends critically on how the light enters it: the side-by-side arrangement makes it very sensitive to the spatial uniformity of light across the filter and the transmittance also changes with angle for each element individually [26]. A mosaic photometer is generally used with some form of diffuser to “mix” the incoming light, both spatially and angularly, in an attempt to improve this undesired performance aspect.

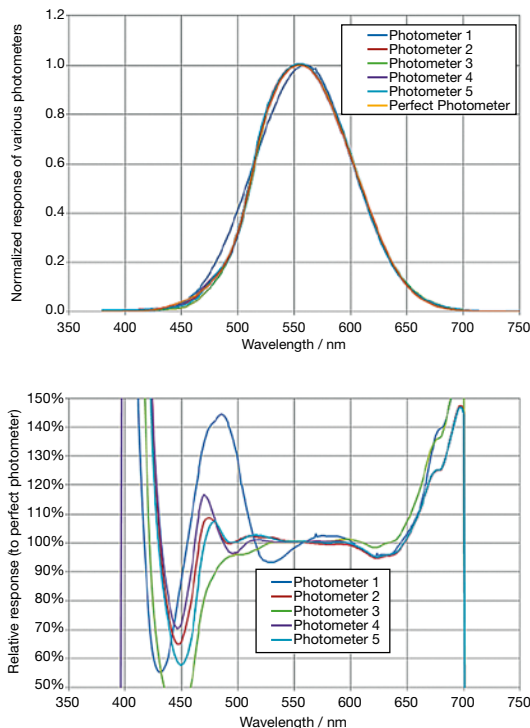


Figure 35:
Five real photometers and the perfect photometer responses with wavelength (top). The ratio of each photometer response to the perfect response (bottom).
Source: Swiss Federal Institute for Metrology (METAS). Data courtesy of P. Blattner

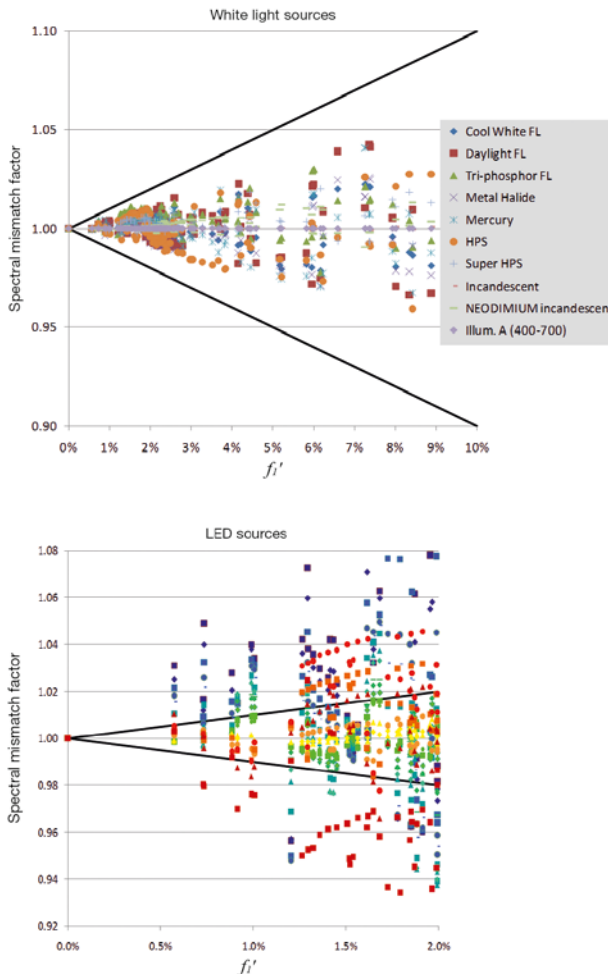
Diffusers inevitably throw away light, decreasing the sensitivity and increasing the measurement time. The filter stack type, which does not inherently require diffusers, should be used if possible for measurements of weak sources or where rapid results are desired. Goniometry is often one of those examples where speed is important, since thousands of angles may be sampled and each one should be done as fast as possible.

When we consider the accuracy of spectral matching to human response, small differences in photometers can have a big impact. However, it also depends on what you are measuring. In Figure 35 several examples of real

photometers are presented. Photometer 1 is obviously the worst match. Yet from Figure 35 (bottom), it shows the smallest errors at 450 nm. Often the “goodness of fit” parameter, f'_i , is used for selection of the best devices [1]. The index f'_i describes how well the relative spectral responsivity of the photometer matches the $V(\lambda)$ function. For white, broadband light sources this is reasonable, and although it is not an indicator of error it does show some correlation, as can be seen in Figure 36 (top) [27].

For single color LEDs, however, there is no correlation, and Figure 36 (bottom) shows that f'_i cannot indicate the quality of the photometer in such measurements. Instead, a simple spectral mismatch correction (the factor shown in Figure 36) can be applied to reduce the errors to a minimum, and this depends more on the measured response than the quality of the photometer. As this can be calculated if the LED is known, it is often the simplest, easiest and best way to achieve the highest accuracy measurements [1].

Figure 36:
Measured spectral mismatch factor versus f'_i for white light sources. The black < shape shows an “error” equal to the f'_i value (top). The same but for single color LED sources, concentrating only on the “best” photometers (bottom). The LED sources range from 465 nm (deep blue data points) to 643 nm (deep red data points).
Source: Swiss Federal Institute for Metrology (METAS). Data courtesy of P. Blattner



It has long been realized that f_i' is not a good selection criterion for photometers used for LED sources and the debate on what might replace it began over a decade ago [28]. That debate still continues without any firm recommendation. Meanwhile, it should be borne in mind that stability and design may be more important than f_i' in the selection of photometers for single color LEDs.

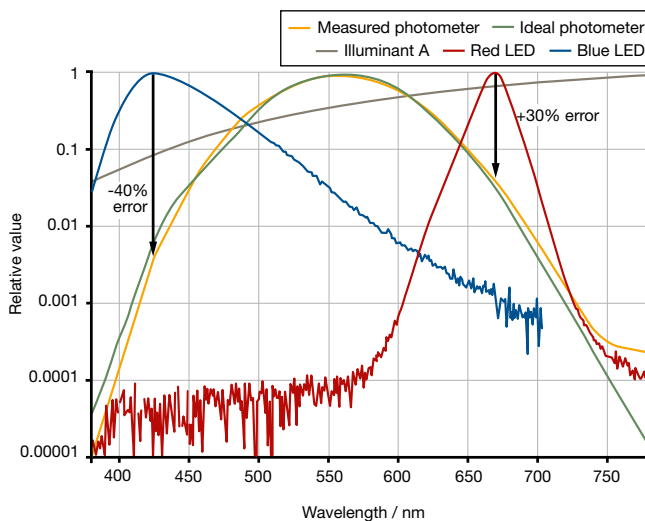
5.2 Comparison of Photometers and Spectroradiometers

Photometers use a broadband detector in conjunction with a $V(\lambda)$ filter to measure photometric values. The output current of this detector is directly proportional to the photometric measured value, i.e. a photometer for luminous intensity is calibrated in cd per unit of photocurrent.

A spectroradiometer measures the total spectral power distribution of the source. The photometric value is calculated (usually by the software) from this measured spectrum weighted by standard CIE tables. This basic difference between spectroradiometers and photometers is extremely important in LED metrology.

Photometers are well suited for carrying out measurements on incandescent white light sources, e.g. Illuminant A (Tungsten-halogen lamp with 2856 K color temperature). These sources have a maximum intensity to their radiation distribution in the infrared region, and the intensity decreases gradually over the visible range of the spectrum. At 400 nm, the value is only 8 % of the maximum. If the photometer's $V(\lambda)$ filter is optimized to this radiation distribution, the accuracy of the correction in the slopes of the $V(\lambda)$ curve is not so important because there is relatively little light in the blue range of the spectrum. A "blue" response deviation from ideal only results in a slight error of the measured photometric values. LEDs, however, have a completely different spectral power distribution, which tends to be approximately Gaussian with a specific peak wavelength and a FWHM of a couple of tens of nanometers. A poor correction of the filter, particularly at the slopes of the $V(\lambda)$ function in the blue and red regions (see Figure 37 green and yellow curves), results in large deviations in the measured value particularly for blue, red and white LEDs. Errors of several 100 % are not unusual for blue LEDs [29] and correct evaluation of the blue peak in white LEDs is critical for an accurate determination of the color coordinates (see also Section 8.2).

Figure 37:
Ideal $V(\lambda)$ photometer response (green) and measured response (yellow) of a real photometer, radiation from standard Illuminant A (grey), and a blue and red LED (blue and red respectively).



A precise spectroradiometer (see next section) avoids these errors because the photometric quantities are calculated from the spectral data with precisely defined CIE functions. Spectroradiometers should therefore be used for LED metrology.

High-accuracy photometers are useful for rapid measurements of white LED luminaires where only luminous intensity distribution and luminous flux are important. However, spectral measurements are almost as fast and essential where color shifts in the radiation pattern are present, or where color parameters or derived parameters, such as CRI, are needed.

5.3 Requirements for a Spectroradiometer

A spectrometer must meet certain basic requirements for carrying out radiometric measurements before it can be used as an accurate spectroradiometer. Accuracy depends on the interaction of all components, including both the optical systems (monochromator/spectrograph, optical probe) and electronics (detector, amplifier and analogue/digital converter). Simple, low-cost spectrometers generally fail to meet these high standards and can lead to significant errors and lack of correlation in measurements.

A spectroradiometer can be designed on the basis of two different principles. Scanning spectrometers use a monochromator¹⁷ with one or several gratings that rotate and a single detector. Array spectrometers have a

¹⁷ An optical device that allows selection of narrow band radiation from a wider range of wavelengths available at the input by mechanical means.

spectrograph¹⁸ with a fixed grating and a detector comprised of many single diodes or CCD elements. The array setup has the advantage of capturing the entire spectrum simultaneously.

5.3.1 Scanning Spectroradiometer

A scanning spectroradiometer (see Figure 38) will generally offer the highest accuracy, but at the expense of longer measuring times (i.e. several to tens of seconds). Switching the dynamic range electronically during the scanning procedure enables precise recording at the steep slopes of very narrow-band LEDs. Using a single detector permits use of an additional baffled slit on the detector side to minimize stray light. This produces an excellent optical dynamic range that may be up to five orders of magnitude when measuring LEDs. For some measurement applications (e.g. assessing the photobiological safety of lamps) even superposition of two single monochromators (see Figure 39) is recommended [30]. When realized properly (e.g. two grating arrangements sharing the same axis of rotation to ensure highest stability and elimination of problems associated with synchronizing the two monochromators), such a double monochromator features extremely good stray light suppression (10^{-9} when measuring LEDs).

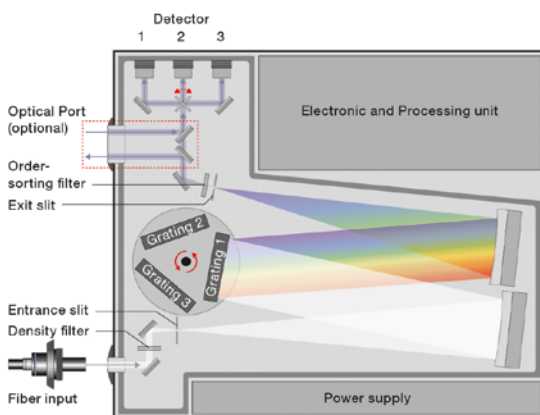


Figure 38:
Illustration of a scanning single monochromator. Light entering through the entrance slit is dispersed by a rotating grating assembly. After passing the exit slit the light is directed to different detectors that can be semiconductor detectors made of silicon, InGaAs, lead sulfide and lead selenide or photomultipliers.

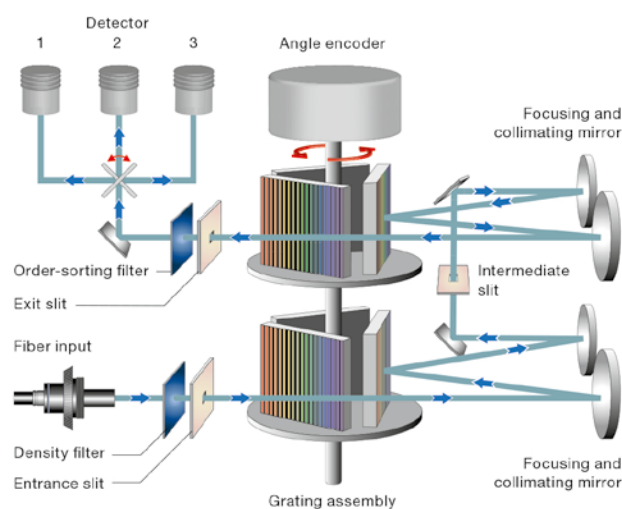
Another advantage of scanning spectroradiometers is the large spectral range combined with high spectral resolution and wavelength accuracy. This enables a wide range of applications, ranging from testing the night vision compatibility (NVIS) of displays and panel graphics¹⁹, to high resolution spectral measurements of plasma sources, transmission and reflection measurements.

¹⁸ An instrument that separates and records light into a frequency or wavelength spectrum.

¹⁹ According to MIL-L-85762A and MIL-STD-3009 standards.

A scanning spectroradiometer is the preferred choice as a reference instrument for R&D and calibration labs.

Figure 39:
Illustration of a double monochromator designed in subtractive configuration (the spectrometers residual dispersion at the exit slit is zero).



5.3.2 Array Spectroradiometer

An array spectrometer can carry out measurements much faster than a scanning spectroradiometer, because the entire wavelength range²⁰ is recorded simultaneously. The fastest measuring times are around a few milliseconds. An increase in sensitivity can be achieved by increasing the integration (measurement) time. An array spectroradiometer cannot exclude stray light as effectively, because it lacks an exit slit. The entrance slit is directly imaged to the detector array. The result is a loss of optical dynamic range of about one order of magnitude compared to a scanning spectrometer. The spectral resolutions of array spectrometers are in the region from 1 to 10 nm, depending on the number of pixels of the detector and the optical resolution of the spectrograph. The design and arrangement of imaging optics in the spectrograph is extremely important to guarantee optimum image quality on the flat detector. Improved imaging characteristics can generally be obtained with longer focal lengths and larger optics. The fast measuring speeds make this type of spectroradiometer ideal for measurements in production control. A crossed Czerny-Turner construction gives low stray light as well as good image quality (see Figure 40).

²⁰ A major disadvantage of array spectrometers is a smaller spectral measurement range compared to scanning spectrometers. In addition, the spectral range is fixed.

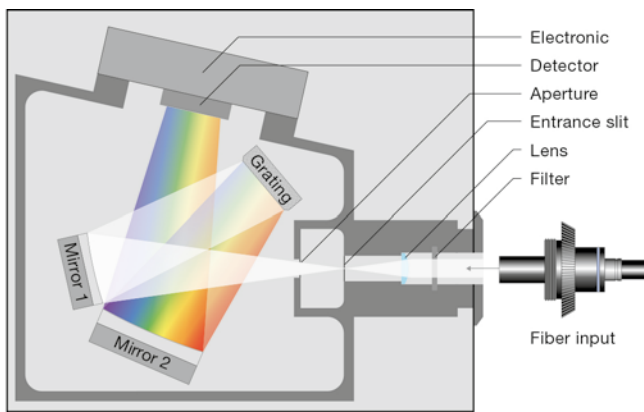


Figure 40:
Design of an array spectroradiometer in crossed Czerny-Turner construction.

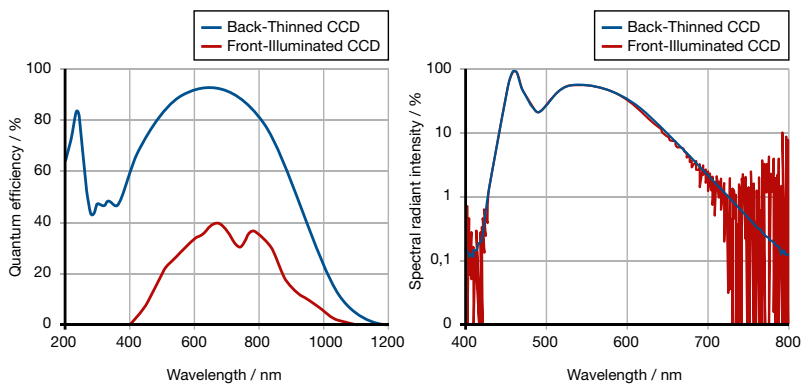
The most common type of detectors used in array spectroradiometers is a CCD. Several types of CCDs exist, as the need for high sensitivity and low noise lead to new design innovations.

CCD pixels can be arranged in a line (1D) or a grid (2D). 1D CCDs are quicker to read out, but have a fixed and relatively small vertical size, which limits their sensitivity. In 2D CCDs a full image can be read out or the columns can be read as one detector (vertical binning) to effectively give a 1D array, but of much higher vertical size and hence sensitivity.

A CCD array must ultimately be read out. In a line transfer CCD the image (charge) from each pixel is transferred vertically to a register, and that register is then read horizontally so each pixel is read in turn. As the CCD may still be exposed during this readout, it is important that the readouts are fast compared to normal exposures, in order to minimize smear. Frame transfer CCDs get around this by transferring the image pixel charges into a parallel set of image pixels that are not exposed to light prior to the readout. Unfortunately, these parallel “dark” pixels also take up space on the CCD, and often reduce the exposed area (and sensitivity) by 50 %.

CCDs traditionally placed the “circuitry” on top of the imaging elements, as this was easier to manufacture. Even though much of it was transparent, the circuits of these front-illuminated devices reflected some light and prevented it from reaching the imaging elements below. In back-illuminated CCDs the silicon wafer is flipped during manufacture, placing the wiring behind the imaging pixels, and the imaging layer is thinned to optimize detection. In this way a front-illuminated device of 60 % efficiency compares to a back-illuminated device of 90 % or more efficiency (see also Figure 41 left). Furthermore, back-thinned CCD sensors are far more sensitive to signals in the shortwave spectrum (higher blue and UV response). Limitations of front-illuminated line CCDs are obvious (see Figure 41 right) when measuring white LEDs.

Figure 41:
Spectral response function of a back-thinned CCD and a front-illuminated CCD (left). Spectrum of a white LED on a logarithmic scale (right). The better performance of a back-thinned CCD is clearly visible.



5.3.3 Selection Criteria

The range of applications for array and scanning spectroradiometers is large, and the selection of a suitable measuring instrument by the user should heavily depend on the desired application. The following Table 8 summarizes the most important selection criteria for both types of spectroradiometers, taking into account specifications of the monochromator or spectrograph, detector and electronics.

Table 8:
Summary of the most important selection criteria for array and scanning spectroradiometers.

Specification	Criterion
Spectral resolution	Depends on the slit width, focal length, dispersion of the grating and the number of pixels of the detector. It should be less than 5 nm (ideally 3 nm). Measurements with poor spectral resolution can lead to errors, particularly for narrow band LEDs.
Wavelength accuracy	Should be better than ± 0.5 nm. Wavelength deviations have a linear effect on peak and centroid wavelength. Errors of 1 nm also lead to similar deviations in calculating the dominant wavelength for red and blue LEDs.
Stray light rejection	Three to four orders of magnitude are the minimum requirement. Section 8.2 discusses examples of the wide-ranging effects of stray light. The influence of stray light might also depend on the wavelength range (see for example UV LEDs in Section 5.4).
Sensitivity	Sensitive detectors are required for testing LEDs in the mcd and mlm range because the optical probes for luminous intensity and luminous flux (diffuser or integrating sphere) result in a considerable loss of light. This criterion is also important with production applications (see Chapter 9)
Signal-to-noise ratio	Excellent signal-to-noise ratio of the detector is important for radiometry because the measured spectra are analyzed over the entire wavelength range and a noisy signal at the spectral extremes leads to errors. Cooled detectors are preferable because these significantly reduce thermal noise and guarantee long-term stability of the dark current.
Linearity	Linearity is an important factor for a spectroradiometer. Any change in the light power launched into the spectrometer must lead to a proportional change in the detector signal. Otherwise, the system is not suitable for radiometric measurements. Array spectrometers must have linearity over the entire specified range of integration times. Often software correction is used to improve this parameter.
Electronic dynamic range	There should be at least four orders of magnitude as in stray-light rejection, and this demands 15-bit analogue-to-digital electronics as a minimum.
Stability and robustness	Important especially when used continuously in rugged manufacturing environments.

5.4 Stray Light Correction of Array Spectroradiometers

A major limitation in the capabilities of array spectroradiometers in photometry and radiometry is the occurrence of stray light in the device. This means that a certain element of the array detector is contaminated by radiation other than that of the given spectral range. The reason for the occurrence of stray light can be found in various mechanisms:

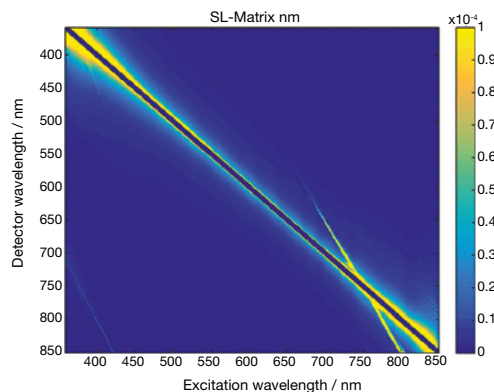
- Stray light from the diffraction grating due to manufacturing inaccuracies in the shape and spacing of lines, or roughness of the surface of the grating
- Higher diffraction orders of the grating
- Double diffraction of the back-reflected light on the grating
- Inter-reflections between the detector and other optical components
- Reflection and scattering of surfaces, in particular of the inner wall of the spectrograph
- Fluorescence of optical elements

The total amount of measured radiant power thus contains a portion of stray light that causes an error. The main objective of the improvement of radiometric performance of the spectroradiometer is to avoid, or at least largely suppress, the stray light by design measures. Thereafter, residual stray light can be effectively corrected by a suitable method of measuring and calibration [31], as outlined in the following.

The complex stray light behavior of an array spectrometer can be determined with the aid of a tunable laser source. The idea is that monochromatic radiation can be attributed for the most part to a certain pixel of the detector. The entire light that is measured outside the bandpass function for this wavelength is the stray light contribution of pixel i that is seen from all other pixels j in the detector.

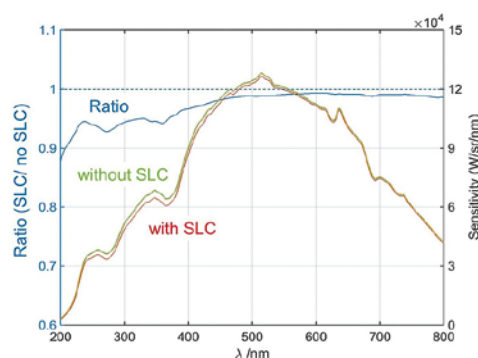
In practical implementation, wavelengths are tuned within the measurement range of the spectrometer in 10 nm increments and spectrum is recorded after each step. The tuning of the wavelength can be performed with the aid of an optical parametric oscillator (OPO) laser. The entirety of all detected spectra over all excitation wavelengths and suitable interpolation results in a device-specific matrix. If the bandpass function of the real signal is subtracted, the result is a so-called stray light matrix (see Figure 42). A stray light matrix can be numerically applied in the calibration and measurements of the spectrometer. Depending on the application, lamp type and observed spectral range, a stray light correction of array spectrometers provides lesser or greater advantages.

Figure 42:
Typical stray light matrix of an array spectroradiometer.



Broadband sources such as halogen lamps and deuterium lamps are normally used for the spectral calibration of spectroradiometers (see also Section 5.5.2). The impact of stray light correction on the spectrum of a broadband source is particularly distinct in the UV and IR spectral range, because the detector of an array spectroradiometer has only a very low sensitivity at the edges. Stray light correction of the spectrum used for calibration is meaningful, because errors in the areas of lower sensitivity are intensified due to the division of the measured spectrum by the reference spectrum.

Figure 43:
Sensitivity curves with and without stray light correction and their relationship.



Comparing the relationship of sensitivities with and without stray light correction after calibration, a stray light portion of about 10 % in the range below 400 nm (Figure 43) can be recognized. A 10 % increase in sensitivity in this range of the already low sensitivity, has a direct effect on the absolute precision. In particular applications based on UV radiometry thus profit from stray light correction, e.g. measurement of UV LEDs, sun simulators or halogen lamps with a high portion of UV radiation [32].

The ultraviolet range is normally subdivided into UVA (320-400 nm), UVB (280-320 nm) and UVC (200-280 nm). UVA radiation is used, e.g. for curing of printing inks, adhesives and coatings. UVC radiation is used, e.g. for disinfection and water purification.

Figure 44 shows spectra of a UVA-LED and a UVC-LED with and without stray light correction in logarithmic presentation. For the UVA-LED, the suppression of stray light by more than one order of magnitude in the UV range to almost 10^{-5} is clearly recognizable. Beyond this, stray light correction improves the precision of radiant intensity by about 3 % in this example. The impact of stray light correction is even greater for UVC-LEDs. It almost reaches the stray light level of a double monochromator and about 4 % more precise radiant intensity. While the peak wavelength (257 nm) does not change at all with the stray light correction, the centroid wavelength shifts by about 0.8 nm in the direction of the peak wavelength.

In the measurement of UV LEDs considerable errors are made in the determination of the absolute value alone by reason of stray light contaminated calibration. As a direct consequence, stray light correction leads to a higher precision in radiometric evaluation. All applications based on UV LEDs profit from this, e.g. curing of adhesives and coatings, lithography, scanning heads, horticulture lighting, biomedical devices, combatting of hospital infections, etc.

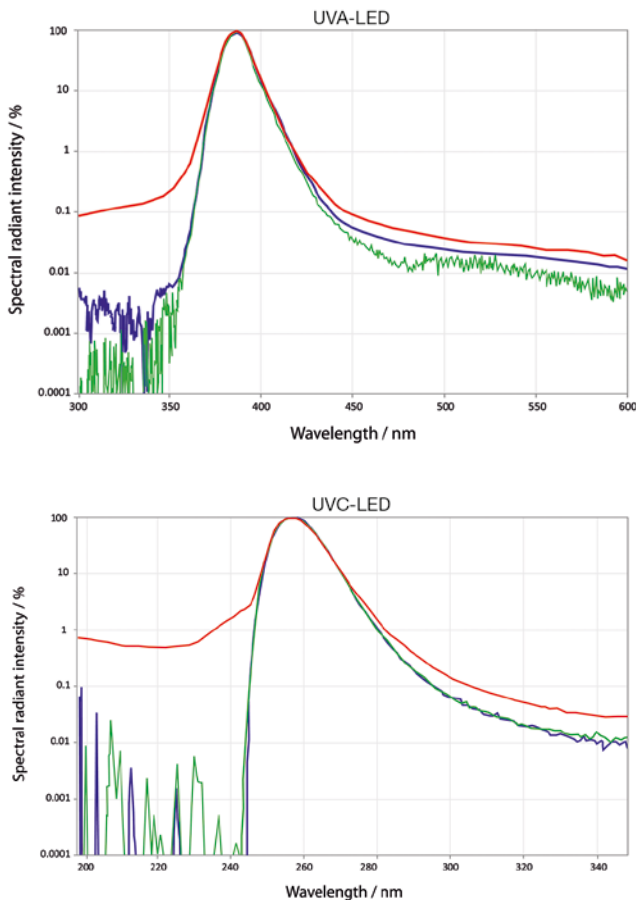


Figure 44:
Logarithmic display of the spectra of an UVA- and UVC-LED without (red) and with stray light correction (blue). For reference, the LEDs are measured with a double monochromator (green).

5.5 Calibration of Spectroradiometers

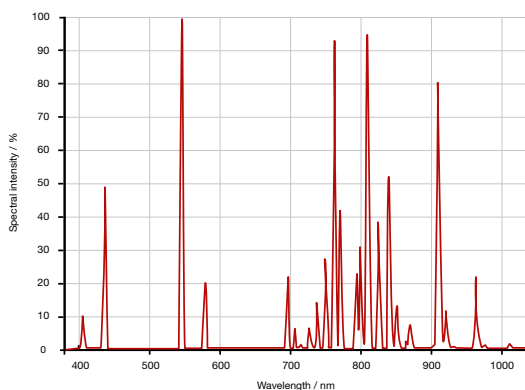
Accurate radiometric measurements require precise calibration of the measuring instrument. Spectroradiometers are calibrated in three stages: the wavelength calibration, the spectral calibration and the absolute calibration. A calibration of an instrument is not only necessary when using it for the first time. A calibration may be necessary after repair or in regular intervals for quality assurance and is always done on the whole measurement system (spectrometer, fiber, connector, measurement adapter e.g. integrating sphere).

5.5.1 Wavelength Calibration

Wavelength calibration is the first stage of the full calibration of a spectroradiometer. A fixed-frequency laser or low pressure Hg or HgAr or Xe lamp with several spectral lines can be used for this purpose (see Figure 45). The frequency of these lines is exactly known from physical models and precise experiments in fundamental physics. That's why these lines are called an intrinsic normal. The known wavelength of an emission peak is assigned to the pixels of the detector (or position of the grating in case of a scanning spectroradiometer). Normally software identifies the peak position of a line using a suitable peak detection algorithm and calculates the wavelength position for the nearest pixels. A table of pixels versus wavelength is then stored as a wavelength calibration file valid only for this particular device. Particularly in the case of array spectrometers many calibration points should be checked to calibrate the entire spectral range.

Air-spaced etalons may be used to refine and correct the wavelength scale [33] for those applications requiring the ultimate in wavelength accuracy. This method has the advantage that a very large number of wavelength reference points are available and distributed across the entire wavelength range of the instrument. It is also a self-consistent method, easily identifying scale errors.

Figure 45:
Spectrum of a
HgAr lamp used for
wavelength calibration.



5.5.2 Spectral Calibration

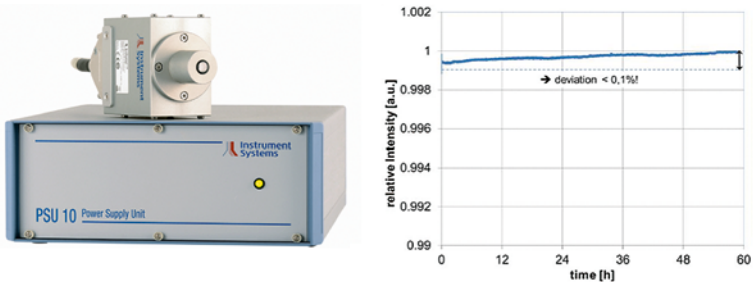
The second stage involves the spectral calibration of the spectroradiometer, i.e. determining the spectral response of the system over the specified wavelength range. Basically, the spectral variation is the result of the sensitivity curves of the detector, the grating and optical probe used. The measured sensitivity curve of the spectroradiometer and the spectral data of a 1,000 W FEL lamp (traceable to a national calibration laboratory) are used to generate the correction function. The lamp emission is very sensitive to applied current, which therefore must be stabilized to within ± 0.0001 A to attain a constant operating state and hence exact values for the spectrum. A change in current leads to a change in lamp temperature. The Planckian radiation distribution is exponentially dependent on temperature, therefore slight changes in color temperature cause significant changes in spectral distribution, particularly in the short wavelength range. Any current error results in a relative irradiance error of 10 times as much. For UV calibrations a calibrated deuterium lamp is used in much the same way.

5.5.3 Absolute Calibration and Verification

The last step is the calibration of the absolute scale. One absolute scale is achieved from the halogen lamp used in the spectral calibration. Verification of the spectroradiometer calibration is carried out using an LED for which the luminous intensity has been determined by a national calibration laboratory. The value for luminous intensity of the reference LED is then compared to the result that has been calculated from integrating the measured LED spectrum which has been weighted with the $V(\lambda)$ curve. The broadband spectral calibration is thus equated with an absolute scale derived from two traceable standard sources. The LED stage corresponds to the substitution method recommended by all national calibration laboratories [34]. The substitution method means using a reference standard for calibrating a measuring instrument such that the properties of the standard are intended to correspond as closely as possible to those of the test specimen. This is the best way of guaranteeing direct traceability to national standard laboratories in a rigorous manner.

When a system is used to measure LEDs, the inclusion of standard LEDs in the calibration process ensures consistent and correct results. Any systematic effects caused by the differences between the FEL calibration lamp and LED sources are removed. Current and temperature stabilized reference LEDs that are traceable to a national laboratory should be used (see Figure 46 left). A special package is normally used with a diffuser as a cap for the LED in order to obtain Lambertian spatial radiation characteristics and ensure uniform chromaticity at all angles.

Figure 46:
Typical LED calibration source with control electronics (left). The temperature of the LED is actively stabilized using a Peltier element. Stability of intensity over a period of 60 hours (right). The deviation is smaller than 0.1 %.



5.6 Imaging Photometers and Colorimeters

The use of imaging photometers and colorimeters for fast capture of photometric and colorimetric quantities with spatial resolution has attracted increasing interest also in Solid-State Lighting, besides the traditional automotive and display applications. Compared with measuring instruments without spatial resolutions, such as spectroradiometers, this technology offers some advantages. In a single image a large number of measurements can be captured simultaneously leading to substantial time-savings. Furthermore, image-processing software functions permit automated methods of analysis, e.g. calculation of homogeneity or contrast.

The absolute measuring precision of imaging photometers and colorimeters is not as high as that of spectroradiometers. This is because of the operational principle using a CCD Sensor in combination with optical filters which can only be adapted with limited precision to the sensitivity of the human eye.

A precision objective lens with downstream $V(\lambda)$ filter is used to image the specimen under investigation on a CCD sensor. A range of resolutions and image sizes can be covered by interchanging the objective lens. The size of the measurement area is determined by the lens type and the distance of the specimen to the camera.

If the imaging device is used as an imaging colorimeter, a set of glass filters is used to match the spectral sensitivity of the CCD sensor to the known CIE tristimulus functions X , Y , and Z (see Figure 47). The filters are successively inserted into the beam path. In high end cameras, two separate filters are used for mimicking the X function, with one filter each for the blue and red range of the spectrum. This four-filter technology considerably improves accuracy compared to conventional filter-based colorimeters. Individual images of the corresponding tristimulus values are recorded sequentially and then calculated to a single image with luminance and color coordinate distribution.

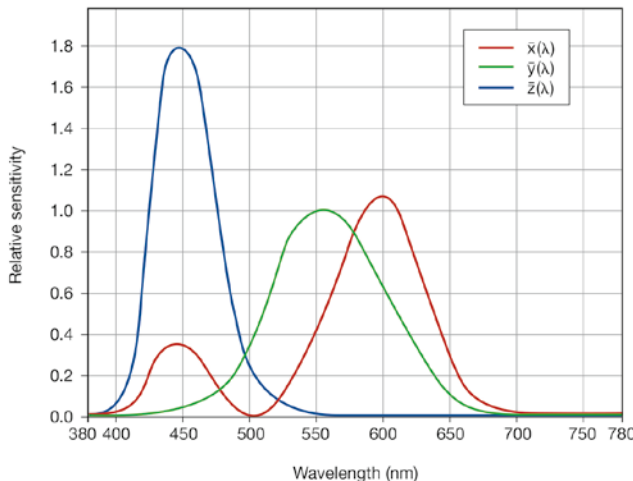


Figure 47:
Sensitivity curves of the CIE 1931 2° standard observer.

A new way to improve accuracy is to use six filters instead of four. Recording data in six channels to determine three parameters (X , Y , Z) results in a redundancy for their calculation. An optimized 3x6 adaption matrix is used for determining the tristimulus values from the six output channels [35]. In this way, the technologically caused residual error of the filter adjustment is eliminated. The higher accuracy of a six-filter colorimeter in determining the color coordinates is also reflected in the calculation of the dominant wavelength (see Figure 48).

Each sensor pixel in the camera is assigned a calibrated luminance or colorimetric value in the final image. This takes into account vignetting by the aperture, lens aberrations, and other effects. A complex flat-field correction must be performed for every aperture and distance setting of the objective lens. The total of these measuring points provides a two-dimensional image that can be used for further evaluation using diverse software analysis tools, such as spotmeter, profile, 3D-box, polygon traverse, etc.

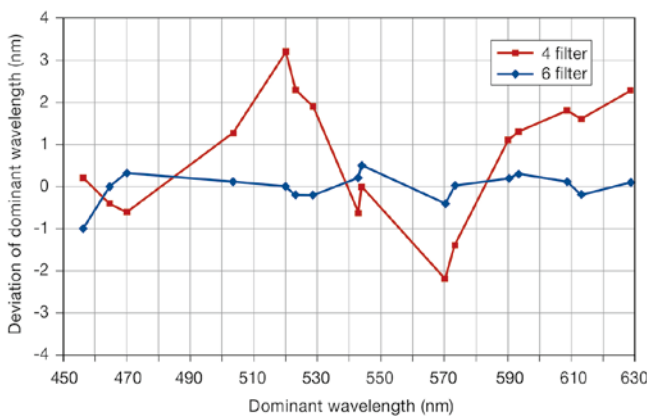
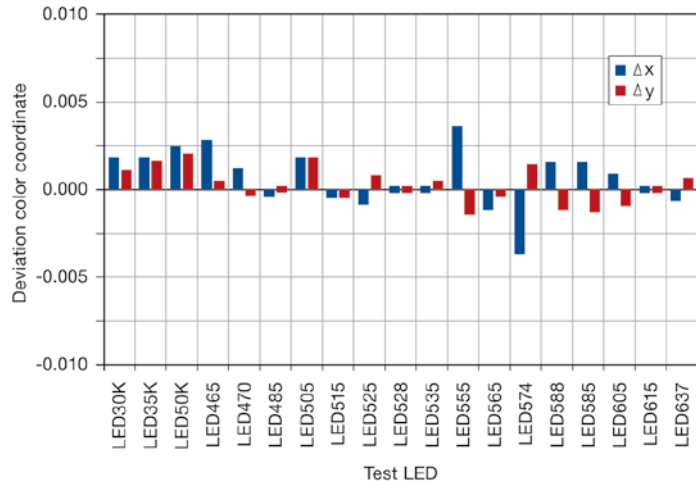


Figure 48:
Deviation of dominant wavelength for a four- and six-filter colorimeter (top). Deviation of color coordinate x and y for a six-filter colorimeter using different test LED sources (bottom).



Imaging photometers and colorimeters are the instruments of choice for measurements of luminance and color distribution of panel graphics and control elements in the automotive industry and avionics, measurement of homogeneity, contrast, mura, and Modulation Transfer Function (MTF) of flat-panel displays and analysis of luminous intensity and CCT distribution of lamps.

A crucial quality criterion for imaging photometers and colorimeters is the filter mismatch, characterized by a parameter f_i' similar to photometers. Other quality features are the dynamics, spatial distortion caused by the optics, CCD specific errors such as smear and blooming, and the stray light.

The dominant wavelength, rather than the color coordinates, is mostly used to analyze the color of narrow band spectra that are virtually 100 % color-saturated. This is particularly the case with color LEDs. The software calculates the dominant wavelength from the x y color coordinates using an algorithm recommended by the CIE. Because the filters do not exactly match the CIE tristimulus functions, a measuring error dependent on the wavelength of the radiation occurs in the color coordinates for narrowband spectra. The entire spectral range can be divided into various segments in which the measuring errors vary considerably. The deviation of dominant wavelength in the range from 560 to 610 nm, for example, is less than 1 nm, because the filters can be precisely matched here. But even small changes in the color coordinates in the red spectral range result in substantial changes in the dominant wavelength. This leads to a relatively large deviation when dominant wavelength is determined for red LEDs. This dependence is strictly systematic and can therefore be corrected.



Figure 49:
Test setup for measuring spatial radiation characteristics of mid-sized light sources using an imaging colorimeter.

With the help of a special test setup, an imaging colorimeter can be used for fast determination of luminous intensity distribution curves, spatial homogeneity of the color coordinates and the color temperature of lamps and luminaires (see Figure 49). This test setup comprises an imaging colorimeter measuring a light-permeable screen which is illuminated by the sample from behind. The system is suitable for small to mid-sized light sources, like single LEDs, LED modules, LED light engines, retrofit lamps and small luminaires. While the test object illuminates the light-permeable screen, the imaging colorimeter measures the luminance distribution arising on the screen from which the spatial radiation patterns are calculated (see Figure 50). The angle-dependent differences in the color coordinates can be determined in the same way. The extremely short measuring times in comparison with a goniophotometric measurement make the test setup ideal for a number of settings including incoming goods inspection or quality assurance.

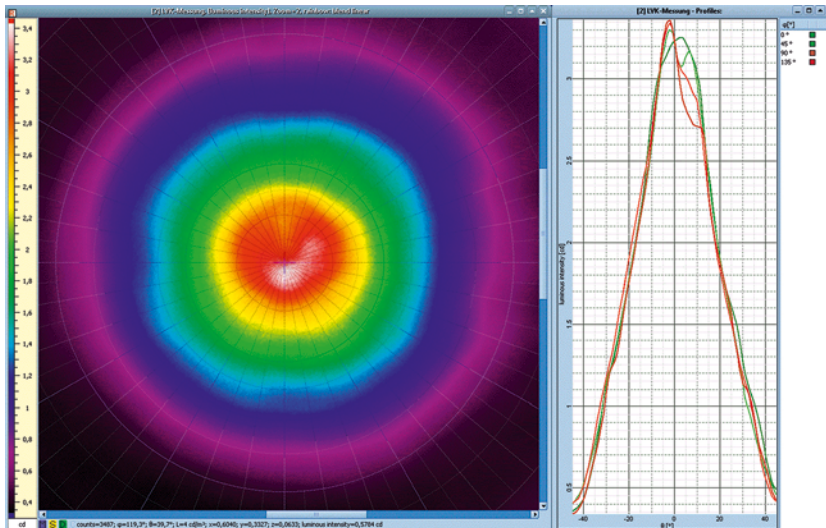


Figure 50:
Image of luminous intensity distribution curves measured with the test setup shown in Figure 49.

6 Basic Properties of Integrating Spheres and Goniometers

Apart from optical measurement equipment like spectrometers or photometers, integrating spheres and goniometers are the most important devices used in the measurement of optical radiation. This section gives an overview of basic properties and concepts of integrating spheres and goniometers.

6.1 Integrating Spheres

Using integrating spheres to determine the radiant power or luminous flux from light sources is one of the most important procedures in light measurement. The interior surface of the hollow sphere is coated with a diffuse reflecting material, e.g. barium sulfate (BaSO_4). Multiple reflections ensure that the light is distributed uniformly throughout the sphere, independently of the original spatial radiation pattern of the light source. Thus, the integrating sphere guarantees complete mixing of the radiation. A detector measures the so-called induced irradiance E_{ind} on the inside sphere wall, which provides a direct measurement for the total luminous flux Φ of the test specimen. Where ρ is the reflectance of the sphere coating and R is the radius of the sphere, the following relationship applies for an ideal integrating sphere derived using the principle of multiple reflections:

$$E_{ind} = \frac{\Phi}{4\pi R^2} \cdot \frac{\rho}{1-\rho} = \frac{\Phi}{4\pi R^2} \cdot M(\rho)$$

The sphere factor $M(\rho)$ specifies how much the throughput of the integrating sphere varies as a function of reflectance. The formula clearly shows that the measured luminous flux does not depend on the position or angle of the detector, but only on the size of the sphere and the properties of the coating. The reflectance of an integrating sphere is a decisive factor for the attainable measuring accuracy. A maximum high reflectance close to 100 % is desirable in order to achieve optimum mixing of the light and a high throughput of the sphere. However, sensitivity of the coating to dirt and ageing goes up as the reflectance increases. The variations in the spectral throughput of the sphere also increase as a result. By contrast, a low reflectance produces greater dependence on the spatial light distribution, alongside lower throughput.

6.1.1 Integrating Sphere Design

Many details must be taken into account for realization of an integrating sphere in order to guarantee the most precise measurement. Potential sources of measurement errors resulting from the sample table, baffles, cables and even the test specimen itself need to be kept as low as possible.

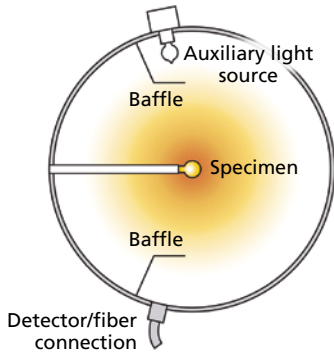


Figure 51:
Cross-section of an integrating sphere and components.

The detector²¹ is positioned at a small port in the wall of the sphere and must be protected against direct irradiation by a baffle in order to comply with the measuring principle of multiple reflections. The detector also needs to have good cosine correction, i.e. the signal sensitivity must change with the cosine of the angle of incidence, in order to obtain an accurate measurement for E_{ind} and hence Φ . The installed baffles must be designed as small as possible and should be located halfway or a third of the distance between the source and the detector as recommended in the guideline IES LM-79.

Holes in the sphere, called ports, are necessary to allow light to be coupled into and out of the sphere. The relative port area to sphere surface area (the port fraction) shall be kept as low as possible.

Light may be introduced via an input port, or the source may be placed directly at the center of the sphere. Figure 51 shows a drawing of an integrating sphere and its basic components with the lamp at the center.

Still on the line between lamp and detector, but now on the opposite side of the lamp, there should be an auxiliary lamp. The auxiliary lamp is also baffled to avoid direct illumination of the test lamp. The auxiliary lamp remains permanently inside the sphere and is switched on when required. It is used to compensate for sphere throughput changes when different standard or test lamps are placed in the sphere. Without this, measurement errors of several percent are likely.

The change in throughput is due to a phenomenon known as self-absorption. Light emitted from the source will be reflected many times and

²¹ Most of integrating sphere designs use an optical probe that is fiber coupled to a spectroradiometer.

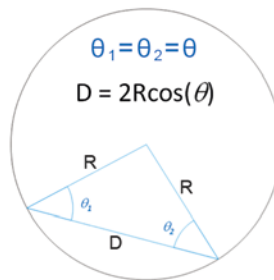
may encounter the source again and be absorbed. The magnitude of the self-absorption effect varies with the physical dimensions of the source, including control gear and holders, and the reflectivity. A sphere must be extremely large compared to the source before this effect is insignificant. Usually all spheres in applications where accuracy is important will have an auxiliary lamp.

6.1.2 Integrating Sphere Theory

Exchange of radiation

An important property of an integrating sphere comes directly from the fact that it is spherical and coated with a diffusing material (Lambertian coating), i.e. all parts of the sphere are “seen” equally by all other parts of the sphere.

Figure 52:
Geometry of a circle (or sphere) for exchange factor calculations.



The exchange of radiation between two differential diffuse surfaces is described by the so-called exchange factor, the fraction of energy leaving one element and arriving at the second element. If an element of surface radiates light at angle θ_1 , and this is then received by an element of surface dA at angle θ_2 a distance of D away, the exchange factor dF will be:

$$dF = \frac{\cos \theta_1 \cdot \cos \theta_2}{\pi \cdot D^2} \cdot dA$$

In a spherical enclosure θ_1 equals θ_2 (see Figure 52) so this reduces to:

$$dF = \frac{1}{4\pi R^2} \cdot dA$$

As the exchange factor is no longer dependent on angle or distance, any part of the sphere “sees” all other parts equally.

This means that a detector placed at any location on the sphere wall can measure the sum of light that strikes all other parts of the sphere surface. If the detector does not feature good cosine response, this relationship no longer applies and the sphere will become sensitive to the directionality of sources.

Integration of light

Consider an integrating sphere with two ports: one input port of area A_i and one exit port of area A_e . We introduce an amount of light, Φ , into the input port. If the “unbroken” sphere surface area is A_s and the coating has a reflectance ρ , after one reflection the amount of light in the sphere is:

$$\Phi \cdot \rho \cdot \frac{A_s - A_i - A_e}{A_s} = \Phi \cdot \rho \cdot (1 - f) \quad \text{where } f = \frac{A_i + A_e}{A_s}$$

The quantity f is known as the port fraction. Expanding this principle to n reflections, the amount of light in the sphere after refection number n is:

$$\Phi \cdot \rho^n \cdot (1 - f)^n$$

Summing all reflections and using an expansion of an infinite power series, this reduces to:

$$\Phi \cdot \rho \cdot (1 - f) \cdot \left\{ 1 + \rho \cdot (1 - f) + \dots + \rho^{n-1} \cdot (1 - f)^{n-1} \right\} = \frac{\Phi \cdot \rho \cdot (1 - f)}{1 - \rho \cdot (1 - f)}$$

From this basic equation we can derive all other equations relating to integrating spheres. For instance, the radiance at the exit port is:

$$L = \frac{\Phi}{\pi A_s} \cdot \frac{\rho}{1 - \rho \cdot (1 - f)} = \frac{\Phi}{\pi A_s} \cdot M$$

M , the sphere multiplier, is related to the throughput of the sphere. When the port areas are small compared to the sphere surface:

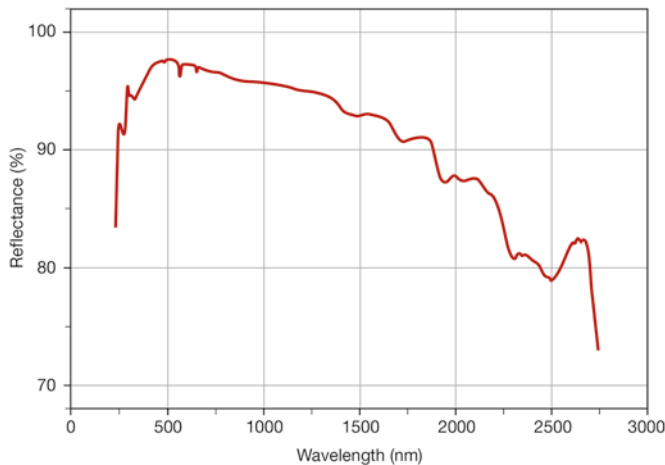
$$M = \frac{\rho}{1 - \rho \cdot (1 - f)} \approx \frac{\rho}{1 - \rho}$$

6.1.3 Coatings

For sphere coatings, white materials that scatter light randomly (Lambertian) are used. These are normally based on barium sulfate (BaSO_4) or polytetrafluoroethylene (PTFE) commonly known by the trade name “Teflon”. Barium sulfate is standard for applications in the visible and near-infrared spectral range but requires careful handling by the user. PTFE is often used for applications in the ultraviolet because of its higher reflectance in the UV spectral range compared to BaSO_4 . High purity is required for both of these products to obtain the correct reflectance properties over a wide wavelength

range. A typical reflectance curve of BaSO₄ is shown in Figure 53. Barium sulfate powder in its raw form is difficult to apply and comes off easily. A binder, usually polyvinylalcohol (PVA) or polymethylmethacrylate (PMMA) is therefore necessary. Although PTFE powder does not adhere readily (non-stick frying pans are coated with it), it does stick to itself under pressure and can be used in the raw state for medium-sized spheres. However, it scatters more weakly than barium sulfate and requires thicker coatings, so it will eventually collapse under its own weight. Bulk-treated PTFE materials, where the powder particles are fused by heat, offer greater strength, but care in machining and handling is required. Such materials are also quite expensive and therefore rarely used for large integrating spheres.

Figure 53:
Typical reflectance of a BaSO₄ coating.



It is clear that high reflectivity is essential for the highest throughput. However, this also makes the integrating sphere very sensitive to objects placed inside the sphere (lamps etc.) and contamination (dust etc.). If, for instance, we have a sphere coating that is 99.5 % reflective, and this is reduced by contamination to 99 %, the throughput changes by a factor of 2. This can be seen by evaluating the (simplified) sphere multiplier for the two values of reflectance:

$$M_{99.5\%} = \frac{0.995}{1 - 0.995} = 199 \quad M_{99\%} = \frac{0.99}{1 - 0.99} = 99$$

Similarly, large self-absorption corrections are required even for slight changes in test lamp properties.

Conversely, spheres coated with low reflectivity coatings of around 80 % show low sensitivity to self-absorption changes and contamination. Taking the above example of 0.5 % coating reflectance change due to contamination, the change in throughput is a factor of only 0.03 (or 3 %).

$$M_{80\%} = \frac{0.8}{1-0.8} = 4 \quad M_{79.5\%} = \frac{0.795}{1-0.795} = 3.88$$

However, low reflectivity coatings have two inherent problems: the throughput is low, making the system much less sensitive to light, and objects in the sphere (baffles etc.) can affect the directional response of the sphere, making some directions more sensitive than others.

Practical spheres are therefore a compromise between several factors involving both design and coating reflectance. A coating reflectance of 94 % to 97 % is considered to be the best for general applications [36].

6.1.4 Sphere Directional Response

The introduction of direct light baffles in an integrating sphere is necessary, but also changes the sphere from the ideal. Light in certain directions must make at least 2 reflections before there is any chance of detection (the shadow area shown in Figure 54). There is also a region where the detector is partially blocked on the first reflection (partial shadow area).

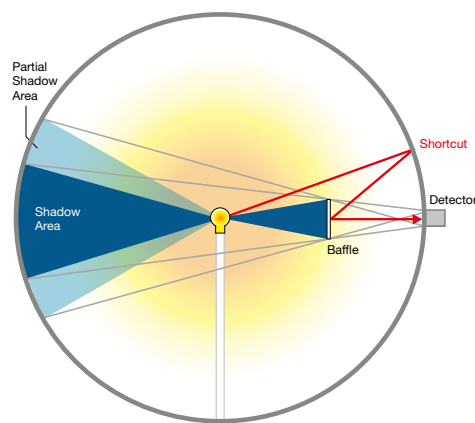


Figure 54:
Illustration of shadowing areas of lower and higher response of an integrating sphere with direct light baffles.

The impact of the extra reflection required in these areas depends on the coating reflectivity; a 99.5 % reflective coating loses only 0.5 % of the light on the first reflection, and hence the effect would be small. An 80 % reflective coating loses 20 % in this first reflection. In addition, light hitting close to the detector can reflect onto the baffle and then to the detector. This “shortcut” results in higher throughput than average for the sphere.

If one places a sphere scanner (a light source providing a pencil beam that can be rotated) at the position of the lamp, the throughput variation with angle can be mapped.

Figure 55:
Sphere scanner map of an integrating sphere response shown from two different perspectives. Colors indicate the relative throughput (red = high, green = low, orange = average).

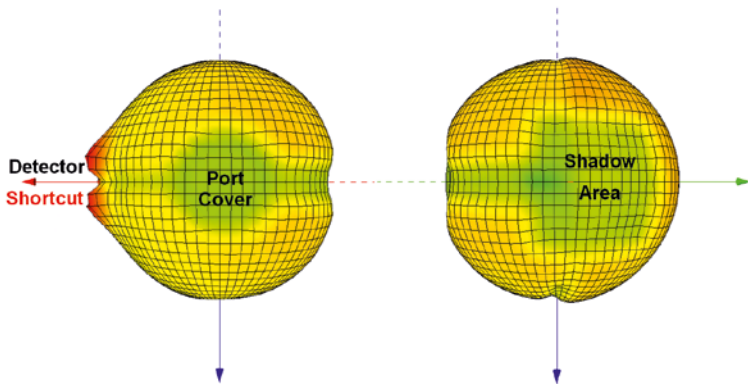


Figure 55 shows an actual 3D map of a sphere (shown from two different perspectives) in which all changes in throughput can be seen. In addition to the baffle shadow, the shadow of the post holding the baffle is also visible. Areas of the sphere that have slightly different coatings, e.g. port covers and the seam between hemispheres, can also be observed with this form of characterization.

When measuring a directional source such as LEDs, it is important to point the emission maximum towards the average areas rather than towards the shadow areas or shortcuts. In this way, the highest possible accuracies are obtained.

6.2 Goniometers

Instead of measuring all directions of emission at once, as in the case of integrating spheres, when using a goniometer each direction is measured individually. Angular resolved measurements are thus possible. A lamp is placed at the center of the virtual sphere and a detector with good cosine response maps the angles around it. A goniometer can be operated together with a photometer as a conventional goniospectrometer, or with a spectrometer as a high-quality goniospectroradiometer. The science of goniospectroradiometry measures luminous flux, luminous intensity distributions and the angular-resolved spatial characteristics of colorimetric values. In contrast to integrating spheres, goniphotometry is a direct measure of photometric values which does not require luminous flux or luminous intensity standards.

6.2.1 Coordinate Systems

Coordinate systems used in goniometry are broadly classified into three types: A, B and C. These are defined by the IES [37] and also by CIE [38] [39] with slightly different definitions. Each of the coordinate systems uses a series of half-planes within which a scan of in-plane angles is made. The combination of in-plane angles and half-plane angles relative to a reference provides the three-dimensional polar coordinates. Goniometers are generally classified by the type of coordinate system employed. The differences between the goniometer systems lie in the orientation of the polar axis, the reference angle, the numbering system and eventually the rotation of the luminaire. The C, γ coordinate system (see Figure 56) is the most popular system used in general lighting.

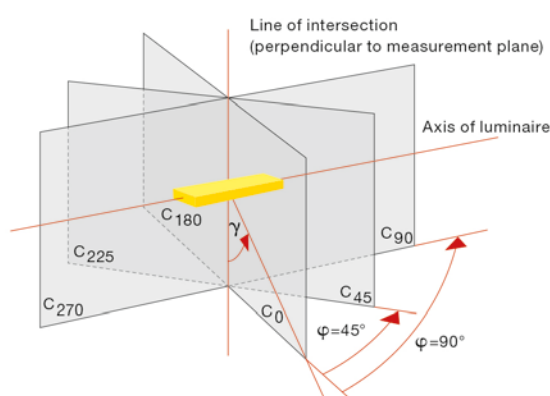


Figure 56:
Definition of the C, γ coordinate system. The in-plane angle γ and the half-plane angle φ is shown.

6.2.2 Goniometer Types

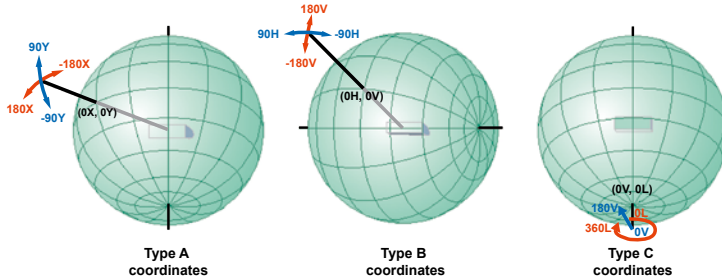


Figure 57:
The coordinate systems for type A, B and C goniometers.

Type A goniometers

The polar axis is vertical and the reference (OX, OY) is horizontal. The optical axis of the luminaire is pointed towards the reference. The luminaire is rotated in X and Y with the detector in a fixed position. A half-plane angle, X, is set

between -180° and $+180^\circ$ and then the in-plane angle, Y, is scanned between -90° and $+90^\circ$. This is repeated for all half-plane angles, X, to complete the 3D scan.

This type of goniometer is most common in the automotive and aviation lighting industries.

Type B goniometers

The polar axis is horizontal and the reference (0H, 0V) is horizontal at 90° to the polar axis. The optical axis of the luminaire is pointed towards the reference. The luminaire is rotated in H and V with the detector in a fixed position. A half-plane angle, V, is set between -180° and $+180^\circ$ and then the in-plane angle, H, is scanned between -90° and $+90^\circ$. This is repeated for all half-plane angles, V, to complete the 3D scan.

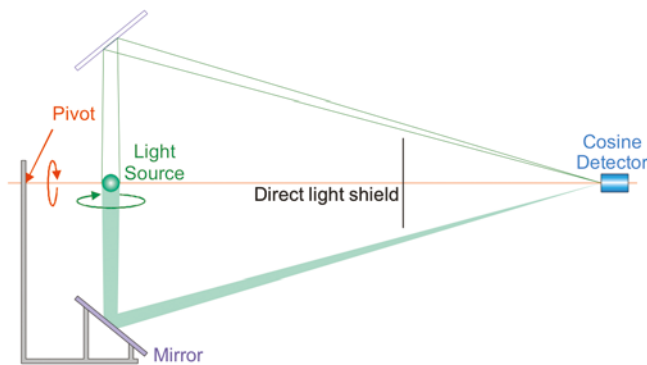
This type of goniometer is most common in the display industry.

Type C goniometers

The polar axis is vertical and the reference (0V, 0L) is downward along the polar axis. The optical axis of the luminaire is pointed towards the reference. The luminaire is rotated in L only and the detector is rotated in V. A half-plane angle, L, is set between 0° and $+360^\circ$ and then the in-plane angle, V, is scanned between 0° and $+180^\circ$. Note the lack of negative numbers in this coordinate system. This is repeated for all half-plane angles, L, to complete the 3D scan.

As the detector is rotated in the vertical plane, considerable vertical space is required for IES Type C goniometers. This sometimes involves building special rooms, spanning several floors of a building. A moving-mirror goniometer is often employed as a compromise between accuracy of measurements and space requirements, but still requires a strong commitment of the user concerning budget and test room dimensions. This type of goniometer is most common in general lighting where the luminaires are very large and sensitive to burning orientation, as for example fluorescent and discharge lamps.

Figure 58:
Schematic drawing
of a moving-mirror
goniometer.



However, the mirrors can lead to polarization sensitivity and the light reaches the detector from different angles (making alignment and symmetry of its response critical factors). IES LM-79-08 recommends that moving mirror goniometers are avoided if the SSL source emission is polarized. Also, the mechanical components holding and rotating the mirror may give stray light errors due to unwanted reflections from the structural parts. Furthermore, keeping the – sometimes very large – mirror clean from dust and other contaminations is often a tedious and time consuming task.

The best way to implement a type C goniometer is the so-called turning detector type goniometer. This type of goniometer allows the device under test to remain in position unchanged and the detector moves on the surface of a sphere around the luminaire. Figure 59 shows the working principle and an example of a practical implementation of a turning detector type goniometer.

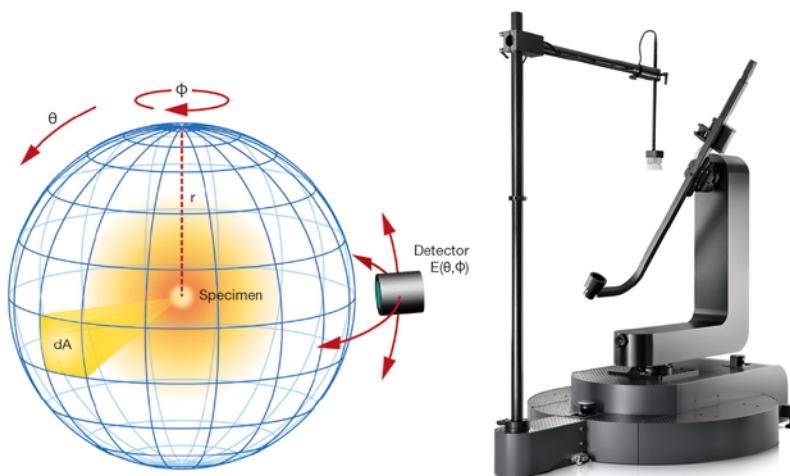


Figure 59:
Working principle (left)
and example setup
for the realization of a
turning detector type
goniometer which
maintains the designed
burning position of the
DUT (right).

Unfortunately, there are severe practical limits to the overall dimension of this type of goniometer. These limitations come from the fact that in modern goniophotometry two boundary conditions have to be met simultaneously: the measurement of large samples on the one hand and the measurement of luminous intensity distributions in the far-field on the other hand. Luminous intensity is defined in the far-field where the DUT can be considered as a point source. The measurement distance required to maintain this photometric distance depends on the type of source and its radiation characteristics. Ten times the largest dimension of the light emitting surface of the DUT is a good rule of thumb, but some sources require even more (narrow intensity distributions or emitting surfaces with large non-luminous spaces). Considering this, the turning detector type measurement of a 0.5 m DUT (easily reached by LED tubes for example) would require a test laboratory with a height of at least 10 m (0.5 m DUT \times 10 \times 2) which is inappropriate for most cases.

Figure 60:
Schematic drawing (top)
and example realization
of a turning luminaire
goniometer (bottom).



An alternative approach is a so-called turning luminaire design (see Figure 60). Such a moving source goniometer is much simpler and more convenient compared to a moving mirror goniometer, and avoids the height restrictions of a turning detector or moving mirror type goniometer. The photometric distance still has to be maintained, but the measurement axis is now horizontal, which places requirements only on the width and not on the height of the laboratory. A turning luminaire goniometer like the one shown in Figure 60 can measure DUTs with 2 m in diameter in a laboratory with a standard ceiling height, which is a big advantage compared to other implementations. The only disadvantage of the system is that it does not maintain the burning position of DUTs which show an effect of changing their position with respect to gravity. This problem is addressed in the next chapter.

6.2.3 Burning Position Correction

LEDs are semiconductor devices that are, in general, insensitive to orientation changes. The optical output of an LED is mostly determined by the temperature of the p-n junction. Used in Solid-State Lighting fixtures, the LED incorporates a passive heat sink in order to keep the junction temperature as low as possible. The passive heat sink of most SSL sources relies on convection induced air flow and is designed for the operating orientation used in the application. The air flow through the cooling fins assures the intended cooling

rate, and with that the anticipated temperature of the LEDs. A disturbed convectional air flow might change the optical properties of the luminaire. Such a perturbation may be induced by operating the device in a position different from the manufacturers intended burning position with respect to gravity. The influence of the operating position is highly dependent on the luminaire type. CIE S025 (see also Section 3.3 on page 18) in principle allows goniometric measurements to be performed in an orientation other than the designed burning position. To meet the requirements of the standard, a suitable correction has to be applied.

The auxiliary photometer method

One possible implementation of the requested correction is the so-called auxiliary photometer method. The basic concept of this correction method is monitoring of the relative optical output of the test specimen in a fixed direction in space while the test specimen changes its orientation with respect to gravity. An auxiliary photometer head whose orientation and distance to the light source is maintained during the movement can provide such monitoring data. Weighted with a reference, the value measured in each different operating position serves as a correction factor for the measurement. The reference value is measured with the light source in the designed operating position after it is thermally stabilized. Figure 61 shows a schematic of the working principle.

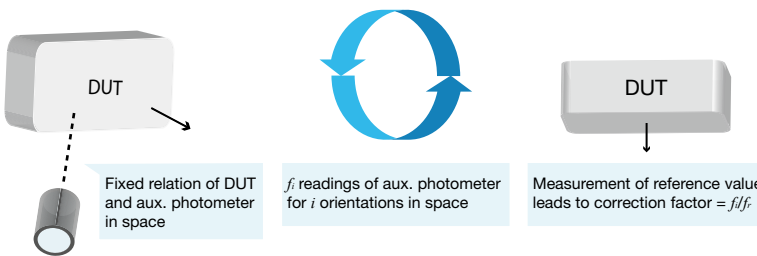


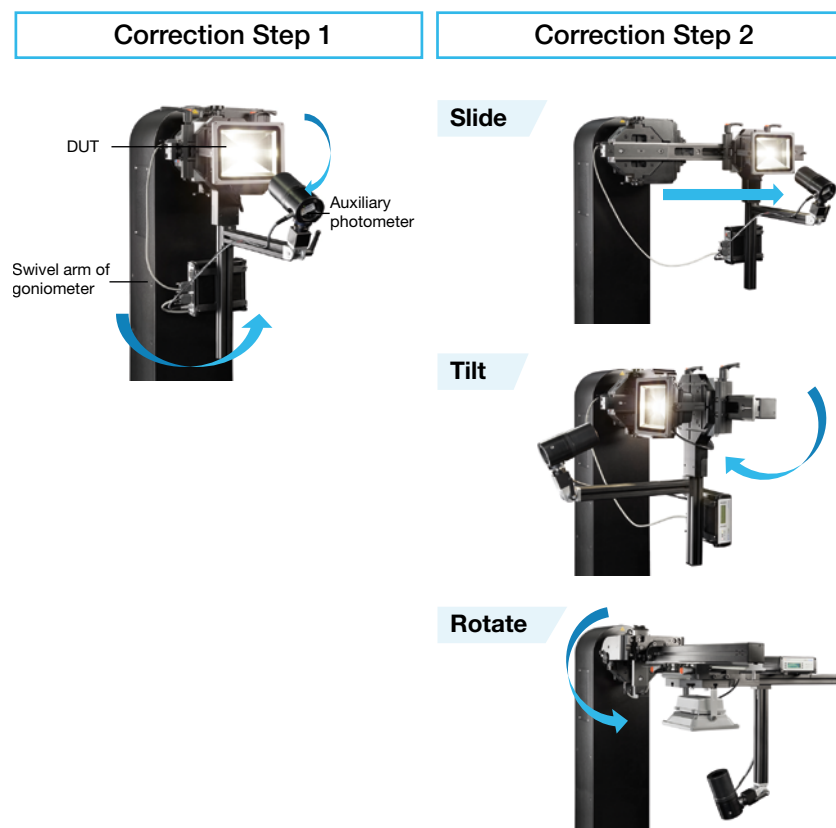
Figure 61:
Schematic working principle of the auxiliary photometer method. The movement of the C and γ axis of the turning luminaire goniometer define i orientations of the DUT in space. The readings f_i of the auxiliary photometer for the i orientations, divided by one reference value f_r measured in the designed operating position, serve as correction factors.

Practical implementation and usability

A suitable implementation of the auxiliary photometer method faces numerous challenges [40]. The photometer hardware must be removable, to allow standard turning luminaire measurements. In addition, it must feature stable positioning with respect to the DUT, but should be adjustable to different sizes of the SSL fixture. This is exceptionally challenging when taking into account SSL sources that can have a broad range in size (e.g. from relatively small retrofits to large fixtures with 2 m in diameter). The positioning of the DUT to record the reference value must be flexible, to account for different designed burning positions (e.g. down- or up-lights). The reference position should be reached without turning off the DUT in order to avoid additional measurement time due to an additional burn-in and stabilization procedure. A possible implementation is shown in Figure 62.

Figure 62:
Correction step 1 implies the connection of an auxiliary photometer and the recording of the photometer readings for the orientations of the DUT defined by the setting of the turning luminaire measurement.

Correction step 2 features the geometric displacement of the hardware adapter in order to position the DUT in the intended burning position. The DUT is slid on an additional cantilever arm. The arm can then be tilted by 90°. With the help of the motorized C-axis of the goniometer, the DUT can be rotated in virtually any desired burning position.



The first step implies the connection of the auxiliary photometer to the DUT and the recording of the readings for the different orientations in space. These orientations are defined by the sequence setting of the turning luminaire measurement.

The second step comprises the geometric displacement of the hardware adapter in order to position the DUT in the burning position intended by the manufacturer. The designed burning position can be reached without power-down of the DUT. This “hot” positioning avoids long additional burn-in times and minimizes the additional time effort for the correction. After the DUT has reached a stable thermal condition, the reference value f_r is recorded.

After the completion of correction step 1 and 2, a set of correction factors for each pair of C- and γ -angles used in the measurement is calculated. This burning position correction file can then be applied to the previously recorded measurement with the turning luminaire goniometer. The file can be reused for other, identical samples out of a larger batch which considerably saves measurement time. The file can also serve as a pure test measurement to judge if a DUT shows a position dependence that needs to be corrected or not.

Measurements and test comparison

To validate the performance of the auxiliary photometer method a reference measurement is needed that represents the “true” performance of the device under test in its designed burning position. For this purpose, all samples are measured using a turning detector type goniometer. This type of goniometer allows the device under test to remain in position unchanged, and the detector moves on the surface of a sphere around the luminaire.

A variation in supply voltage was used to simulate a series of high position dependencies [40]. A 12 W SSL downlight was measured at lower operating voltages with the tuning luminaire goniometer, and this inevitably led to a lower luminous flux. The reference value in the standard burning position at the rated voltage of 230 V was recorded after adequate burn-in time and used for subsequent position correction. With this method, a series of different luminous fluxes ranging from -4 % to -26 % compared to the reference value could be realized. Even the high deviations to the reference measurement could be corrected to around 1 % over the entire range. The graphical summary of Figure 63 shows the corrected curve (blue) in close proximity to the reference (grey). Therefore, light sources showing highly pronounced position dependence can be measured accurately and in conformity with CIE S025 using a turning luminaire goniometer with subsequent burning position correction.

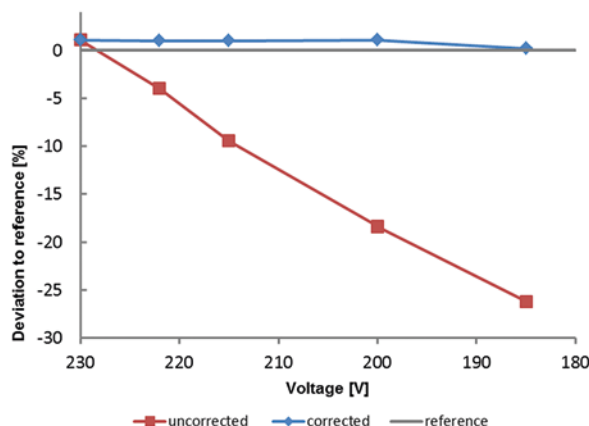


Figure 63:
Application of the burning position correction method to high position dependencies induced by varying the supply voltage. The high deviations to the reference measurement could be corrected to around 1 % over the entire range. The corrected curve (blue) is in close proximity to the reference (grey) whereas the uncorrected curve (red) shows an increasing deviation with decreasing supply voltage.

7 Optical Characteristics of LEDs, Modules, SSL Lamps and Luminaires

This chapter deals with the measurement of optical characteristics of LEDs and SSL sources. Typically luminous flux and radiant power are the most important optical parameters for LEDs although the spatial intensity distribution and colorimetric quantities are sometimes also required. For single LEDs averaged LED intensity in condition B is still common. Partial LED flux is a quantity that is based on a specific measurement geometry. It is sometimes required for particular applications but still not widely used. For SSL sources, the photometric and colorimetric radiation characteristics are important.

7.1 Luminous Flux and Radiant Power

The two principal methods for measuring total radiant power and luminous flux are using either an integrating sphere or a goniophotometer/goniospectroradiometer. The next two sections explain these two measuring methods with consideration of typical measurement challenges.

7.1.1 The Integrating Sphere Method

Measuring geometries

The luminous flux quantity is sometimes called total luminous flux to emphasize the fact that it is the total for all directions. It is also referred to as 4π flux since a complete sphere has 4π steradians of solid angle. To collect all light within the 4π steradians the source must be at the center of the sphere. This 4π geometry is the conventional configuration for measuring luminous flux (see Figure 64 left). The radiation emitted in all directions is captured and the total luminous flux is measured.

For light sources which have negligible or no radiation directed backwards, the total flux can be measured in the more convenient forward flux, or 2π geometry. Here, the light source is located at a port in the wall of the sphere. Only the light radiation emitted in the front hemisphere is recorded for the measurement (see Figure 64 right). This forward radiation is typical for most LED products. The integrating sphere must be calibrated absolutely based on the measuring geometry in conformity with the substitution principle. This principle states that the test light source should always be measured by comparison to a standard source having similar spatial and spectral distributions.

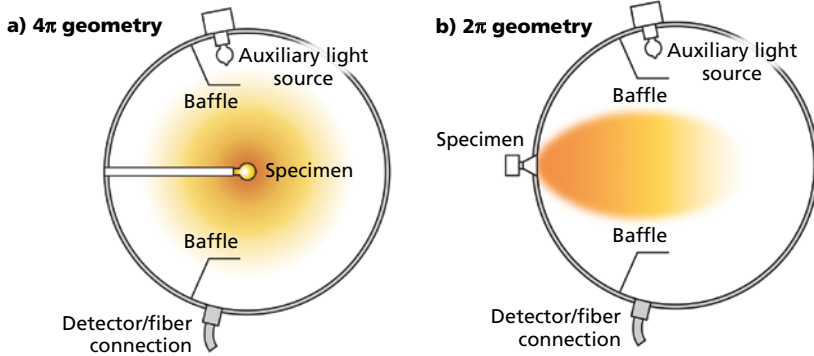


Figure 64:
CIE recommended sphere geometries for all sources (left) and for sources with no backward emission (right).

Guidelines for selecting the correct size

The test specimen should always be significantly smaller than the internal diameter of the sphere, in order to keep the interference factor caused by the sample itself as low as possible. However, the incident light intensity on the detector decreases as the sphere gets bigger. As a rule of thumb, the light throughput of an integrating sphere is a function of the inverse square of the sphere's radius. Selecting the correct relationship between the size of the test object and the size of the sphere is therefore crucial for an effective balance between high measuring quality and good throughput (see also Figure 65).



Figure 65:
A 1 m in diameter sphere (left) is ideal for measuring most LEDs and modules in the 4π and 2π recommended geometries. A 2 m sphere (right) is ideal for large luminaires and SSL products.

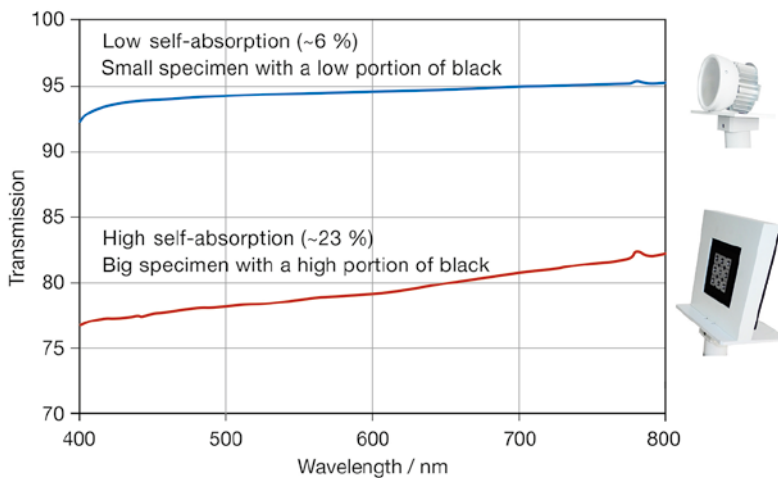
There are guidelines for selecting the correct size of a sphere for a given size of test sample. Using the 4π geometry, the total surface of the test sample should be smaller than 2 % of the surface of the sphere. The length of a linear lamp should be less than 2/3 of the diameter of the sphere. Using the 2π geometry, the diameter of the measuring port and hence the maximum extension of the test specimen should not exceed 1/3 of the sphere diameter.

Self-absorption correction

The test object itself contributes to the absorption of light radiation in the integrating sphere. This form of interference known as self-absorption can

result in a significant attenuation of light radiation and leads to deviations in measurement. This attenuation becomes more pronounced as the test specimen becomes bigger and darker. Figure 66 shows two typical examples of test specimen and the resulting transmission versus wavelength. Self-absorption can lead to a correction of up to several ten percent.

Figure 66:
Self-absorption spectra
for two typical DUTs.



A self-absorption correction with the assistance of a suitable auxiliary light source is therefore essential for precise measurements. A halogen lamp covering a wide spectral range is typically used for this purpose. The auxiliary light source must be positioned behind a baffle in order to avoid illuminating the sample directly and it should be operated by a stable power supply. This light source is used to determine the spectral absorption behavior of the device under test, the sample holder and the connecting cables, and then offset with the actual measurement. The effect of self-absorption increases as the reflectance of the coating rises and the ratio of the area of the sphere to the test specimen decreases.

Near-field absorption

Any object (such as a socket for example) that is in close proximity of the light source absorbs light significantly and may cause large errors. This so-called near-field absorption cannot be corrected by a self-absorption measurement. The cause of this effect should thus be avoided. The object should be placed as far away from the lamp as possible and the formation of cavities should be avoided. In addition, coating the object surface with a high-reflectance material is recommended. As an example, a good solution for a linear tube holder is shown in Figure 67.



Figure 67:
Example of avoiding near-field absorption effects. The holder of the linear tube is placed as far away as possible from the light source and coated with a high-reflectance material.

Burning position

As described in Section 3.3, measurements of passively cooled SSL sources should be performed in the burning position defined by the manufacturer. This also applies to sphere photometry. When measuring in the 4π geometry, it is convenient to use an internal lamp post that can be mounted up-down or down-up, to realize the designed burning position of the light source. In the case of 2π geometry, a rotatable sphere is the method of choice (see for example Figure 68). The complete sphere can be rotated within its mounting frame. The measuring port is therefore located at the side, top or bottom side.

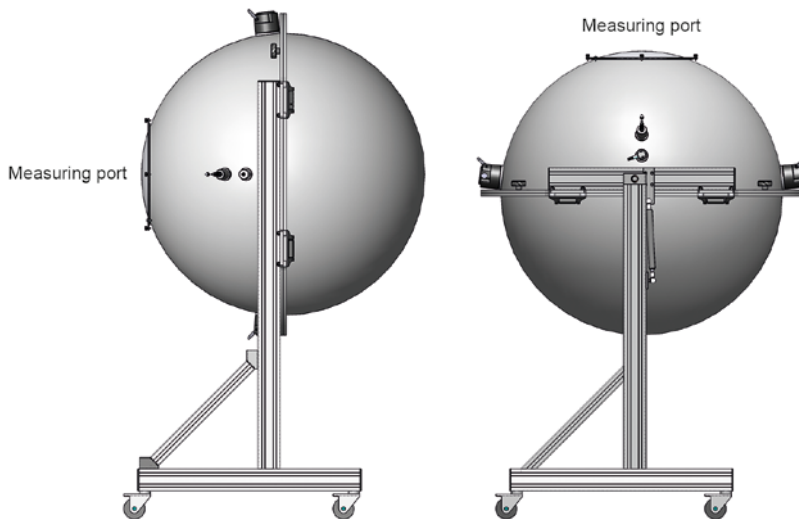


Figure 68:
A rotatable 1 m sphere. Position-sensitive light sources can be measured in their designed operating position.

Consideration of measurement errors

Contributions to measurement errors are manifold. An error analysis when using a spectroradiometer as detector can be found in Chapter 8. The wide range of radiation characteristics shown by LEDs can introduce calibration

errors in measuring luminous flux. A variation of 5 % can be obtained for components with diffuse emission, but deviations of more than 10 % are possible with narrow-angled LEDs.

As described above, selecting the right sphere size, performing a self-absorption correction, avoiding near-field absorption and measuring in the designed burning position of the light source is crucial for a high accuracy measurement. In addition, a regular recalibration of the sphere is recommended to compensate aging effects of the sphere coating.

Another big portion of error contributes when starting the measurement before the source is thermally stable (refer also to Section 8.5.4). Furthermore, when testing according to CIE S025 or EN 13032-4, an ambient temperature of 25 °C is recommended. Putting a source which generates heat into an enclosure (the integrating sphere) the ambient temperature (temperature in the sphere) will rise and it will be different to the “normal” operating conditions. When measuring in the 4π configuration, it is therefore recommended to stabilize the source with the sphere hemispheres apart. The sphere should be closed just before the measurement. This way, ambient conditions in normal operation can be simulated best. Care should be taken to close the sphere in a subtle manner in order to avoid air movement which might contribute in an undesired way to thermal management.

7.1.2 The Goniophotometer Method

Although measuring luminous flux or radiant power with a goniophotometer is more time-consuming compared to integrating spheres, it is much more precise. This measuring procedure does not require luminous flux standard lamps as a reference value as it is the case in sphere photometry. It is the method of choice if lamps with different luminous intensity distributions are to be measured, and it is the baseline for calibrating luminous flux standard lamps which provide the reference value for other test procedures. Another distinguishing feature of goniophotometry compared to sphere photometry is the ability to measure partial luminous flux and angle of half intensity. These values must be determined when measuring characteristics relating to energy efficiency [41] [42] and conformity to Zhaga specifications (see Section 3.7).

The method can be best described by an imaginary sphere enclosing the source (see Figure 59 left). A cosine-corrected detector moves on the surface of the sphere along specific paths at distance r (the sphere radius). The detector is used to determine irradiance E arising as a result of the partial radiant flux $d\Phi$ incident on detector area dA as a function of θ and φ .

$$E(\theta, \varphi) = \frac{d\Phi}{dA}$$

Several measurements are taken for each angle θ with angle φ varying from 0° to 360° . Individual zones are scanned corresponding to a constant degree of latitude of the sphere. Total radiant power Φ is then

$$\Phi = r^2 \int_0^{2\pi} \int_0^\pi E(\theta, \varphi) \cdot \sin \theta \cdot d\theta d\varphi$$

Alternatively, instead of moving the detector which might require considerable mechanical effort, a stationary detector can be used and the SSL source is scanned. However, for modules and luminaires that have convection cooling this may not apply and a correction for the luminaire position might be indicated (refer to Section 6.2.3).

Figure 69 shows the setup for this kind of goniophotometer. The angle φ is adjusted by rotating the source about its mechanical axis and angle θ by pivoting about its tip. The detector sits on an optical rail to permit measurements at various distances.



Figure 69:
Goniophotometer with a compact light shielding enclosure. The DUT is moved instead of the detector. The angle φ is adjusted by rotating the LED about its mechanical axis and angle θ by pivoting about its tip.

Large distances are a requirement for luminous intensity distribution to meet the far-field condition. For measurements of total flux using a goniometer, the large distances are not required. Providing the detector has good cosine response, the irradiance can be measured accurately at all angles. As described in Section 2.1.3, irradiance is not a property of the lamp, but instead the light falling onto a surface. By measuring the irradiance at sufficient locations around a virtual sphere enclosing the lamp, the total flux can be derived by integration. Providing that no interactions between source and detector occur, the size of the source can be almost the size of the virtual sphere.

Efficiency and Efficacy

If the total optical power emitted by a LED, module or luminaire is known then it can be combined with electrical power P [W] supplied to the unit to give efficiency:

$$\varepsilon_e = \frac{\Phi_e}{P} \quad \frac{[W]}{[W]}$$

Efficiency is unitless (the units in the numerator and denominator cancel) and specific to the conditions of measurement. Driver efficiency may be included or excluded, and temperature de-rating to operational conditions may be required for practical applications.

Luminous efficacy is similarly calculated but using total luminous flux:

$$\eta_v = \frac{\Phi_v}{P} \quad \frac{[lm]}{[W]}$$

Luminous efficacy is expressed in units of $[lm\ W^{-1}]$. Like efficiency, luminous efficacy values are specific to measurement conditions, and may include or exclude driver efficiencies and temperature effects.

7.2 Luminous Intensity and Radiant Intensity

Luminous intensity is the most frequently measured parameter for low-power LEDs. According to the definition, luminous intensity must be measured at a distance where the sample can be considered an approximated point light source. The distance of the detector from the test specimen required for conformity with this criterion is known as the photometric distance. It varies with the size of the light source to be measured. The minimum factor, given by the ratio of the distance to the detector and the maximum extent of the light emitting surface, varies between 5 and 15 depending on the applied standard and the prevailing spatial radiation pattern.

One method of determining luminous intensity I_v involves calibrating the detector in illuminance E_v and calculating luminous intensity using the inverse square law:

$$E_v = \frac{I_v}{r^2}$$

Apart from maintaining the far-field condition, the validity of this calculation requires the precise measurement of the distance r between the detector and LED. The many different designs available make it difficult to determine the precise position of the emission center (also known as the goniometric centroid) of the LED.

7.3 The “Averaged LED Intensity” Concept

Many LEDs have a relatively large emitting area compared to the short distance that is generally used for a measurement. Lenses, if present, may dramatically shift the apparent position of the emitting center. A point source cannot be assumed and therefore the inverse square law no longer holds. The irradiance measured at the detector is not easily related to the intensity of the source. Therefore measurements done with different geometrical setup will most likely lead to different results and are difficult to compare.

Because of this, the CIE developed the concept of “averaged LED intensity” to solve the problem that occurs under near field conditions [6]. This concept no longer corresponds to the physically precise definition of luminous intensity but relates more to a measurement of illuminance at a fixed distance and detector size. The LED is positioned in such a way that its mechanical axis is directly in line with the center point of a round detector with an active area of 1 cm², and the surface of the detector is perpendicular to this axis.

CIE recommendation	Distance between LED tip and detector	Solid angle
Condition A	316 mm	0.001 sr
Condition B	100 mm	0.01 sr

The CIE gives two recommendations for the distance between the LED and the detector surface (see Table 9). Condition B is the most commonly used geometry since it is also suitable for weak LED light sources. The front tip of the LED is always taken as the reference point for the distance. This guarantees that the same geometry is always used when measuring luminous intensity in different laboratories irrespective of the design of the LED.

Table 9:
CIE recommendations for the concept of averaged LED intensity. The area of the detector is always 1 cm². The relevant solid angle is determined by the distance between the LED tip and the detector.



Figure 70:
Intensity probe that conforms to the standard CIE condition B for 100 mm distance together with a precision test socket for mounting the LED. The test socket is inserted into the tube of the condition B adapter for measurement.

Figure 70 shows a realization of this concept in practice. The intensity probe comprises a tube with a length corresponding to the desired CIE condition into which an LED test socket can be inserted. The distance between the tip of the

LED and the detector is exactly 100 mm in the case shown in Figure 70. Two baffles in the beam path help to reduce stray light. A fiber bundle is attached to the detector (a diffuser or small integrating sphere with a 1 cm^2 measurement port) to guide the light into a calibrated spectroradiometer.

7.4 The “Partial LED Flux” Concept

Sometimes neither the luminous intensity nor the luminous flux represent the usable light for a particular application, and something in between is required. The quantity of partial LED flux was introduced in CIE publication 127-2007.

Luminous intensity involves a flux and a solid angle and is the ratio of the two; hence its unit is the candela, which is the lumens per steradian. Partial LED luminous flux also involves a flux and an angle, but is expressed as the flux within the angle as opposed to a ratio; hence its unit is lumens (with the angle specified).

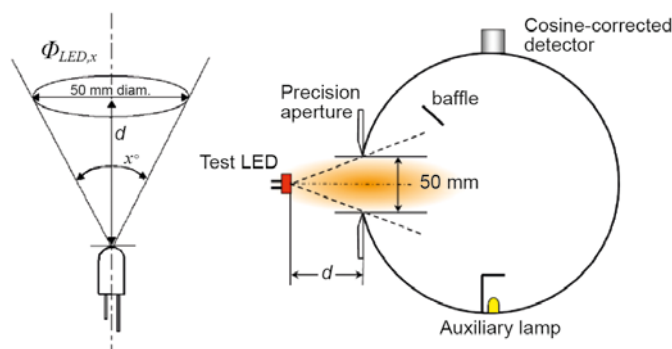
Like averaged LED intensity, partial LED flux is a near-field measure and hence is similarly defined in terms of physical geometry rather than being a fundamental unit. This is why the term “LED” is included in the quantity. This distinguishes it from the partial flux that may be calculated from far-field goniometric measurements.

Distance d is set for a desired half cone angle x as given by

$$d = \frac{25}{\tan \frac{x}{2}} \quad [\text{mm}] \quad \text{where } 0^\circ \leq x \leq 180^\circ$$

The symbol for this quantity is $\Phi_{LED,x}$ – with the value of x being the cone angle (diameter) in degrees. For example, $\Phi_{LED,180}$ is the flux emitted in the front half hemisphere (forward flux) in which case, $d = 0$. Any flux emitted in the directions other than in the given cone angle is ignored. Figure 71 left shows the basic concept.

Figure 71:
Concept (left) and
experimental realization
(right) of partial LED flux.



The reference point of the LED is the tip of the enclosure of the LED, though it may not be the effective center of light emission, because it can be easily identified for any type of LED while the effective center of emission is difficult to determine and sometimes unknown. It is chosen for simplicity and reproducibility of measurement. The diameter of the aperture (50 mm) is fixed in order to achieve reproducibility in measurement. As this is a near-field measurement, results vary if apertures of different sizes are used for the same cone angle.

For the measurement of partial LED flux, an integrating sphere of, for example, 250 mm in diameter can feature an input port with a precision aperture of 50 mm in diameter (see Figure 71 right). By varying the distance d , different cone angles can be realized and measured.

Although the unit of partial LED luminous flux is the lumen, and hence the same as the total luminous flux, the quantities are different and should not be confused. Total luminous flux is a measure of all the light emitted by the LED, whether 2π or 4π . Partial LED flux is the flux within a set measurement geometry, and hence may be all or a fraction of the total flux emitted, depending on the LED radiation pattern. Care should therefore be exercised in comparing partial LED fluxes, to ensure the same cone angle x is used and is appropriate for the application.

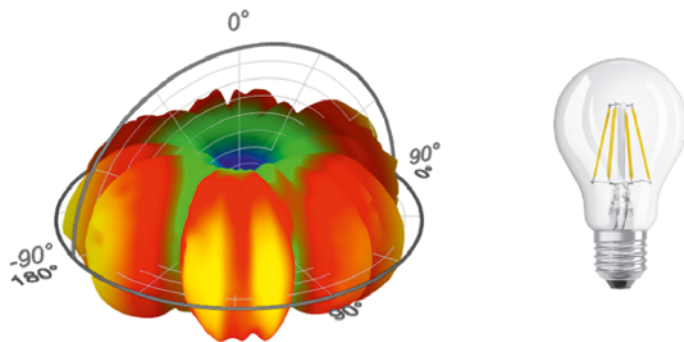
7.5 Spatial Radiation Characteristics

The many different packages and types of LEDs generate different spatial radiation characteristics. Precise knowledge of the angle-dependent distribution of radiation is necessary for some applications. For example, a full-color (red, green, blue) LED display may appear white when observed at a normal angle if all three colors are illuminated simultaneously. However, if the LEDs have a different spatial distribution of radiation for the individual colors, a color change may occur when the display is observed off axis.

Luminous intensity distributions

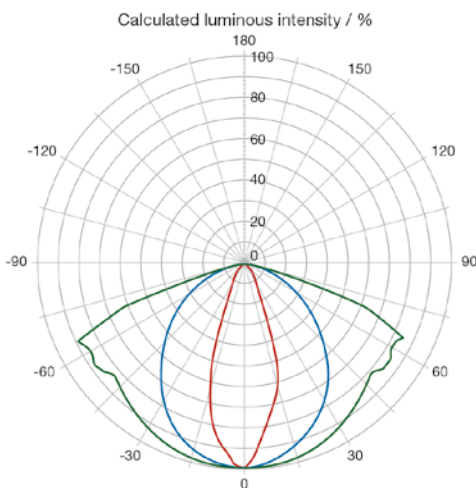
Characterizing luminous intensity distributions of LEDs and SSL sources is a pure photometric measurement task that can be performed by a goniometer unit used together with a spectroradiometer or photometer. A photometer allows very fast “on-the-fly” measurements and is recommended for pure photometric measurements and time-critical test sequences. Spectroradiometers offer the distinct advantage that all characteristics – radiometric, colorimetric and photometric – can be determined with maximum precision. Nevertheless, goniospectroradiometers have longer measurement times.

Figure 72:
Luminous intensity distribution in 3D representation (left) of a filament LED bulb (right).
The spatial radiation characteristic of the 6 filaments are clearly visible.



Luminous intensity is measured in the far-field (maintaining the photometric distance, see Section 7.2) for different azimuth and elevation angles. Using a C, γ coordinate system, leads to a complete spatial radiation pattern of luminous intensity (luminous intensity distribution). As an example refer to the luminous intensity distribution in 3D representation of a filament LED bulb (Figure 72). A single profile generated by scanning the γ angle is also known as a luminous intensity distribution curve of a single C-plane. An example of different luminous intensity distribution curves gives the radial plot of Figure 73. A source with near-Lambertian distribution (blue curve), a narrow-angled source (red curve) and an LED with distinct intensity shape for special applications (green curve) are shown. In general, different display options for spatial radiation patterns such as radial, semi-radial, Cartesian, spherical and 3D are commonly used for data evaluation.

Figure 73:
Different luminous intensity distribution curves displayed in a radial plot.



The data generated in goniophotometry can be used in lighting simulation programs. Lighting fixture manufacturers and others are using two different types of file format for specification of luminaire photometry, especially luminous

intensity distributions from light sources. One is the Illuminating Engineering Society (IES) standard and the other is the EULUMDAT data file format. The file extension is .ies and .ldt, respectively. The IES-standard is defined in the document LM-63-02 [43]. The EULUMDAT format is the European equivalent to the IES file format.

Colorimetric spatial radiation patterns

Colorimetric spatial radiation characteristics can only be measured using a gonirospectroradiometer (or a gonio-colorimeter, but this filter-based method is not recommended for absolute measurement of color quantities). With a gonirospectroradiometer, all relevant color information such as color coordinates, dominant wavelength, color temperature, color rendering index, etc. can be recorded simultaneously in an angular resolved measurement. Analyzing a potential angular variation of colorimetric quantities is important for LED manufacturers, as well as for module and luminaire manufacturers. For example, the color coordinates of a white LED often show a significant blue shift at certain viewing angles because the light path through the yellow phosphor is angle dependent (see Figure 74).

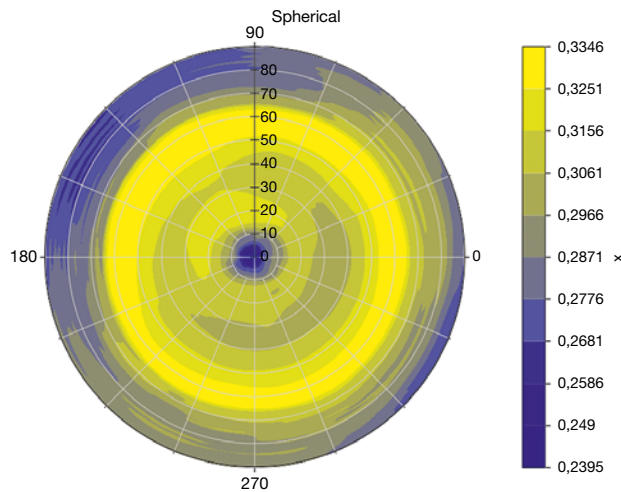
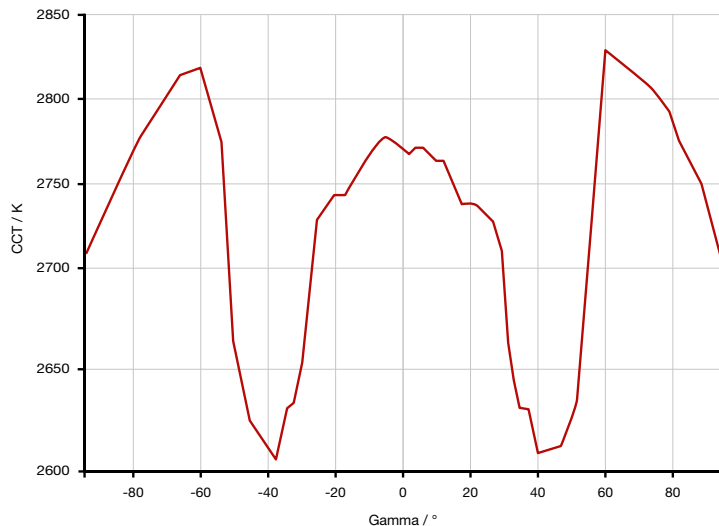


Figure 74:
Color coordinate x of an angle-dependent measurement of a white LED in a spherical plot. A significant blue shift is seen in the center and edges of the beam.

Significant variations of correlated color temperature with angle can be observed for LED modules. Figure 75 shows the angular profile of CCT variations for an LED module in a Cartesian plot.

Figure 75:
CCT variations with angle for an LED module.



Typical measurement times

The measurement of angular-resolved photometric or colorimetric distributions can be very time-consuming. The measurement time depends greatly on the details of the measurement. The type of detector used, the characteristics of the sample and the anticipated resolution contribute to the time a user has to invest. Although it is impossible to give a reliable answer to the question of measurement time for all cases, typical times can be estimated [44]. The basic idea is to analyze the behavior of two typical sources, one with a broad, and one with a narrow luminous intensity distribution.

To cover the contribution of the detector, both sources are measured using a photometer, a spectroradiometer with a fixed integration time and a spectroradiometer in autoranging mode. The fixed integration time is set by adjusting the spectroradiometer near saturation at the angle with highest signal level. The autoranging measurement will adjust the integration time of the spectroradiometer automatically during the angular scan (each change in integration time must follow a dark current measurement). Obviously, this procedure is the slowest.

To cover the aspect of anticipated resolution, the deviation of the measurement result to the “real” value of luminous flux is evaluated for measurements using different angular increments.

The results are summarized in Figure 76. The upper half and the lower half of the figure correspond to a single C-plane scan of samples having a broad and a narrow angular distribution, respectively. The left side shows the measurement time in minutes versus the angular increment used. An on-the-fly measurement is clearly the fastest measurement and with approximately 15 seconds per C-plane nearly independent of the resolution used. Both measurements with the spectroradiometer (fixed integration time and autoranging) show a

similar behavior. The measurement time rises steeply as a finer resolution is approached. From these measurements recommendations for the anticipated resolution and also an estimation of measurement time can be given. Since a narrow angular distribution leads to a rise in the deviation of luminous flux with increments $> 2^\circ$ - 3° , a scanning increment of approximately 2° is the optimum choice. If the task is to measure such a source with a spectroradiometer, the recommendation would be to use a fixed integration time (the deviation is nearly the same for fixed integration time and for autoranging). From the lower left plot in Figure 76, one can estimate a measurement time of 2.5 minutes per C-plane for this increment. A measurement of 16 C-planes in this configuration would therefore last approximately 40 minutes.

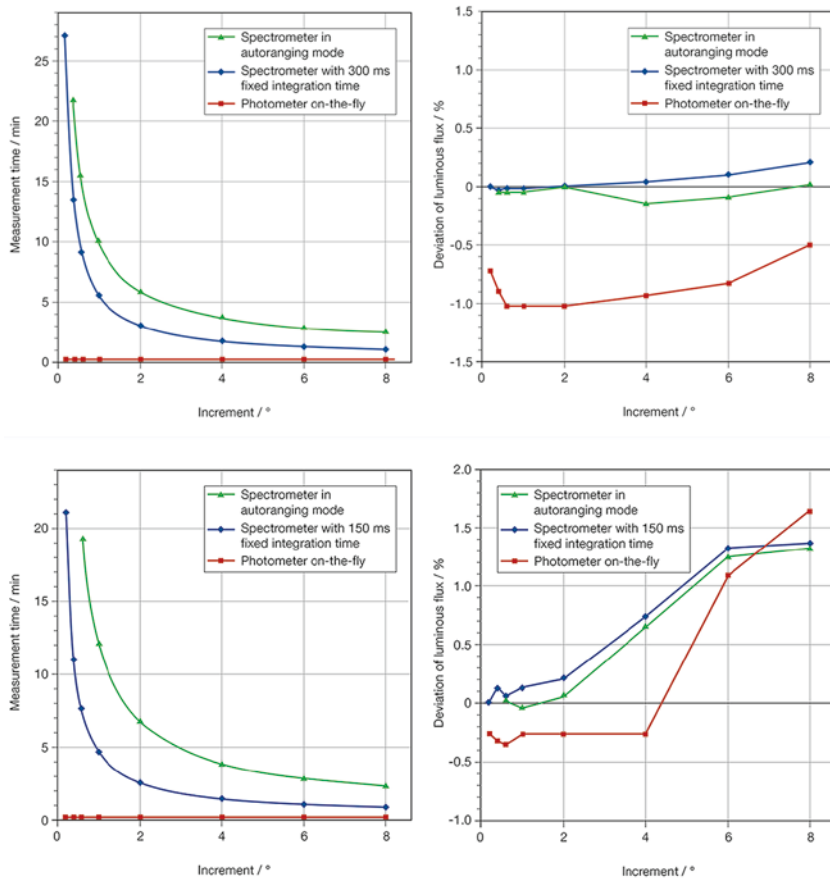


Figure 76:
Results of an analysis to estimate typical measurement times. The upper half corresponds to a source having a broad angular distribution. The lower half corresponds to a narrow distribution. The left side shows the result of measuring time versus used angular increment of one C-plane. Deviations of luminous flux with angular increment are shown on the right hand side.

7.6 Uniformity and Glare

Uniformity

The definition of luminance uniformity (or non-uniformity) often depends on application. For displays, uniformity with respect to position on the display and angle to the display are required [45]. In general uniformity is defined as:

$$\mathcal{U} = 100\% \cdot \frac{L_{\min}}{L_{\max}}$$

And non-uniformity as:

$$\mathcal{N} = 100\% \cdot \left(1 - \frac{L_{\min}}{L_{\max}}\right) = 100\% \cdot \left(\frac{L_{\max} - L_{\min}}{L_{\max}}\right)$$

For SSL general lighting, the uniformity of irradiance is important but often the luminance uniformity is not considered. This is changing, with several groups working on definitions of uniformity that can be generally applied. However, the above definition is inadequate as the locations of L_{\min} and L_{\max} are irrelevant. This means that the panels in Figure 77 have the same uniformity because they have the same L_{\min} and L_{\max} .

Figure 77:
Example panels illustrating problems in the definition of uniformity for SSL general lighting. Both panels have the same uniformity.



Clearly, the eye perceives these as different uniformity because it is sensitive to the rate of change of luminance and not just their absolute values. Several possible methods for describing uniformity based on frequency or values over a specific pattern are currently under discussion, but none are standard as yet.

Glare

When bright sources such as the sun or its reflection in water are in a person's field of view, they can affect the ability to see the other details of a scene. Glare is generally divided into two types: disability glare and discomfort glare.

Disability glare is the reduction in visibility caused by intense light sources in the field of view, but is not necessarily uncomfortable. In fact, some lighting designs deliberately create disability glare to add "sparkle" to a scene.

Discomfort glare is the sensation of annoyance or even pain induced by excessively bright sources. Both types of glare are subjective and vary from person to person. However, there is a general increase in sensitivity to glare with age.

For indoor sources the most commonly employed measure of discomfort glare is the CIE unified glare rating, UGR. It is defined [46] [47] as:

$$UGR = 8 \cdot \log_{10} \left(\frac{0.25}{L_b} \cdot \sum \frac{L^2 \cdot \omega}{p^2} \right)$$

Where L_b is the background luminance [cd/m^2].

L is the luminance [cd/m^2] of the luminous parts of each luminaire in the direction of the observer's eye.

ω is the solid angle [sr] of the luminous parts of each luminaire at the observer's eye.

p is the Guth position index (displacement from the line of sight) for each luminaire.

8 Discussion of Sample Measurements with Error Analysis

This section discusses possible sources of error in LED and SSL measurements. Examples are used to show the influence of optical and electronic properties of a spectrometer on measurement accuracy. It emerges that the quality of the spectrometer and calibration is highly important. Furthermore, parameters other than the contributions of a spectroradiometer that might influence measurement accuracy are discussed.

8.1 Effects of the Dynamic Measuring Range

The dynamic measuring range of a spectrometer is determined by its electronic and optical properties.

The electronic dynamic range is given by the quantum well depth of the CCD, but limited on the low signal level end by the accuracy and the number of digitalization steps of the A/D converter and the low-noise performance of the amplifier. Another limitation for low signal levels is given by the dark noise of the CCD induced by thermal noise, external radiation and stray currents. The optical dynamic range is determined by the stray light properties of the monochromator or spectrograph. Measurements on a red LED are used as an example to demonstrate the influence of the dynamic measuring range (see Figure 78).

Figure 78:
Three measurements of a red LED as a relative logarithmic representation with different dynamic measuring ranges (10^2 , $10^{2.5}$ and $10^{3.5}$). The black line corresponds to the CIE color matching function $\bar{x}(\lambda)$.

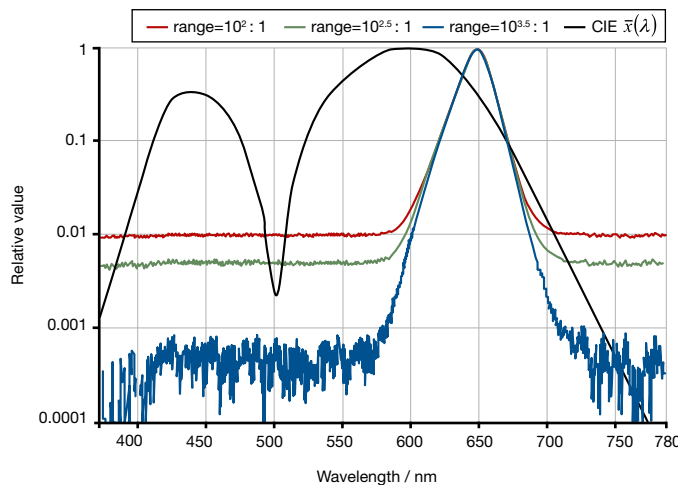


Table 10 lists the relevant measurement results of the spectra shown in Figure 78. Correlation between measured color values and the corresponding dynamic measuring range can be clearly seen. The stray light and noise in the spectral range from 380 nm to approximately 570 nm (where the actual spectrum of the LED begins) contributes more to calculating the color coordinates as the dynamic measuring range decreases (becomes poorer). The optical and electronic dynamic range of the spectrometer must be at least one order of magnitude greater than the range covered by the weighting curves to prevent this performance artifact exerting an influence on the chromaticity values.

Dynamic range	x	y	Purity
10^2	0.6402	0.2957	81 %
$10^{2.5}$	0.6721	0.2918	89 %
$10^{3.5}$	0.7088	0.2873	99 %

Table 10:
Measurement results
of the example spectra
of a red LED shown in
Figure 78.

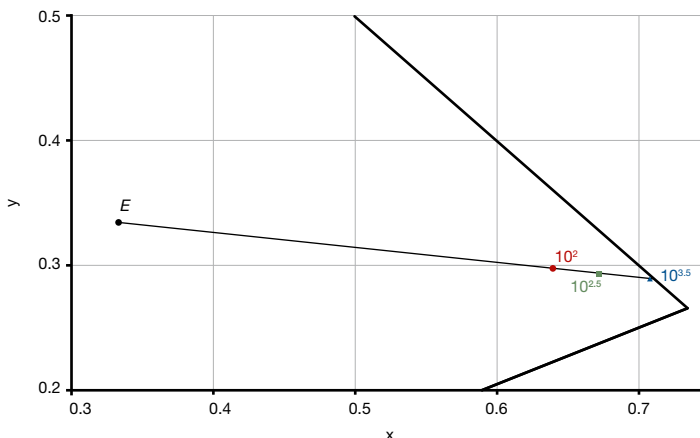


Figure 79:
Color coordinates from
Table 10 are indicated
in this section of the CIE
1931 x,y chromaticity
diagram (the blue triangle
corresponds to the
color coordinates of the
measurement with 99 %
purity, the green square
to 89 % purity and the
red circle to 81 % purity).

Values of purity lower than 99 % measured for red (GaAs) LEDs that should actually be located (almost) on the monochromatic locus (refer to Figure 79), are nearly always an indication of a poor dynamic measuring range [48].

8.2 Influence of Stray Light on White LEDs

This section will focus on the question of stray light rejection and the effects of stray light on the measurement accuracy for white LEDs. Stray light in this context is a property of the spectrometer and should not be confused with ambient or background light. An introduction to stray light and stray light correction of array spectrometers has already been given in Section 5.4.

There are different methods of determining stray light performance of a spectrometer. The following procedure provides the most useful information

for a spectroradiometer: Light from a halogen lamp²² is launched into the spectrometer through a yellow filter with a cut-off wavelength of 455 nm. The yellow filter has absorption of 6 orders of magnitude below this wavelength and hence radiation detected below this cut-off wavelength must be caused by stray light artifacts from the monochromator or spectrograph.

Figure 80:

Results of stray light tests from three different spectrometers. The blue curve was determined using a scanning spectrometer and turquoise and red curves using two different array spectrometers. The spectrum of a halogen lamp is also indicated (green curve) for reference. All curves were normalized at 480 nm.

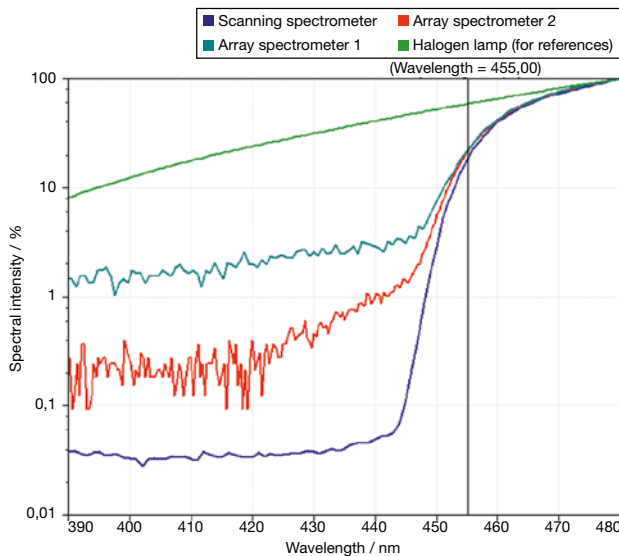


Figure 80 shows curves from the three different spectrometer types used in the stray light test described above. The curve with the best stray light rejection was measured using a scanning spectrometer and the other two curves were measured using array spectrometers of different quality. The cut-off wavelength at 455 nm is marked by a cursor.

Erroneous calibration caused by stray light

Section 5.5.2 on calibration of array spectroradiometers described how a Planckian radiator with a color temperature of approximately 3000 K and maximum intensity in the near infrared range is used for spectral calibration. At blue and UV wavelengths there is much less intensity and hence the calibrations are susceptible to stray light. This is compounded by lower responsivity of the spectroradiometer (see also the left side of Figure 41 on page 52) at these wavelengths, leading to many decades between the highest and lowest signals.

Stray light is caused by scattering of light so in an array spectrometer it no longer falls on the correct pixel but is detected at some other pixels. For instance, if blue light components are weak compared to the rest of the

²² The spectrum of halogen lamps is close to that of Planckian radiators.

spectrum and the CCD is more sensitive to other wavelengths, then scattered “other wavelength” light will reach the “blue” pixels and add significant signal. Since the signal does not come entirely from the calibration lamp at the blue wavelength indicated, the calibration factor will contain a stray light error.

If the same type of source is being measured, i.e. a tungsten halogen lamp similar to the calibration lamp, the measurement also contains the same stray light error and the two errors cancel each other out. However, if the source being measured differs spectrally from the calibration lamp as virtually all LEDs do, the errors do not cancel each other out and can bias intensity and color results.

Measurement errors resulting from stray light

Stray light errors are normally associated with low signal levels in the presence of higher signals at other wavelengths. This is seen in Figure 81 at short wavelengths. However, the stray light in the calibration can lead to incorrect values of the blue peak in white LEDs, even though there is high signal from the LED. Where both signals are strong the effect is usually insignificant. The different weighting of the blue and yellow peak caused by the calibration stray light will lead to wrong results of the color values of the LED.

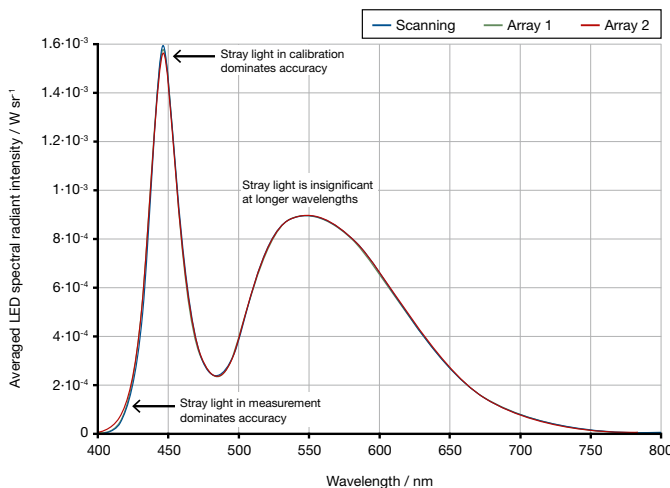


Figure 81:
Effect of stray light on
spectral calibrations and
measurements.

Scanning spectroradiometers generally obtain the correct result because of their sufficient stray light rejection. Measurements with array spectrometers can give rise to substantial deviations depending on the quality of the spectrometer (see Table 11).

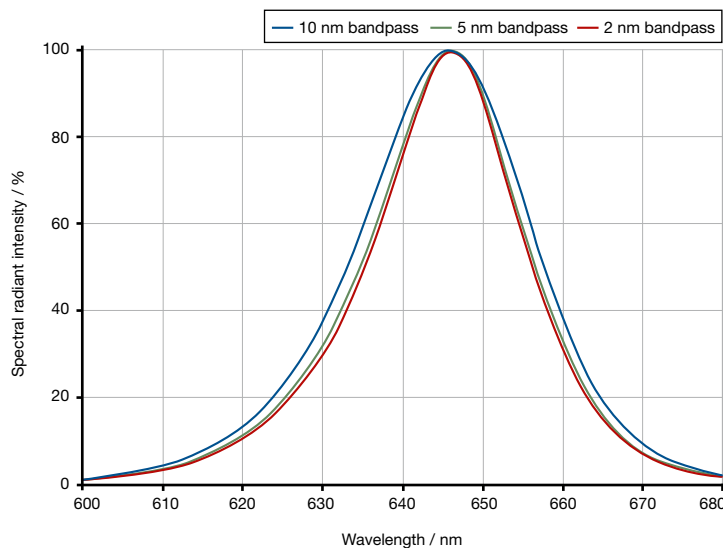
Spectrometer	x		y	
Scanning	0.3169	$\Delta x_{\text{scanning}}$	0.3425	$\Delta y_{\text{scanning}}$
Array spectrometer 1	0.3174	0.0005	0.3435	0.0010
Array spectrometer 2	0.3173	0.0004	0.3444	0.0019

Table 11:
Results of color
coordinates for the three
spectroradiometers
measured in Figure 81.

8.3 Influence of Bandpass

The bandpass determines the spectral resolving power of the spectrometer. The measurement result of a spectroradiometer is always a convolution of the spectrometer bandpass with the actual spectrum of the light source. Provided that the spectrum of the light source is significantly wider than the spectral resolving power, e.g. in a halogen lamp, the measured spectrum also corresponds to the actual spectrum of the light source. Conversely, the measured full width at half maximum (FWHM) will correspond to the bandpass for a very narrow laser line.

Figure 82:
Spectral power distributions of the same red LED, measured at different spectral resolutions. Differences in the convolution of the spectrometer bandpass with the actual spectrum of the light source are clearly visible. Influence of measurement results shows Table 12.



Although the centroid wavelength remains virtually the same within the scope of the measuring accuracy, the measured FWHM increases substantially with a bandpass of 5 nm or more. The increase in FWHM causes a shift in the dominant wavelength of up to 1 nm for large slits. Wrong color coordinates leading to a change in the dominant wavelength will be calculated by widening the spectrum.

Figure 82 and Table 12 show how different bandpass functions affect the measuring results of a red LED with a spectral bandwidth of 20 nm full width at half maximum. Although the centroid wavelength remains virtually the same within the scope of the measuring accuracy, the measured FWHM increases substantially with a bandpass of 5 nm or more. The increase in FWHM causes a shift in the dominant wavelength of up to 1 nm for large slits. Wrong color coordinates leading to a change in the dominant wavelength will be calculated by widening the spectrum.

Bandpass [nm]	$\lambda_{\text{dom.}}$ [nm]		λ_c [nm]		FWHM [nm]	
0.5	634.17	$\Delta_{0.5\text{nmBP}}$	644.71	$\Delta_{0.5\text{nmBP}}$	20.75	$\Delta_{0.5\text{nmBP}}$
1	634.15	0.02	644.59	0.12	20.80	0.05
2	634.13	0.04	644.62	0.09	20.95	0.20
5	633.91	0.26	644.56	0.15	21.82	1.07
10	633.26	0.91	644.43	0.28	24.49	3.74

A description of how this behavior can be explained in theoretical terms can be found in [49]. The interaction between the spectrum and the resulting color coordinates is modeled on a mathematical formulation. This analysis shows that the dominant wavelength in certain spectral ranges – below 480 nm and above 590 nm – is heavily influenced by the spectral width of the measured LED spectrum. However, practical measurements show less dependence than the mathematical model because the bandpass does not contribute fully to the measured FWHM [50].

A recommendation for the spectral resolution of a spectrometer used for SSL measurements can be derived from these experiments. The bandpass should be approximately 20 % of the FWHM of the LED for measurements of narrow band LEDs, i.e. should not significantly exceed 3 nm.

8.4 Performance Indices

The CIE developed performance indices for photometers [51]. Those indices that are applicable to using array spectroradiometers in photometric measurements can be applied to instrument performance. In addition, the CIE technical committee 2-51 is preparing a report for publication that extends these indices to specific performance requirements of array spectroradiometers. Although not yet published, these include amongst others the indices listed in Table 13.

Name of Index	Group	Symbol	Description
Directional Response Index	Imaging input optics	$f_{2,g}$	Luminance in the field of measurement is not constant
Surround Field Index	Imaging input optics	$f_{2,u}$	Surrounding area is of different luminance
Polarization Dependence Index	Imaging input optics	f_8	Specular reflections and certain luminaires may cause light to be polarized
Focusing Distance Index	Imaging input optics	f_{12}	Measuring scenes where a large depth of field is required
Response Uniformity Index	Imaging input optics / Diffuser and integrating sphere input optics	f_9	Non-uniform distribution of light over sensitive area of detector

Table 12:
Measurements of dominant wavelength, centroid wavelength and spectral bandwidth of a red LED obtained with different spectral resolutions.

Table 13:
Possible performance indices for array spectrometers.

Name of Index	Group	Symbol	Description
Directional Response Index	Diffuser and integrating sphere input optics	f_2	Cosine correction of the measurement head for light under non-normal angles
Spectral Broadening Index	All array spectroradiometers	f_{31}	Effects of bandpass when measuring narrow peaks such as LEDs
Stray Light Index	All array spectroradiometers	f_{32}	A general comparative performance with respect to spectral stray light
Fixed Integration Time Linearity Index	All array spectroradiometers	$f_{3,1}$	The linearity at fixed integration time, using a variable source intensity
Fixed Source Intensity Linearity Index	All array spectroradiometers	$f_{3,2}$	Linearity at fixed source intensity, using a variable integration time

8.5 External Influences

There are a number of other parameters apart from the spectrometer that influence the measuring accuracy of LEDs. Amongst others, these are the quality of the current source, design aspects of the test socket, the precise mechanical setup and the stabilization of the DUT before measurement.

8.5.1 Accuracy and Stability of the Current Source

Usually the luminous flux and intensity are directly proportional with the driving current of the LED. However, at higher currents the efficiency droop of LEDs results in a slower increase of the intensity with the current. Changes of the driving current will also lead to shifts of the LED's spectral emission which in turn may affect the luminous flux or intensity output. This can even compensate the power droop of the LED. For example, in the case of a red LED a change of 1.1 % in the value for luminous intensity was observed for a deviation of 1 % in the current. Figure 83 shows a typical dependency of the luminous flux vs. forward current for a white LED.

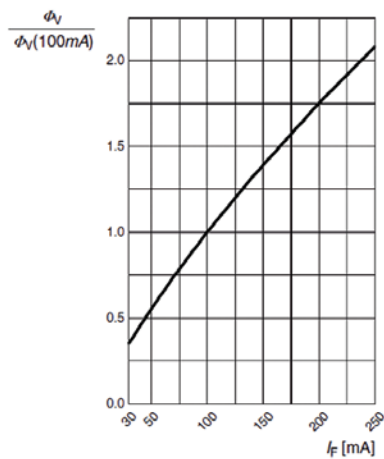


Figure 83:
Relative luminous flux
versus forward current
for a white LED.
Source: OSRAM Opto
Semiconductors GmbH,
Duris P5 datasheet

In any case, inaccurate settings or instabilities of the LED's forward current will directly result in measurement errors. For accurate and reproducible measurements it is essential to use accurate and calibrated power supplies. As with spectroradiometers, the calibration of the power supply or source meter unit should be updated at regular intervals. If lower quality power supplies are used, it is advisable to monitor the value of the current using a separate multi-meter.

Monitoring of the forward voltage of an LED should be done using a four-wire connecting scheme to allow for separate power and sense lines (see Figure 84). This requires test sockets with separate leads and sense points to the electrodes of the LED.

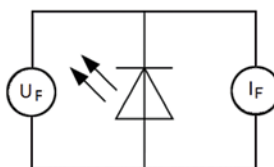


Figure 84:
Four-wire connecting
scheme.

8.5.2 Quality of LED Test Sockets

Test sockets as shown in Figure 85 are needed to hold the LEDs in a defined position and contact them electrically. A clamping mechanism is used to hold the LEDs in place, since gluing or soldering the LEDs would make an exchange difficult and the LEDs could not be reused after testing.

Figure 85:
Precision test sockets for different LED packages.
The socket should permit identical alignment of the mechanical axis.



As a critical component in the LED measurement setup, the test sockets must be carefully designed to avoid shadowing effects of the clamps and reflections from the socket. Especially for small SMD LED types, such effects can easily lead to measurement errors of 10 to 15 % or more.

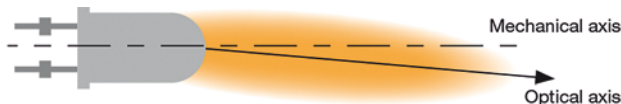
The mounting mechanism always holds the LED package in the same way and thus permits identical alignment of the mechanical axis for all LEDs with the same package. This setup follows the CIE recommendation that the mechanical axis of the LED, rather than the optical axis, should be taken as the reference axis for measurements.

The test sockets will also affect the thermal properties of the LED. The clamps, electrodes and the material of the test socket will influence the heat management of the LED leading to different stabilization times and operating temperatures of the LEDs. Test sockets must be designed to minimize such effects, but they can never be excluded completely.

8.5.3 Precision of Mechanical Setup

The precise mechanical setup plays an important role. Most measurements of single LEDs follow the CIE127-2007 recommendations. These define the mechanical setup with the tip of the LED positioned on the optical axis of the test setup in a defined distance from the detector. Mechanical and optical axes of a LED may not be coincident (see Figure 86). A reproducible test setup is a prerequisite for precise measurements in order to guarantee that the detector always sees the same section of the radiation cone. CIE therefore recommends to align the mechanical axis of the LED parallel to the optical axis of the test setup.

Figure 86:
Example of a skewed radiation cone of an LED.



This type of measurement results in 3 potential sources of errors: distance from the detector, lateral position from the optical axis and angular tilt between optical and mechanical axis.

Distance errors

Under the widely used condition B for measurement of averaged LED intensity, a distance from the LED tip to the diffuser of precisely 100 mm is required. The inverse square law²³ means that a deviation of just 2 millimeters leads to an error of approximately $\pm 4\%$. This effect applies to (almost) all LEDs independently of the individual spatial emission characteristics.

Often the same LED test socket can be used with several LED types of different outer dimensions. To accommodate LEDs with different body lengths some sockets use adjustment or spacer rings to ensure the correct position of the LEDs. However, it is the responsibility of the user to use the correct spacer with the LED under test. As shown in Figure 87, if a wrong spacer is used the distance will be wrong and errors of several percent will result easily.

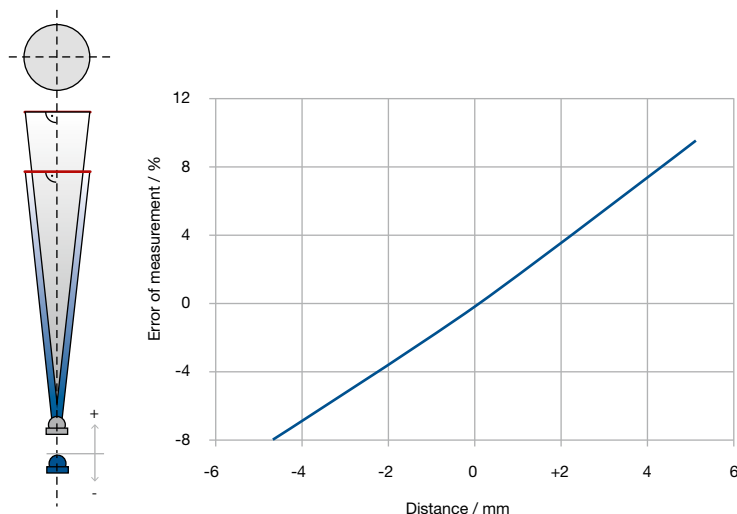


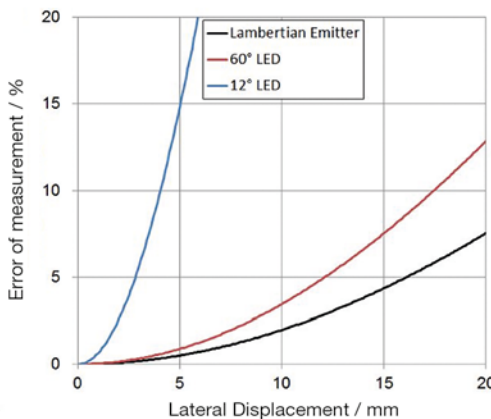
Figure 87:
Schematic (left) to illustrate distance deviations of an LED from the detector. Measurement errors (right) resulting from distance deviations.

Lateral displacement

The lateral displacement of the LED from the optical axis is usually less critical than a distance deviation since mechanical tolerances allow the LEDs to be positioned with an accuracy of a few tenth of a millimeter at the optical axis. Figure 88 shows the optical setup and the theoretical deviations for a Lambertian emitter and LEDs with 60° and 12° emission cone (FWHM). Even for narrow angled LEDs such errors are usually less than 1 % with standard test sockets. Real deviations, however, depend on the exact emission pattern of the LED and the cosine correction of the detector. Furthermore, the detectors are usually equipped with internal baffles which limit the field-of-view in order to reduce stray light effects. Such baffles will cause shadowing effects on the detector once the LED is at the edge of the field-of-view.

²³ Note that the inverse square law does not apply exactly to LEDs.

Figure 88:
Schematic (left) illustrating a lateral deviation of an LED from the optical axis. Measurement errors (right) resulting from the lateral deviation.



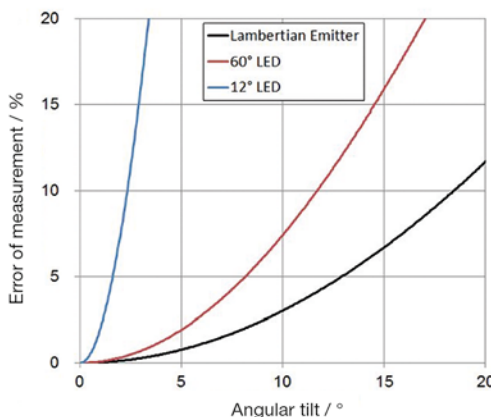
Angular tilt

More critical than lateral displacement is an angular tilt of the LED in the socket. This is often hard to control since the LED is clamped from the side, while at the same time the electrical contacts press against the bottom of the LEDs. If the socket is not carefully engineered a tilt of the LED may occur.

This may be of considerable importance particularly in the case of clear, narrow-angled LEDs. Reproducible alignment of the mechanical axis of the LED must be guaranteed to achieve a reproducible measurement of luminous intensity. An investigation revealed that a precision socket guarantees a standard deviation of 0.1 % for measurements on a green narrow-angled LED while simpler test sockets without special lock mechanisms show standard deviations of 3 % and more.

Figure 89 shows the effect of an angular tilt of the LED calculated for the same LEDs as in Figure 88. Again, the effect is much more critical for narrow angle LEDs than for wide angle devices. As with the lateral displacements, the effect of a tilt angle depends a lot on the emission pattern of the LED and must be evaluated individually for each LED type.

Figure 89:
Schematic (left) illustrating an angular tilt of an LED. Measurement errors (right) resulting from the angular tilt.



8.5.4 Temperature Stabilization Time

Single LEDs

For single LEDs (see Section 4.2 on page 32) the stabilization time exerts a considerable influence. Figure 24 on page 33 shows that beginning the measurement at different points in time can lead to results differing by several percent. The stabilization time depends on the LED type and external conditions such as ambient temperature. It is therefore not possible to give a general recommendation for the time of measurement. The forward voltage of the LED gives an indication of when the steady state has been attained at which point the measurement can be performed.

LED lamps and luminaires

For LED lamps and luminaires stabilization is strongly related to thermal equilibrium of the components. CIE S025 and LM-79 give detailed guidelines how to stabilize the DUT before measurement. Differentiation is made regarding the type of DUT (lamp or luminaire) and regarding the application of a pre-burning procedure²⁴. This differentiation leads to 5 different stabilization routines which are applicable. They differ with respect to pre-operation time (amount of time with the DUT burning before the actual monitored stabilization time), the monitored stabilization time, the allowed relative deviation of light output and electrical power and the allowed time-out (time after which the DUT can be tested, although it shows a higher deviation than allowed during the monitored time)²⁵. Table 14 shows a summary of the five stabilization routines. As an example, a lamp that has not been pre-burned should be stabilized according to CIE S025 as follows:

The lamp should be operated for at least 30 minutes (15 minutes pre-operation time and at least 15 minutes monitored stabilization time). The lamp is considered as stable if the relative difference of maximum and minimum readings of light output and electrical power observed over the last 15 minutes is less than 0.5 % of the minimum reading. If stabilization conditions are not achieved within 45 minutes the measurement can be performed and the observed fluctuations must be reported.

²⁴ It has to be demonstrated that a pre-burning procedure produces the same stabilized condition as when using the normal procedure.

²⁵ Only valid for DUTs that show random fluctuations. The observed fluctuations must be reported. A slow decrease of gradient of the measured value is not a random fluctuation and the stabilization criteria have to be met.

Table 14:
The five stabilization routines for LED lamps and luminaires according to CIE S025, EN 13032-4 and IES LM-79.

Stabilization routine	Observables	Pre-operation time [min]	Monitored stabilization time [min]	Relative deviation [%]	Time-out [min]
CIE S025 / EN 13032-4 for lamps	Simultaneous observation of light output and electrical power at least at an interval of 1 minute	15	15	0.5	45
CIE S025 / EN 13032-4 for luminaires		15	15	0.5	150
CIE S025 / EN 13032-4 for pre-burned lamps		0	15	0.5	45
CIE S025 / EN 13032-4 for pre-burned luminaires		0	15	0.5	150
IES LM-79		0	30	0.5	120

LED modules

For LED modules²⁶ thermal measurement conditions are given by their performance temperature measured at the t_p -point. The t_p -point is a location on the surface of the LED module specified by the manufacturer. The temperature of an LED module can be adjusted using active cooling methods described in Section 4.3.2 on page 36. The module is considered to be stable if it maintains the specified performance temperature within $\pm 1^\circ\text{C}$ for 15 minutes.

²⁶ LED light engines incorporating heat sinks are not modules with regard to stabilization time. Such DUTs should be measured following the procedure of LED lamps and luminaires.

9 LED Measurements in the Production Line

During the manufacturing process of LEDs electrical, optical and thermal measurements are performed directly in the production line. The results are used to discard malfunctioning LEDs and to sort out good LEDs. The sorting process is called binning. Each bin contains LEDs of similar electro-optical properties that can be tightly specified despite large variation across a whole production batch. Furthermore, the results of in-line tests are used to adjust processes directly during manufacturing to enhance production yield.

This chapter will address important aspects of the optical measurements in a production environment.

9.1 Conditions and Requirements in Production Testing

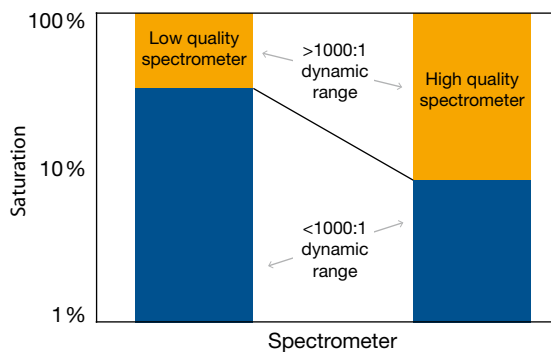
The main difference compared to a laboratory measurement is speed. Measuring 10 LEDs in 1 second is the order of magnitude for a production line. That means there is no time to move the LED into the perfect position for measurement. For example, for a luminous flux setup with an integrating sphere the LED is usually placed in 2π position, often even a few millimeters outside the sphere radius. Part of the emission meant to be detected will not enter the sphere and is lost. Additionally, the imperfect light shielding against the environment allows ambient light to enter the sphere and disturb the measurement. Therefore, a correction of the measurement result is required in most cases.

The optical measurement devices must match the speed of the mechanical handling equipment in a production line. The measurement times must be as short as possible. Space for the optical probes and devices is very limited, due to mechanic or pneumatic picking, contacting and visual inspection equipment. Temperature and humidity in the production area are not always controlled well, and can fluctuate significantly. The test equipment is also exposed to vibrations and has to endure uninterrupted operation. Thus, the conditions in a production environment require highly robust and low maintenance devices, while the measurements must still be accurate and reproducible.

Measuring LED parameters in production is particularly challenging for metrology equipment because CIE-compliant measuring adapters have very low light throughput and a wide diversity of LEDs are to be tested (ranging from low power to High Power devices). At the same time, short measuring times are necessary to ensure a high throughput in terms of units per hour (UPH).

Photometers and color measuring heads performing integral measurements are generally used in production control because measuring speed is a critical factor for this application. The basic problems with photometers have been discussed in Section 5.2. The quality of photometer based testers in production was reasonable for testing green, yellow and red LEDs, but not sufficient for blue and white LEDs.

Figure 90:
Line-integration of area detectors results in a less noisy signal allowing a larger measurement range due to a good signal-to-noise ratio even at low detector saturation.



The robust construction of array spectrometers and their short measuring time make them ideal for production applications. The biggest disadvantage has been the lack of sensitivity and dynamic range. Integration times in the millisecond range could not be obtained using an optical probe compliant with CIE recommendation B (refer to Section 7.3) and a diffusor that reduced light throughput dramatically.

The development of a new generation of high quality back-illuminated CCD sensors with a significant increase of sensitivity overcomes this restriction. The increase in effective full quantum well capacity by using an area detector head increases the usable dynamic range and reduces the noise level, which means better reproducibility (see Figure 90). Array spectroradiometers with this type of detector are preferable for production control of LEDs, because they eliminate the disadvantages of photometers without compromising measurement time.

9.2 Process Integration

All measurement equipment in a production line is automatic and must communicate to interact. A mechanical handling machine for the LEDs will initiate a series of measurements whenever an LED is placed in testing position. This is triggered by a Start of Test (SOT) signal. The set of measurement devices, probes and software performing the tests are called a tester unit. After receiving the SOT signal, the tester will trigger a series of electrical tests by a sourcemeter, as well as one or more optical tests by a spectroradiometer while lighting up the LED at an operating current. These test jobs are different

for each LED type and manufacturer. The tester will evaluate the measurement quantities according to a process tailored for the test job. The result is a bin number for the LED. The information is transmitted along with the End of Test (EOT) signal to the handling machine. Now the cycle starts again with receiving the next SOT signal. The flow diagram is shown in Figure 91 for an arbitrary device under test (DUT).

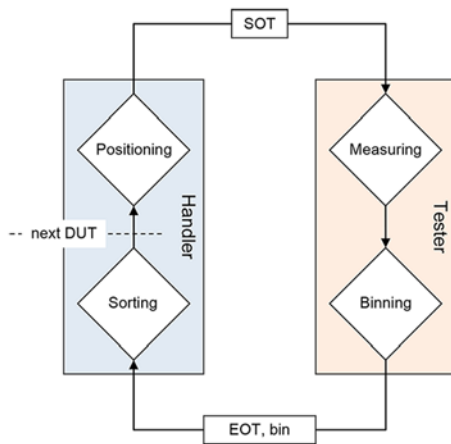


Figure 91:
Process diagram for the interaction of a mechanical handling machine and a tester unit.

Signals can be exchanged either by analog electrical signals or by a protocol for digital signals. Each manufacturer uses its own language for the machines; there is no standard. However, most machines can communicate via TTL gates. The foremost network protocol used is TCP/IP. If the tester software is integrated into the handling machine software it can be a library (dll or dylib) with the basic tester functions.

To improve an existing production line or establish a new one, a key to success is correct measurement data with good absolute accuracy. By logging the spectrum for each device under test, all optical measurement data can be derived from this raw data. For the regular production flow, the level of data logging can be decreased again to the level required for quality control and feedback to earlier production steps.

9.3 Reproducibility and Accuracy

9.3.1 Correction Factors

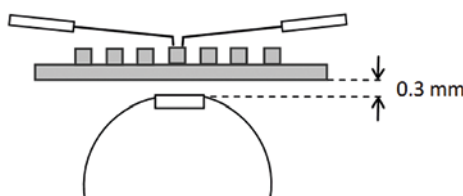
Systematic errors of a measurement need to be known and subtracted to obtain correct results. Sources of systematic errors are discussed in this section.

The luminous flux of an LED is strongly dependent on the junction temperature and can fluctuate by several percent when changing the junction temperature by 10 K. For an exemplary type of white LEDs with blue chip and phosphor the color drift of the x and y coordinates is in the range of 0.02 for 10 K²⁷. This is about 50 K for the CCT. For this chapter, we will disregard the obstacles of measuring and controlling the LED temperature and concern ourselves with the optical measurements for a certain electrical driving. A common practice is to test low power LEDs at room temperature, typically 25 °C, and High Power LEDs at 85 °C, which is within the range of normal operating temperatures. They are operated only a few milliseconds for testing, which does not allow them to reach thermal equilibrium.

Non-equilibrium correction

The emission of a typical LED requires a stabilization time of up to one minute (see Section 4.2). LEDs in the production line are lit up for about 10 ms, meaning they are operated in a non-equilibrium state. Making a simplified assumption the ambient temperature, the soldering point temperature and junction temperature are equal. The values measured under these test conditions differ from those obtained under steady state conditions. However, there is generally a reproducible correlation between the two test conditions (see Section 4.3). The manufacturers of LEDs are responsible for determining this correction function for individual LED types and taking it into account in production testing.

Figure 92:
Typical wafer probing set-up for the measurement of flip chip LEDs in a constant distance to the integrating sphere port.



²⁷ The color shift depends on the type of LED. Another example would be InGaAlP based red LEDs which exhibit a stronger color drift with temperature.

Measurement geometry correction

A measurement of light sources at a certain distance from the side port of the integrating sphere is always a measurement of partial luminous flux and not total luminous flux (see also Figure 92). The opening angle and distance of the source must be fixed and the same as during calibration. If present, the protective window or dome is part of the calibrated device and should not be removed or exchanged. The same holds true for luminous intensity adapters. If the calibration is done properly, only a small correction is required, owing to the individual emission directions of the LEDs tested.

Inter-line correction

For LEDs from different production lines the optical measurement results should be comparable for the same bin type. This is achieved by applying a further correction to match the measurement results of several testers. This will not increase the accuracy, but rather decrease it to some extent. Only the spread of the measurement results between different production lines becomes smaller (see also Figure 93).

9.3.2 Reproducibility

For small bin sizes – small in terms of the allowed range of each optical property – it is important to measure with a high precision, so that the deviations between LEDs in one bin are small. This does not mean that the measurement is accurate. Rather than the precision, the reproducibility of a measurement is used to quantify the performance of a spectroradiometer in LED production. The reproducibility is inherent to the measurement device and the measurement conditions. A low noise spectroradiometer is required for a sufficient signal-to-noise ratio. The power source must be sufficiently stable (refer to Section 8.5.1 for details). The measurement should be shielded from ambient light and mechanical vibrations altering the measurement geometry randomly (see Section 8.5.3).

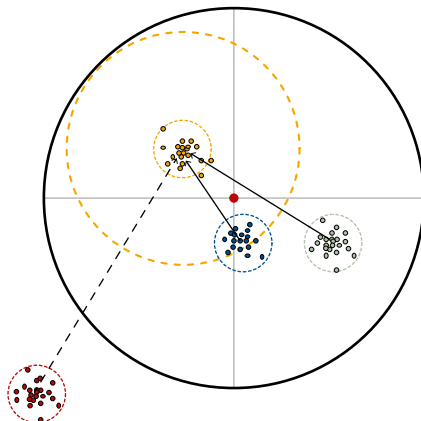
9.3.3 Accuracy

For specifying the bins correctly, the measurement must be accurate. Best accuracy can only be achieved by a proper calibration that can be traced to national calibration standards. Accuracy is important for reference measurements in the laboratory, but also for the production line equipment. By measuring sample LEDs (so called golden samples) in the laboratory, the assumed true value is transferred to the production line by measuring the same samples there and applying a correction. However, a large correction

will impose major problems on the measurement quality of the production line equipment. The response of spectroradiometers is not linear with intensity, and derived values like color coordinates and CCT are hard to correct. The correction should be as small as possible which can only be achieved by using accurate and well-calibrated equipment.

Figure 93 illustrates the corrections applied for testers in production (blue, red and green dots) to match a reference laboratory measurement of a golden sample (yellow dots). The inner dashed circles give the precision of the measurements. The outer dashed circles give the accuracy, it is indicated only for the yellow dots (laboratory), omitted for the blue, red and green dots (production). The true value (light red dot in the center) must be within the accuracy. While a small correction of the production values towards the laboratory values are acceptable (black arrows for the blue and green dots) a large correction will lead to unpredictable measurement deviations (black dashed arrow for the red dots).

Figure 93:
Illustration of corrections applied for testers in production (blue, red and green dots) to match a reference laboratory measurement of a golden sample (yellow dots).



The best practice is therefore to have accurate, precise and well-calibrated spectroradiometers in the production line and laboratory. The laboratory spectroradiometers are checked and recalibrated frequently to a reference standard that can be traced back to national calibration standards. For bringing the production line equipment to the values measured in the laboratory, only a small correction within acceptable limits is necessary.

Not maintaining a good level of calibration will cause problems if LEDs from different factories or from different dates of production are combined during storage or delivery. LEDs in bins that are labeled alike will have different properties, and the quality and trueness to the specifications of a combined batch will be insufficient (see Figure 94 for example).

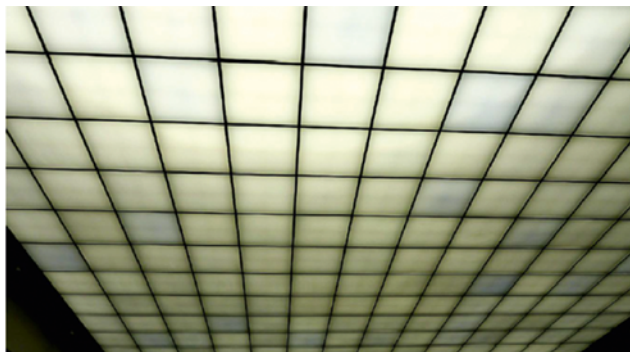


Figure 94:
Not maintaining a good level of calibration will cause problems if LEDs from different factories or from different dates of production are combined during storage or delivery.

9.4 Field Installation of Measurement Equipment

The production process of LEDs in which optical testing plays a role, can be divided into several steps. Typically, it starts with a wafer that is cut into dies. The dies are then separated changing their optical properties to some extent. For phosphor-converted white LEDs a phosphor is selected and brought onto the die by a variety of techniques. For multi-chip white LEDs three or four dies are combined. Finally, the contacted die is packaged creating an individual LED. Depending on the final use the LEDs can be mounted on circuit boards and combined with driving electronics and possibly lenses and reflectors.

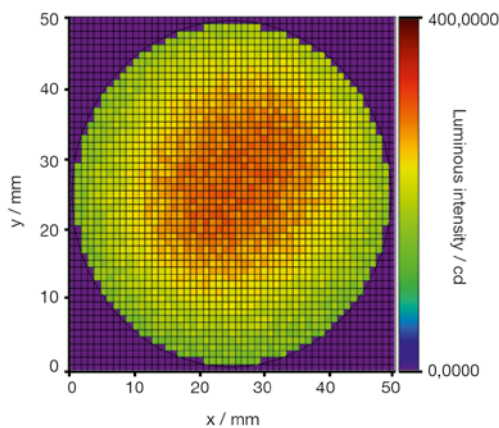
By knowing the photopic properties of the wafer, phosphor, die and package or even modules one can learn which process steps lead to which changes. This knowledge can be applied to influence the binning statistics actively and to increase the yield by bringing out-of-spec chips back into the specifications by using the correct phosphor or phosphor density/mixture, respectively.

The following sections give an insight into typical optical measurements along the four main production steps. There will be a focus on white LEDs as they are in the highest demand and of the highest complexity.

9.4.1 Wafer Level Testing

Measuring at the wafer stage of manufacturing [52] is necessary for an early decision on further process steps to optimize the yield. Wafer must be handled in clean room environments. The probing is usually done by mounting an integrating sphere over the wafer. The unseparated die to be tested is moved beneath the center of the sphere port and contacted by probing needles (see Figure 96). This procedure is described first, followed by more uncommon or novel methods. The optical tests performed are usually for luminous flux and dominant wavelength. A typical result is a so-called wafer map as shown in Figure 95.

Figure 95:
A wafer map (plot of x and y coordinate on the wafer indicating differences in luminous intensity) is a typical result of wafer level testing.



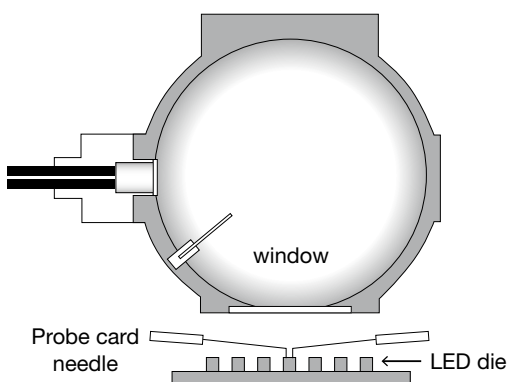
Wafer testing with an integrating sphere

Due to tight space requirements for wafer probing applications and the general production requirement of short optical integration times, the design of the integrating sphere should be as small as needed, but as big as possible. For wafer probing, a sphere with a diameter of 100 mm meets best the requirement for the accuracy and size restriction. Spheres with diameters between 75 mm and 250 mm can be used as well, depending on the application. The maximum size of the entrance port should be 1/3 of the sphere diameter, e.g. 33 mm measurement opening for a 100 mm sphere.

A fused silica window may be used to protect the barium sulfate coating of the sphere against contamination and environmental influences (see Figure 96).

In the case of flip chip LEDs, the sphere can be placed from the bottom side very close to the LED. As illustrated in Figure 92, the distance can be less than 1 mm and it is in good approximation a measurement of total luminous flux.

Figure 96:
Integrating sphere with 100 mm diameter for wafer-probing with a protective fused silica window as a dust protection.



Wafer testing with an optical fiber

A special development for taking fast measurements on wafers without hindering visual inspection is the fiber-optic probe. It features particularly high light throughput and permits very short measuring times, even for low light levels. The compact design enables it to be positioned between the alignment microscope and wafer without compromising the visual inspection of the contacts (see Figure 97). This probe is usually calibrated for illuminance or for known measurement distances for luminous intensity but not for luminous flux. A diffusor can be mounted for measuring with less dependency on the coupling angle. The fiber-optic probe can also be used for measuring separated dies.

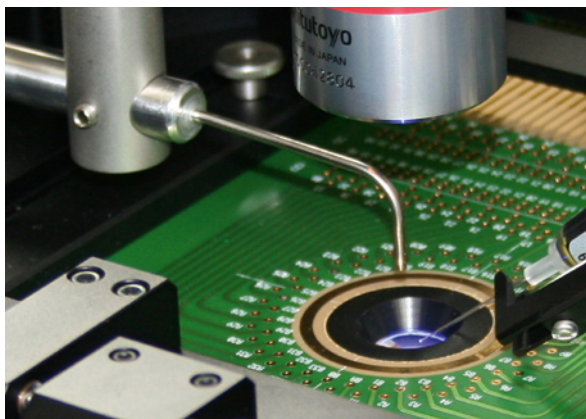


Figure 97:
Fiber-optic probe for fast
wafer inspection.
Source: Cascade
Microtech GmbH

Wafer testing through a microscope

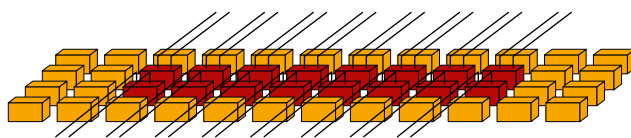
A technique often seen on wafer probing systems is the optical measurement of LED dies through a microscope. This is an imaging procedure which actually provides luminance measurement. It is not representative for measurements of luminous flux or intensity and is not recommended. Errors due to the inhomogeneity of the emitting chip may occur. Also, color deviations are likely because of spectral transmission of the microscope.

Multi-channel probing

Multiple die testing can speed up wafer probing. To minimize time consuming mechanical prober movements 4, 8, 16 or more dies are contacted at the same time and the optical probe is positioned above this group of dies (see Figure 98). The current source is multiplexed and switched subsequently from die to die. The multi-channel testing procedure thus permits the successive measurement of multiple dies without moving the wafer. Since the electrical switching times (one or a few milliseconds) are significantly shorter than the stopping times of the probes (ten or a few ten milliseconds), the throughput increases. Multiplexed multi-channel testing can increase the throughput by a typical factor of four. A faster method is to use multiple channel current

sources that operate in parallel. The electrical testing of all contacted dies is performed at the same instance of time. The optical testing still has to be performed subsequently, to be able to differentiate the emission.

Figure 98:
Contacting the LED chips on the wafer with a special probe card for multi-die testing.



9.4.2 Die Level Testing

The electro-optical properties of a die change when it is isolated from the wafer. Testing at the level of isolated dies is the next step for optical and electrical testing along the production process. For low quality LEDs this step can be omitted, but is essential for the process control required to manufacture high quality LEDs.

The separation can be performed by placing the sliced wafer on a so-called blue tape, a polymer foil. When the foil is expanded, the dies separate. Special taping probers can contact the dies in this stage for electrical and optical testing. Another possibility is to pick up one die after the other by a mechanical handler machine and place it on a separate test table for contacting and testing it with a special die prober.

The optical tests performed are usually for luminous flux and dominant wavelength. In case of white LEDs using the conversion of blue chip emission by a phosphor, the results can be used to select the phosphor for the desired white. This, of course, requires knowing and measuring the optical properties of the phosphors as well. One possibility when using phosphor plates on the die is to have a handling machine for optically testing and binning the phosphor plates as well. Then a bin of phosphor plates can be matched to a bin of dies to create the desired emission properties. To vary the optical properties of the phosphor a mixture of two, three, or even more phosphors can be used. Another possibility is to deposit the phosphor directly on the chip. Phosphor matching in this case requires a very good knowledge of the deposition process to give the ability to control it via phosphor concentrations and mixtures.

The optical probe of choice is an integrating sphere with a diameter of 75 mm to 150 mm, depending on the space restrictions of the handling machine and LED type.

9.4.3 Package Level Testing

Testing packaged LEDs involves slightly different observables compared to wafer and die testing. Assuming white LEDs, the optical tests performed are usually for luminous flux, luminous intensity, color coordinates and CCT. A development for general lighting applications is using the CRI as a variable for binning. Some LED manufacturers specify LED batches with either a typical CRI value, meaning there can be any spread around that value, or with a minimum CRI value, so all LEDs will be better, but probably most will be very close to the specified CRI.

Compared to the die, the directionality of the light output has changed for packaged LEDs due to contacting, packaging and light propagation in the phosphor or in an attached lens. Manufacturing tolerances lead to a very individual directional characteristic.

Package testing with an integrating sphere

For luminous flux measurements, a directional characteristic means that the emitted light will hit the inner surface of the integrating sphere on a different position for each individual LED. Inhomogeneities in the sphere coating and shape will lead to deviations in the measurement which makes it very important to use a high-quality sphere. Otherwise reproducibility will decrease significantly. Good integrating spheres for production applications have no optical elements opposite to the entrance port for the LED. There is only the unaltered barium sulfate-coated wall, which minimizes the directional dependence of the measurement value.

If the sphere can be positioned very close to the LED, or the LED is mechanically positioned just inside the (theoretical) sphere radius, a fused silica dome must be used for protecting the sphere from dust and loose parts entering it. A flat window would reduce the effective acceptance angle, due to the large reflections under large entry angles. For an illustration of this geometry, refer to Figure 99 on the left side. When there is a larger distance between the LED package and sphere, a flat glass window can be used.

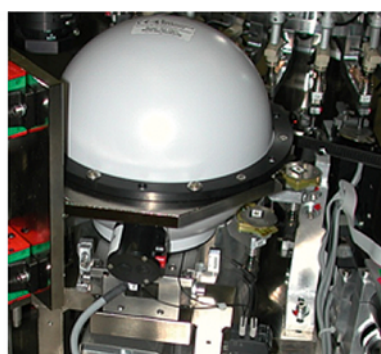
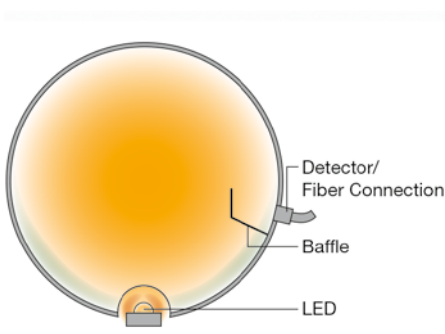


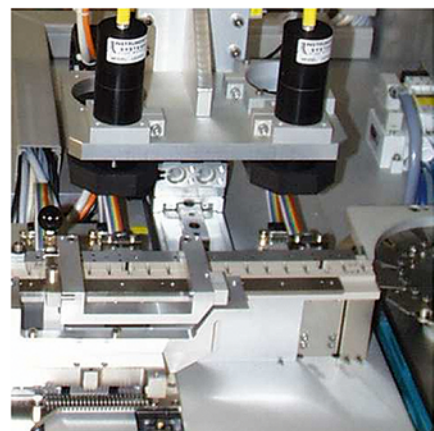
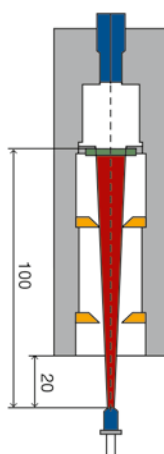
Figure 99:
Integrating sphere with 100 mm diameter for package testing with a fused silica dome (left). The integrating sphere is designed for minimum directional sensitivity due to an undisturbed hemisphere opposing the entrance port. The right side shows an example of a setup in a package handler.

Source: Ismeca Europe Semiconductor S.A.

Package testing with an LED intensity adapter

Luminous intensity is measured by a special adapter that contains a cosine-corrected detector with a well-defined detection area. The LED sample is placed at a given distance from the adapter, but is not in contact with the latter in order not to obscure the movement by the handler. As a consequence, light can enter and escape the volume between emitter and detector, and will influence the measurement value. The detector is shielded by the adapter housing and two baffles (see the schematic drawing on the left side of Figure 100), but still a reasonably dark measurement environment is recommended. The entrance port for the adapter can be protected from dust by a window. The transmittance of the optical fiber connecting the measurement adapter with the spectrometer should be independent of the fiber movement induced by the mechanical vibrations in the handling system.

Figure 100:
Schematic drawing (left) of a CIE condition B averaged LED intensity adapter used in production applications. The optical measurement setup integrated in a sorting system for LEDs (right). The optical probes are LED adapters for luminous intensity measurements.
Source: OSRAM Opto Semiconductors GmbH



Because of the high directionality of LED emission, precise positioning of the mechanical LED axis along the optical axis of the intensity probe is important (refer to Section 8.5.3). Even small deviations can lead to a noticeable difference in measured luminous intensity. This places exacting demands on the accuracy of mechanical positioning systems.

9.4.4 Module Level Testing

Having a module that includes the electrical driving and possibly contains multiple LEDs adds a level of complexity to testing. The optical properties depend on the driving of the LED. This means that testing can only be for a specific driving condition, or the test must be performed while automatically altering the driving, thus gaining information for a smart driving in the end application.

If the module contains several LEDs, testing each LED individually will lead to a number of bins equal to the single LED bin number raised by the power of the number of LEDs in that module. Therefore, measuring all LEDs together is a way to simplify the binning. This can be achieved either by powering up all LEDs at the same instance, or by measuring one by one and combining the spectra by software, then deriving the colorimetric and photometric quantities.

Because the driving electronics is now part of the measured system, the lumen per watt can be a parameter for binning that is important to many end customers.

The dimensions and light output of modules require larger integrating spheres that will range between 250 mm and 1,000 mm. The testing principles are the same as described in the above sections.

9.4.5 OLED Testing

The younger field of OLED mass production has many similarities in terms of optical measurements. The larger emitting area requires bigger integrating spheres for measuring the luminous flux in 2π configuration. The luminance is measured by optical probes uncommon in traditional LED manufacturing, but well-established in display production testing. Areal luminance homogeneity and angular characterization can rely on equipment from display measurement as well. Going into detail on these measurements would exceed the range of this handbook.

Optical testing procedures for OLED production are not yet established. Modules from different manufacturers point to common properties that are worth measuring [53]. An attempt at listing properties likely to be tested in mature production lines is given in Table 15.

Measured value	LED	OLED
Luminous flux	Yes	Yes
Radiant flux	Non-visible (UV/NIR) LEDs	No
Luminous intensity	Yes	No
Radiant intensity	Non-visible (UV/NIR) LEDs	No
Luminance	No	Yes
Luminance homogeneity	No	Yes
Color coordinates	Yes	Yes
CCT	Yes	Yes
CRI	Yes	Yes
Dominant wavelength	Monochrome, e.g. blue chip for white LEDs	Rarely
Centroid wavelength	Rarely	No
Angular characterization	Only in laboratory	Laboratory and pilot lines

Table 15:
Summary of measured properties for LEDs and OLEDs.

List of Figures

Figure 1:	Diagram showing the $V(\lambda)$ curve (human eye response function)	3
Figure 2:	Luminous flux and radiant power geometry. Light from the source spreads in all directions. The flux is the amount of optical radiation (or visible light) emitted by the source	4
Figure 3:	Luminous intensity and radiant intensity geometry. Radiation from a point source emitted per unit solid angle in a given direction	4
Figure 4:	The solid angle $d\Omega$ of a cone is defined as the ratio of the area dA cut out on a spherical surface to the square of the radius r of the sphere	5
Figure 5:	Illuminance and irradiance geometry. A surface of area dA is illuminated by a light source or ambient light	5
Figure 6:	Luminance and radiance geometry. Light is emitted from a surface of area dA in a solid angle $d\Omega$ and a given direction	6
Figure 7:	Drawing to illustrate the cosine law. The apparent area becomes smaller as the angle increases with respect to normal	8
Figure 8:	A radial plot showing examples of sources: Isotropic (same intensity in all directions), Lambertian (the value changes with the cosine of the angle) and an LED with 60° view angle	8
Figure 9:	The CIE 2 ° observer color matching functions (left). 1931 CIE chromaticity diagram for 2 ° observer (right)	10
Figure 10:	MacAdam ellipses shown at 10x actual size	11
Figure 11:	CIE 1960 u v diagram, showing a test source chromaticity and the corresponding chromaticity on the Planckian locus joined by the iso-temperature line (Fit). The temperature of the blackbody on the Planckian locus is the correlated color temperature. D_{uv} is the distance between the chromaticities ...	12
Figure 12:	Examples of source spectra with their respective CCT	13
Figure 13:	Representation of the rendering of the 14 tiles used in color rendering index calculations under test and reference sources. A white tile is included for reference	14
Figure 14:	The spectral power distribution of a blue LED and relevant spectral parameters	15
Figure 15:	Relationship between set value, expanded measurement uncertainty, tolerance and acceptance interval. The definition of the tolerance interval does not take account of measurement uncertainty	21

Figure 16: CIE x y chromaticity diagram showing the 8 Energy Star® nominal quadrangles defining color binning. The red line is the Planckian locus. 7-step MacAdam ellipses are shown as a reference.	
Source: ANSI_NEMA_ANSLG C78.377-2008	22
Figure 17: Smooth transition of daylight and blackbody locus as reference source for TM-30-15	24
Figure 18: Gamut Index versus Fidelity Index with approximate limits for the combination of the two measures (left). The shaded areas are not achievable for practicable white light sources and for sources on the Planckian locus. Color Vector Graphic for a typical white light source (right). Tangential vectors to the reference circle indicate hue shifts. Vectors pointing inside/ outside the reference circle indicate decreased/increased saturation for the specific color	25
Figure 19: Fidelity Index R_f by hue bin	25
Figure 20: Example of socketable, circular LED modules designed according to Zhaga Book 5. Source: GE Lighting Infusion LED module product family.....	27
Figure 21: Luminance property evaluation areas according to Zhaga Book 3	27
Figure 22: Illustration of different package designs for LEDs. From left to right: Traditional Dual In-line Package (DIP), Surface Mount Device (SMD) LED, Chip on Board (COB) LED module	31
Figure 23: Comparison of a conventional lateral chip design with bonding wires and Flip-Chip Technology	32
Figure 24: Stabilization period of a white LED. Time [s] is entered on the x-axis and luminous intensity [cd] and corresponding forward voltage [V] on the y-axes	33
Figure 25: Thermal model of a simple LED package. “Hot” is the p-n junction of the LED and “cold” is the thermal connection to the outside world	34
Figure 26: Simulated cumulative structure function (thermal capacitance versus thermal resistance) and the discrete structure for the package in Figure 25	35
Figure 27: Simulated dynamic impedance for the package in Figure 25. The red curve describes an active cooling and the blue curve a passive air-cooling system. Outside the package, the active cooled system stabilizes much faster	36
Figure 28: Thermal map of a High Power LED connected to an active cooling system	36

Figure 29:	Laboratory test setup for High Power LEDs. A TEC test adapter providing active temperature control is mounted at the side port of a medium sized integrating sphere	38
Figure 30:	Spectrum of a typical phosphor-converted white LED. The blue luminescence peak at 460 nm and the broad phosphorescence peak from approximately 500 to 650 nm are clearly visible. The resulting spectrum is perceived as white by the human eye	39
Figure 31:	Example of a 3 chip RGB LED spectrum	40
Figure 32:	Basic structure of an OLED. Graded hetero-junction devices are gaining in popularity owing to their inherently higher efficiency	42
Figure 33:	Spectra of different sources used in general lighting. The OLED spectrum is generally broadband, showing some structure due to several types of organic layers	43
Figure 34:	A simple photometer with a filter stack (left) and with a mosaic filter (right). Practical mosaic detectors may include some stack elements as well as mosaic elements	44
Figure 35:	Five real photometers and the perfect photometer responses with wavelength (top). The ratio of each photometer response to the perfect response (bottom). Source: Swiss Federal Institute for Metrology (METAS). Data courtesy of P. Blattner	45
Figure 36:	Measured spectral mismatch factor versus f_i' for white light sources. The black < shape shows an “error” equal to the f_i' value (top). The same but for single color LED sources, concentrating only on the “best” photometers (bottom). The LED sources range from 465 nm (deep blue data points) to 643 nm (deep red data points). Source: Swiss Federal Institute for Metrology (METAS). Data courtesy of P. Blattner	46
Figure 37:	Ideal $V(\lambda)$ photometer response (green) and measured response (yellow) of a real photometer, radiation from standard Illuminant A (grey), and a blue and red LED (blue and red respectively)	48
Figure 38:	Illustration of a scanning single monochromator. Light entering through the entrance slit is dispersed by a rotating grating assembly. After passing the exit slit the light is directed to different detectors that can be semiconductor detectors made of silicon, InGaAs, lead sulfide and lead selenide or photomultipliers	49

Figure 39:	Illustration of a double monochromator designed in subtractive configuration (the spectrometers residual dispersion at the exit slit is zero)	50
Figure 40:	Design of an array spectroradiometer in crossed Czerny-Turner construction	51
Figure 41:	Spectral response function of a back-thinned CCD and a front-illuminated CCD (left). Spectrum of a white LED on a logarithmic scale (right). The better performance of a back-thinned CCD is clearly visible	52
Figure 42:	Typical stray light matrix of an array spectroradiometer.	54
Figure 43:	Sensitivity curves with and without stray light correction and their relationship	54
Figure 44:	Logarithmic display of the spectra of an UVA- and UVC-LED without (red) and with stray light correction (blue). For reference, the LEDs are measured with a double monochromator (green)	55
Figure 45:	Spectrum of a HgAr lamp used for wavelength calibration	56
Figure 46:	Typical LED calibration source with control electronics (left). The temperature of the LED is actively stabilized using a Peltier element. Stability of intensity over a period of 60 hours (right). The deviation is smaller than 0.1 %	58
Figure 47:	Sensitivity curves of the CIE 1931 2 ° standard observer	59
Figure 48:	Deviation of dominant wavelength for a four- and six-filter colorimeter (top). Deviation of color coordinate x and y for a six-filter colorimeter using different test LED sources (bottom)	59
Figure 49:	Test setup for measuring spatial radiation characteristics of mid-sized light sources using an imaging colorimeter	61
Figure 50:	Image of luminous intensity distribution curves measured with the test setup shown in Figure 49	61
Figure 51:	Cross-section of an integrating sphere and components	63
Figure 52:	Geometry of a circle (or sphere) for exchange factor calculations	64
Figure 53:	Typical reflectance of a BaSO ₄ coating	66
Figure 54:	Illustration of shadowing areas of lower and higher response of an integrating sphere with direct light baffles	67
Figure 55:	Sphere scanner map of an integrating sphere response shown from two different perspectives. Colors indicate the relative throughput (red = high, green = low, orange = average)	68
Figure 56:	Definition of the C , γ coordinate system. The in-plane angle γ and the half-plane angle φ is shown	69

- Figure 57:** The coordinate systems for type A, B and C goniometers 69
- Figure 58:** Schematic drawing of a moving-mirror goniometer 70
- Figure 59:** Working principle (left) and example setup for the realization of a turning detector type goniometer which maintains the designed burning position of the DUT (right) 71
- Figure 60:** Schematic drawing (top) and example realization of a turning luminaire goniometer (bottom) 72
- Figure 61:** Schematic working principle of the auxiliary photometer method. The movement of the C and γ axis of the turning luminaire goniometer define i orientations of the DUT in space. The readings f_i of the auxiliary photometer for the i orientations, divided by one reference value f_r measured in the designed operating position, serve as correction factors 73
- Figure 62:** Correction step 1 implies the connection of an auxiliary photometer and the recording of the photometer readings for the orientations of the DUT defined by the setting of the turning luminaire measurement. Correction step 2 features the geometric displacement of the hardware adapter in order to position the DUT in the intended burning position. The DUT is slid on an additional cantilever arm. The arm can then be tilted by 90°. With the help of the motorized C-axis of the goniometer, the DUT can be rotated in virtually any desired burning position 74
- Figure 63:** Application of the burning position correction method to high position dependencies induced by varying the supply voltage. The high deviations to the reference measurement could be corrected to around 1 % over the entire range. The corrected curve (blue) is in close proximity to the reference (grey) whereas the uncorrected curve (red) shows an increasing deviation with decreasing supply voltage 75
- Figure 64:** CIE recommended sphere geometries for all sources (left) and for sources with no backward emission (right) 77
- Figure 65:** A 1 m in diameter sphere (left) is ideal for measuring most LEDs and modules in the 4π and 2π recommended geometries. A 2 m sphere (right) is ideal for large luminaires and SSL products 77
- Figure 66:** Self-absorption spectra for two typical DUTs 78
- Figure 67:** Example of avoiding near-field absorption effects. The holder of the linear tube is placed as far away as possible from the light source and coated with a high-reflectance material 79
- Figure 68:** A rotatable 1 m sphere. Position-sensitive light sources can be measured in their designed operating position 79

Figure 69: Goniospectroradiometer with a compact light shielding enclosure. The DUT is moved instead of the detector. The angle φ is adjusted by rotating the LED about its mechanical axis and angle θ by pivoting about its tip	81
Figure 70: Intensity probe that conforms to the standard CIE condition B for 100 mm distance together with a precision test socket for mounting the LED. The test socket is inserted into the tube of the condition B adapter for measurement	83
Figure 71: Concept (left) and experimental realization (right) of partial LED flux	84
Figure 72: Luminous intensity distribution in 3D representation (left) of a filament LED bulb (right). The spatial radiation characteristic of the 6 filaments are clearly visible	86
Figure 73: Different luminous intensity distribution curves displayed in a radial plot	86
Figure 74: Color coordinate x of an angle-dependent measurement of a white LED in a spherical plot. A significant blue shift is seen in the center and edges of the beam	87
Figure 75: CCT variations with angle for an LED module	88
Figure 76: Results of an analysis to estimate typical measurement times. The upper half corresponds to a source having a broad angular distribution. The lower half corresponds to a narrow distribution. The left side shows the result of measuring time versus used angular increment of one C-plane. Deviations of luminous flux with angular increment are shown on the right hand side	89
Figure 77: Example panels illustrating problems in the definition of uniformity for SSL general lighting. Both panels have the same uniformity	90
Figure 78: Three measurements of a red LED as a relative logarithmic representation with different dynamic measuring ranges (10^2 , $10^{2.5}$ and $10^{3.5}$). The black line corresponds to the CIE color matching function $\bar{x}(\lambda)$	92
Figure 79: Color coordinates from Table 10 are indicated in this section of the CIE 1931 x y chromaticity diagram (the blue triangle corresponds to the color coordinates of the measurement with 99 % purity, the green square to 89 % purity and the red circle to 81 % purity)	93
Figure 80: Results of stray light tests from three different spectrometers. The blue curve was determined using a scanning spectrometer and turquoise and red curves using two different array spectrometers. The spectrum of a halogen lamp is also indicated (green curve) for reference. All curves were normalized at 480 nm	94

Figure 81:	Effect of stray light on spectral calibrations and measurements	95
Figure 82:	Spectral power distributions of the same red LED, measured at different spectral resolutions. Differences in the convolution of the spectrometer bandpass with the actual spectrum of the light source are clearly visible. Influence of measurement results shows Table 12	96
Figure 83:	Relative luminous flux versus forward current for a white LED. Source: OSRAM Opto Semiconductors GmbH, Duris P5 <i>datasheet</i>	99
Figure 84:	Four-wire connecting scheme	99
Figure 85:	Precision test sockets for different LED packages. The socket should permit identical alignment of the mechanical axis	100
Figure 86:	Example of a skewed radiation cone of an LED	100
Figure 87:	Schematic (left) to illustrate distance deviations of an LED from the detector. Measurement errors (right) resulting from distance deviations	101
Figure 88:	Schematic (left) illustrating a lateral deviation of an LED from the optical axis. Measurement errors (right) resulting from the lateral deviation	102
Figure 89:	Schematic (left) illustrating an angular tilt of an LED. Measurement errors (right) resulting from the angular tilt.....	102
Figure 90:	Line-integration of area detectors results in a less noisy signal allowing a larger measurement range due to a good signal-to-noise ratio even at low detector saturation	106
Figure 91:	Process diagram for the interaction of a mechanical handling machine and a tester unit	107
Figure 92:	Typical wafer probing set-up for the measurement of flip chip LEDs in a constant distance to the integrating sphere port	108
Figure 93:	Illustration of corrections applied for testers in production (blue, red and green dots) to match a reference laboratory measurement of a golden sample (yellow dots)	110
Figure 94:	Not maintaining a good level of calibration will cause problems if LEDs from different factories or from different dates of production are combined during storage or delivery	111
Figure 95:	A wafer map (plot of x and y coordinate on the wafer indicating differences in luminous intensity) is a typical result of wafer level testing	112
Figure 96:	Integrating sphere with 100 mm diameter for wafer-probing with a protective fused silica window as a dust protection	112

- Figure 97:** Fiber-optic probe for fast wafer inspection
Source: *Cascade Microtech GmbH* 113
- Figure 98:** Contacting the LED chips on the wafer with a special probe card for multi-die testing 114
- Figure 99:** Integrating sphere with 100 mm diameter for package testing with a fused silica dome (left). The integrating sphere is designed for minimum directional sensitivity due to an undisturbed hemisphere opposing the entrance port. The right side shows an example of a setup in a package handler.
Source: *Ismeca Europe Semiconductor S.A.* 115
- Figure 100:** Schematic drawing (left) of a CIE condition B averaged LED intensity adapter used in production applications. The optical measurement setup integrated in a sorting system for LEDs (right). The optical probes are LED adapters for luminous intensity measurements.
Source: *OSRAM Opto Semiconductors GmbH* 116

List of Tables

Table 1:	Important radiometric and photometric quantities	2
Table 2:	General classification of correlated color temperature and examples	12
Table 3:	The standard test conditions and tolerance intervals of CIE S025	19
Table 4:	Summary of special requirements defined by the CIE S025 standard for measuring instruments	20
Table 5:	Nominal CCT categories according to ANSI_NEMA C78.377-2008	23
Table 6:	Overview of the Book 1 to Book 18 published or in development by the Zhaga Consortium	26
Table 7:	Relative partial luminous flux tolerances from Zhaga Book 3. Ideal values of a Lambertian light source are given for reference ...	27
Table 8:	Summary of the most important selection criteria for array and scanning spectroradiometers	52
Table 9:	CIE recommendations for the concept of averaged LED intensity. The area of the detector is always 1 cm ² . The relevant solid angle is determined by the distance between the LED tip and the detector	83
Table 10:	Measurement results of the example spectra of a red LED shown in Figure 78	93
Table 11:	Results of color coordinates for the three spectroradiometers measured in Figure 81	95
Table 12:	Measurements of dominant wavelength, centroid wavelength and spectral bandwidth of a red LED obtained with different spectral resolutions	97
Table 13:	Possible performance indices for array spectrometers	97
Table 14:	The five stabilization routines for LED lamps and luminaires according to CIE S025, EN 13032-4 and IES LM-79	104
Table 15:	Summary of measured properties for LEDs and OLEDs	117

References

- [1] CIE Publication 069-1987, "Methods of Characterizing Illuminance Meters and Luminance Meters", 1987.
- [2] CIE Publication 015-2004, "Colorimetry, 3rd Edition", 2004.
- [3] G. Wyszecki and W. S. Stiles, "Color Science: Concepts and Methods, Quantitative Data and Formulae (2nd edition)", Wiley-Interscience, 2000.
- [4] CIE S 014-4/E:2007, "Colorimetry -Part 4: CIE 1976 L*a*b* Colour Space", 2007.
- [5] CIE Publication 013.3-1995, "Method of Measuring and Specifying Color Rendering Properties of Light Sources", 1995.
- [6] CIE 127-2007, "Measurement of LEDs", 2007.
- [7] IES LM-79-08, "Approved Method: Electrical and Photometric Measurements of Solid-State Lighting Products", 2008.
- [8] IESNA LM-78-07, "IESNA Approved Method for Total Luminous Flux Measurement of Lamps Using an Integrating Sphere Photometer", 2007.
- [9] CIE S025:2015, "Test Method for LED Lamps, LED Luminaires and LED Modules", 2015.
- [10] IES LM-80-08, "Approved Method: Measuring Lumen Maintenance of LED Light Sources", 2008.
- [11] IES TM-21-11, "Projecting Long Term Lumen Maintenance of LED Light Sources", 2011.
- [12] ENERGY STAR® Program Requirements Product Specification for Lamps (Light Bulbs). Eligibility Criteria Version 1.0, DRAFT 1, 2011.
- [13] ANSI_NEMA_ANSLG C78.377-2008, American National Standard for electric lamps "Specifications for the Chromaticity of Solid-State Lighting Products", 2008.
- [14] ENERGY STAR® Program Requirements for Integral LED Lamps - Partner Commitments, amended 3/22/2010.
- [15] CIE TC 1-69 "Color Rendition by White Light Sources".
- [16] IES TM-30-15 "IES Method for Evaluating Light Source Color Rendition", 2015.
- [17] IEC/TR 62732 Edition 1.0 2012-01, "Three-digit code for designation of colour rendering and correlated colour temperature", 2012.
- [18] ISO 9001:2008, "Quality management systems – Requirements", International Organization for Standardization, 2008.
- [19] ANSI/NCSL Z540.3, "Requirements for the Calibration of Measuring and Test Equipment", 2006.

- [20] ISO/IEC 17025, “General requirements for the competence of testing and calibration laboratories”, International Organization for Standardization, 2005.
- [21] S. Chhajeda et. al, “Junction temperature in light-emitting diodes assessed by different methods”, presented at SPIE Photonics West 2005.
- [22] L. Jayasinge, Y. Gu, N. Narendran, “Characterisation of thermal resistance coefficient of High Power LEDs”. Sixth International Conference on Solid-State Lighting, Proceedings of SPIE 6337, 63370V, 2006.
- [23] M. Rencz, V. Székely, “Structure function evaluation of stacked dies”, 20th IEEE SEMI-THERM Symposium, 2004.
- [24] M. Rencz, V. Székely, A. Morelli, C. Villa, “Determining partial thermal resistances with transient measurements and using the method to detect die attach discontinuities”, SEMITHERM, 2002.
- [25] Y. Ohno, “Spectral design considerations for white LED color rendering”, Optical Engineering 44 (11), 111302, 2005.
- [26] DIN EN 13032, page 36: Translation from the original German text: “The construction of some photometer heads can lead to significant dependence of the responsivity (including spectral responsivity) to the incidence-light position in the acceptance area.”, 2004.
- [27] Reproduced with permission from “Basic concept of Photometry”, P. Blattner, Presented at CIE Expert Symposium on Spectral and Imaging Methods for Photometry and Radiometry, 2010.
- [28] R. Young, K. Muray, C.F. Jones, “Quantifying photometric spectral mismatch uncertainties in LED measurements”, Proceedings of 2nd CIE Expert Symposium on LED Measurement, 2001.
- [29] G. Heidel, “Actual problems at the industrial optical measurement of LEDs”, Proceedings of the CIE LED Symposium 1997 on Standard Methods for Specifying and Measuring LED Characteristics, 1997.
- [30] CEI/IEC 62471, CIE S009:2002, “Photobiological safety of lamps and lamp systems”, 2006.
- [31] Y. Zong et al, “Simple spectral stray light correction method for array spectroradiometers”, Appl. Opt. 45, 1111-1119, 2006.
- [32] Đ. Konjhodžić, „Application of stray light corrected array spectroradiometers for UV measurements“, UV-News 11, 46-48, 2016.
- [33] R. Young, R. Häring, “Wavelength Calibration of Array Spectrometers”, Proceedings of CIE 27th Session, South Africa, Volume 1, Part 1, 2011.
- [34] G. Sauter, “LED radiation and measurement uncertainty”, CIE LED Workshop and Symposium, Vienna, 1997.
- [35] Đ. Konjhodžić, P. Khrustalev, R. Young, „Advanced Imaging Colorimetry“, Information Display Vol. 31 5/15, 36-40, 2015.

- [36] Đ. Konjhodžić, R. Distl, "Metrology for LED Lamps and Modules", Light & Engineering, 19(1), 2011.
- [37] IESNA LM-75-01, "Goniometer Types and Photometric Coordinates", 2001.
- [38] CIE 121-1996, "The Photometry and Goniophotometry of Luminaires", 1996.
- [39] CIE 070-1987, "The Measurement of Absolute Luminous Intensity Distributions", 1987.
- [40] G. Leschhorn, Đ. Konjhodžić, "Auxiliary photometer method for goniophotometric measurements", Laser and Photonics, 78-81, January 2016.
- [41] EU regulation Nr. 1194/2012 "Implementing Directive 2009/125/EC of the European Parliament and of the Council with regard to ecodesign requirements for directional lamps, light emitting diode lamps and related equipment", 2012.
- [42] EU regulation Nr. 874/2012 "Supplementing Directive 2010/30/EU of the European Parliament and of the Council with regard to energy labelling of electrical lamps and luminaires", 2012.
- [43] IES LM-63-02 (R2008), "ANSI Approved Standard File Format for Electronic Transfer of Photometric Data and Related Information", 2008.
- [44] G. Leschhorn, "Practical Estimation of Measurement Times in Goniospectroradiometry and Goniophotometry", LED professional Review Issue 47 Jan/Feb 2015, 2015.
- [45] ICDM/SID, "Information Display Measurements Standard", 2012.
- [46] CIE 117-1995, "Discomfort Glare in Interior Lighting", 1995.
- [47] CIE 190:2010, "Calculation and Presentation of Unified Glare Rating Tables for Indoor Lighting Luminaires", 2010.
- [48] P.A. Boynton, Y. Ohno, E.F. Kelley, "Interference-Filter Characterization of Spectroradiometers and Colorimeters", SID Intl. Symp. Digest. Tech. Papers 18, 1997.
- [49] C. Jones, "Colorimetry, chromaticity space and LEDs", CORM Meeting 1998.
- [50] Y. Ohno, "Colorimetric accuracies in spectroradiometry of LEDs", CORM Meeting 1999.
- [51] CIE S023/E:2013 "Characterization of the Performance of Illuminance Meters and Luminance Meters", 2013.
- [52] Đ. Konjhodžić, contribution to Technical Report from CIE TC 2-64, "High speed testing methods for LEDs", to be published by CIE.
- [53] T. Kawabata, Y. Ohno, "Optical measurements of OLED panels for lighting applications", Journal of Modern Optics, 2013.

About Instrument Systems

Founded by Richard Distl in Munich in 1986, Instrument Systems is today one of the world's leading manufacturers of high-precision array and scanning spectrometers as well as complex photometric systems. Our name stands for premium class, innovative products and outstanding expert knowledge in optical measurement technology. Specialized sales engineers can be relied on to provide a solution for even the most demanding measurement tasks, exactly tailored to the needs of our customers.

For many years Instrument Systems has been establishing global standards for spectroradiometric measurement in the LED industry. We are involved in standardization committees and associations such as DIN and CIE, and cooperate with the leading metrological institutes. Virtually all renowned companies in the automotive and aviation industry place their trust in our measurement systems for the qualification of lighting components and displays in the vehicle interior or cockpit. We place the focus of our product development on the use of our systems not only in laboratories but also in fast production tests.

Since 2012 we have been a member of the Konica-Minolta Group and benefit from an international network, supplemented by our experienced representatives. As a continuously growing, medium-sized technology company Instrument Systems stands for customer proximity and the highest level of reliability in product quality, service and support.



The Authors

Dr. Günther Leschhorn received his PhD in Physics during his work with the Max-Planck Institute of Quantum Optics in Munich, Germany. He specialized in the field of single molecule spectroscopy and ultra-fast laser interaction. He was a member of the Munich-Centre of Advanced Photonics, a cluster of excellence of the German Research Foundation and holds a stipend of the International Max-Planck Research School of Advanced Photon Science.

In 2011 he served as a post-doc at the University of Freiburg (Germany) and was heading a group interested in the field of quantum computation.

He joined Instrument Systems as product manager for Spectrometers, Spectroradiometry and Solid-State Lighting in 2012. Today he is head of the product management department of Instrument Systems.

Dr. Richard Young's interest and contributions to light measurement span over 40 years. Dr. Young was educated in England, where he received a B.A. honours degree and Ph.D. in Chemistry.

In 1983 he moved from academia to industry when joined Glen Creston Ltd. in London. In 1994 he relocated to the USA and joined Optronic Laboratories, Inc. where he was promoted to vice president at the end of 1994.

In 2010 he joined Instrument Systems as Chief Scientist. He is an active member of many CIE technical committees and chairs committees on array spectroradiometers and on spectroradiometry. Richard Young recently retired from his role as Chief Scientist and is now working as a consultant for Instrument Systems.

The Handbook of LED and SSL Metrology

Rapid developments in LEDs over the past decade have created a major growth market with completely new applications. Full color displays for large areas only became possible with the introduction of high-intensity blue LEDs, while high-power white LEDs are becoming widely used in general lighting and the automotive industry. These applications have placed increasingly stringent demands on the optical characterization of LEDs and Solid-State Lighting devices.

Specific expertise is needed in order to achieve precise and reproducible results. This handbook discusses the special characteristics of LEDs and emerging OLEDs. It provides an overview of state-of-the-art measurement equipment and gives recommendations for obtaining accurate measurement results. The main goal of this handbook is to give readers new to this subject an introduction into LED metrology. However, this handbook is also a useful reference work for more experienced readers.

The “Handbook of LED and SSL Metrology” is a truly exciting work in that it crosses the need of a broad set of participants in the LED space. Newcomers to LED lighting can use the book to quickly develop a knowledge base while experienced industry participants will find ongoing value in the book as a constant technical reference on their bookshelf.

Maury Wright, Editor-in-Chief, LEDs Magazine

Congratulations on this very helpful handbook. It is a fantastic reference with valuable information about light measurement technology and gives expert advice on the application.

Klaus Ludwig, Segment Leader Luminaires/Multimedia, TÜV SÜD Product Service

This handbook provides the reader with detailed information on the basics of photometry demonstrated by hands-on application.

Emre Onur, Editor-in-Chief, LICHT Magazine

In this extensively updated edition of the “Handbook of LED and SSL Metrology”, the authors stay abreast of changes due to the introduction of LEDs. They explain, in a coherent way, all one needs to know about metrology in general as well as the specifics of SSL metrology. In short, it is a book every lighting specialist dealing with measurement should have on his or her bookshelf.

Arno Grabher-Meyer, Editor-in-Chief, LED Professional Magazine